micromachines

MDPI

Review

PDMS Microfluidic Technological Solutions for Studying Blood Flow and Vascular Dynamics

José Pereira [1,*], Reinaldo Souza [1] and Ana Moita [1,2]

[1] IN+ Center for Innovation, Technology and Policy Research, Instituto Superior Técnico, Universidade de Lisboa, Avenida Rovisco Pais, 1049-001 Lisboa, Portugal; reinaldo.souza@tecnico.ulisboa.pt (R.S.); anamoita@tecnico.ulisboa.pt (A.M.)
[2] CINAMIL, Centro de Investigação Desenvolvimento e Inovação da Academia Militar, Academia Militar, Instituto Universitário Militar, Rua Gomes Freire, 1169-203 Lisboa, Portugal
* Correspondence: sochapereira@tecnico.ulisboa.pt

Abstract

Polydimethylsiloxane (PDMS) microfluidic platforms have become essential experimental systems for probing the fluid mechanics of blood owing to their optical transparency, biocompatibility, and rapid prototyping capabilities. Advances in soft lithography have enabled the fabrication of microchannel architectures that emulate vascular geometries, permitting controlled investigations of shear-dependent rheology, multiphase interactions between red blood cells and plasma, and microcirculatory flow phenomena under physiologically relevant conditions. Despite their widespread use, however, the PDMS devices introduce non-negligible fluid-mechanical artifacts. Wall compliance alters pressure–flow relationships, surface hydrophobicity modifies boundary conditions, and analyte absorption perturbs near-wall rheology and apparent viscosity. These effects complicate the interpretation of the blood-flow measurements, particularly in regimes where the non-Newtonian behavior, cell deformability, and confinement effects dominate. This review synthesizes the recent advances in PDMS microfluidic fabrication and surface-modification strategies while presenting a physics-based framework that links channel geometry, wall mechanics, and blood rheology to the resulting flow regimes. Emphasis is placed on understanding how the PDMS material properties influence the shear-thinning behavior, RBC aggregation, and flow resistance in microvascular-scale geometries, as well as on emerging hybrid materials and stiffened elastomers that mitigate compliance-driven distortions. Finally, the review discusses applications in thrombosis modeling, microvascular diagnostics, and organ-on-chip systems, highlighting how next-generation PDMS platforms can be engineered using fluid-mechanical design principles to enable reproducible and quantitatively accurate blood-flow research.

Keywords: PDMS; blood flow; microfluidics

Check for updates

Academic Editor: Qasem Ramadan

Received: 3 November 2026
Revised: 22 November 2026
Accepted: 24 November 2026
Published: 27 November 2026

Copyright: © 2026 by the authors. Licensee MDPI, Basel, Switzerland. This article is an open access article distributed under the terms and conditions of the Creative Commons Attribution (CC BY) license.

1. Introduction

Understanding blood flow at the microscale is essential for elucidating the biophysical and biochemical mechanisms that govern human health and disease. Blood behaves as a heterogeneous, non-Newtonian suspension whose flow characteristics arise from complex interactions among Red Blood Cells (RBCs), leukocytes, platelets, plasma proteins, and the vascular endothelium [1]. Many clinically relevant phenomena—including microvascular occlusion, thrombosis, inflammation, and impaired tissue perfusion—originate within geometries on the order of tens to hundreds of micrometers, where confinement, shear

gradients, and cell–wall interactions influence transport [2]. Conventional macroscale assays often obscure these behaviors by averaging out cell-scale dynamics, making microscale blood-flow analysis indispensable for advancing both fundamental hemodynamic research and biomedical applications.

Within this context, polydimethylsiloxane (PDMS) has become the predominant material for microfluidic platforms capable of replicating microvascular flow environments [3,4]. PDMS offers a unique combination of properties relevant to fluid-mechanical experimentation: optical transparency supporting high-resolution velocimetry and cell-scale imaging [5], gas permeability that maintains cellular viability under flow [6], mechanical flexibility that enables compliant channel architectures [7], and biocompatibility suitable for blood-contacting applications [8]. Equally important is the accessibility of PDMS fabrication through soft lithography [9], which allows rapid prototyping of custom microchannel geometries. These advantages have positioned PDMS as a central tool for modeling vascular networks, manipulating blood components, and probing hemodynamic phenomena under precisely controlled boundary conditions [10]. Figure 1 shows the timeline of the PDMS microfluidics introduction, expansion, and further improvements.

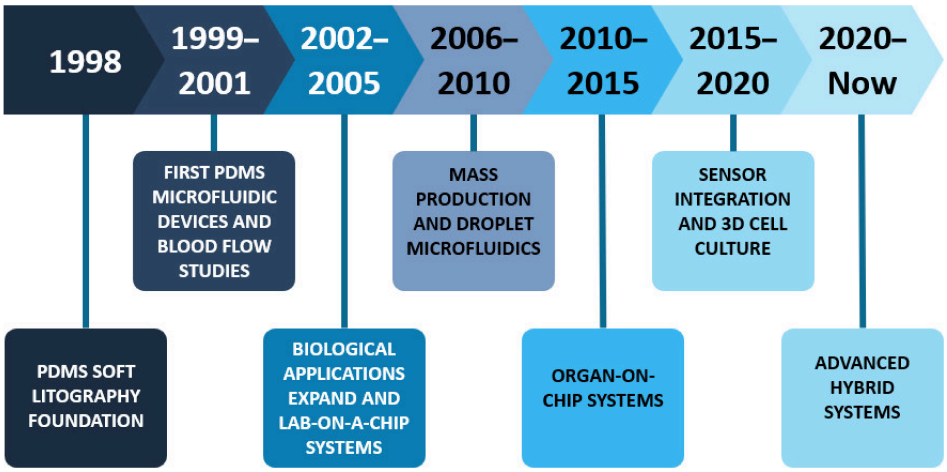

Figure 1. PDMS microfluidics timeline.

Despite the progress enabled by PDMS microfluidics, traditional blood-flow assays—such as cone-and-plate viscometers, parallel-plate flow chambers, and bulk rheometers—remain limited in their ability to reproduce physiological microscale environments. Operating at macroscale dimensions, these systems average out cell-level interactions, mask spatial heterogeneity, and cannot impose localized shear gradients or capture confinement-driven phenomena. They also lack the ability to visualize individual cell deformation, platelet activation, and leukocyte trafficking. As a result, they provide only partial insight into the mechanisms underlying microcirculatory disorders and blood–material interactions. PDMS platforms overcome these limitations by enabling precise control of flow rate, channel geometry, and biochemical cues at physiologically relevant scales, while supporting observation of non-Newtonian and multiphase blood-flow behavior. More broadly, the microfluidic technologies have emerged as powerful tools for reproducing vascular dimensions, mechanical conditions, and disease-specific microenvironments, enabling the investigation of blood-flow phenomena that are difficult to capture using conventional experimental platforms [11].

This review synthesizes recent advances in PDMS microfluidic technologies for blood-flow analysis, with emphasis on fabrication methods, device architectures, and the fluid-mechanical phenomena they enable. By examining both the strengths and limitations of PDMS systems, the present work aims to provide a comprehensive understanding of how

these platforms have shaped modern blood-flow research and where future opportunities lie. The objectives are to summarize the state of knowledge and to highlight the technological gaps, methodological challenges, and promising directions for the microfluidic systems that more accurately capture the physics of microvascular flow.

Although numerous reviews have examined PDMS microfluidics, lab-on-a-chip technologies, and blood microfluidic applications, most studies primarily focus on device fabrication, biological assays, diagnostic applications, and organ-on-chip systems. Comparatively less attention has been devoted to understanding how the properties of PDMS influence the underlying fluid mechanics of blood flow and the quantitative interpretation of the experimental results. The present review addresses this gap by adopting a fluid-mechanics-oriented perspective. Rather than reviewing the PDMS merely as a fabrication material, it is examined how channel compliance, surface properties, molecular absorption, and geometric confinement interact with the non-Newtonian rheology of blood to influence flow resistance, shear distribution, cell migration, and microvascular transport phenomena. Furthermore, this review proposes a unified framework linking PDMS material behavior, device configuration, and blood rheology to the resulting flow regimes. By emphasizing the physical mechanisms responsible for measurement distortions and discussing emerging material and design solutions for minimizing these effects, this work provides a perspective that complements existing reviews and supports the development of more physiologically relevant blood-flow microfluidic systems.

To guide the reader, the manuscript is organized into several sections. Section 2 defines the literature search and classification methodologies. Section 3 introduces the fundamental properties of PDMS and the principles of microfluidic operation relevant to blood flow. Section 4 surveys major categories of PDMS microfluidic platforms, ranging from simple straight channels to complex biomimetic vascular networks. Section 5 explores biological and biophysical phenomena elucidated using PDMS devices, including RBC mechanics, platelet adhesion, and leukocyte dynamics. Section 6 discusses limitations of PDMS—such as hydrophobicity, molecular absorption, and mechanical compliance—and their implications for experimental accuracy. Section 7 reviews strategies to overcome these challenges, including surface-modification techniques, hybrid material systems, and device-level solutions. Finally, Section 8 outlines the future directions for advancing PDMS microfluidics toward greater physiological relevance and clinical translation, followed by concluding remarks in Section 9.

2. Literature Search and Classification Methodology

The literature considered in this review was identified through searches conducted in the Scopus, Web of Science, and Google Scholar databases. The searches were performed between January and June 2026 and covered publications published between January 2000 and March 2026. The search strategy employed combinations of keywords including “PDMS microfluidics”, “blood flow”, “red blood cells”, “RBC deformability”, “hematocrit”, “blood rheology”, “microcirculation”, “blood diagnostics”, “cell mechanics”, and “blood analog fluids”. The representative search queries included the following:

- “PDMS microfluidics” and “blood flow”.
- “PDMS microchannels” and “red blood cells”.
- “PDMS” and “RBC deformability”.
- “PDMS microfluidics” and “disease diagnostics”.
- “blood analog fluids” and “PDMS”.
- “Microcirculation” and “PDMS devices”.

A total of 600 records were initially identified. After screening the titles, abstracts, and keywords for relevance, approximately 350 publications were retained for detailed

analysis. Publications were included when they focused on PDMS-based microfluidic devices applied to blood flow, blood-cell mechanics, blood diagnostics, blood analog fluids, and related hemodynamic phenomena. Studies not involving PDMS devices, publications unrelated to blood and blood analog fluids, and conference abstracts lacking sufficient technical information were excluded. For the thematic analysis presented in this work, the retained publications were manually classified according to their primary research objective. Each publication was assigned to a single category to avoid double counting. The classification categories were as follows: (i) RBC deformability, (ii) disease diagnostics, (iii) flow visualization and hemodynamics, (iv) blood analog fluids and PDMS microfluidics, and (v) other blood-related studies. The resulting distributions are intended to provide an overview of the dominant research themes represented within the literature dataset analyzed in this review. They should not be interpreted as a comprehensive bibliometric analysis of all publications in the field. Table 1 summarizes the main items of literature search and classification methodology and Table 2 shows the percentage distribution of the classification categories and corresponding number of publications.

Table 1. Main items of literature search and classification methodology.

Item	Description
Databases	Scopus, Web of Science, Google Scholar
Search period	January 2000–March 2026
Search date	January–June 2026
Records identified	600
Records retained after screening	350
Inclusion criteria	PDMS microfluidic studies involving blood, blood cells, blood analog fluids, diagnostics, hemodynamics, or microcirculation
Exclusion criteria	Non-PDMS studies, non-blood applications, duplicate records, abstracts with insufficient technical information
Classification categories	RBC deformability, disease diagnostics, flow visualization and hemodynamics, blood analog fluids and PDMS microfluidics, other blood-related studies
Classification method	Manual categorization according to the primary research objective

Table 2. Percentage distribution of the classification categories and corresponding number of publications.

Category	Percentage Distribution	Number of Publications
RBC Deformability	38	133
Disease Diagnostics	28	98
Flow Visualization and Hemodynamics	18	63
Other Blood-Related Studies	12	42
Blood Analog Fluids and PDMS Microfluidics	4	14
Total	100	350

3. PDMS

3.1. Properties of PDMS

3.1.1. Optical Transparency

The PDMS exhibits excellent optical transparency across the visible spectrum, transmitting more than 90% of incident light between 600 and 1600 nm [12]. This high transmittance enables brightfield, fluorescence, and high-speed microscopy, allowing real-time visualization of blood-flow phenomena such as RBC deformation, plasma skimming, and thrombus formation [13]. The low autofluorescence of PDMS supports velocimetry and particle-tracking analyses involving fluorescently labeled cells and biomolecules.

3.1.2. Gas Permeability

The PDMS is highly gas permeable due to its flexible siloxane backbone and relatively large free volume, which facilitate the diffusion of small molecules through the polymer matrix. Reported permeability coefficients for PDMS are approximately 600–800 Barrer for oxygen and 3000–4000 Barrer for carbon dioxide, values that are higher than those of many thermoplastics used in microfluidics. Water-vapor permeability is also significant, enabling moisture transport across device walls. These properties support gas exchange in cell-culture systems and contribute to maintaining physiological oxygen levels within endothelialized channels and organ-on-chip platforms [14]. The high gas permeability of PDMS is particularly advantageous for blood-related microfluidic studies because oxygen and carbon dioxide can diffuse through the channel walls without requiring dedicated gas-exchange structures. However, the gas transport also introduces fluid-mechanical challenges. Water evaporation through the PDMS matrix gradually increases solute concentration, hematocrit, and apparent blood viscosity during long duration experiments. Furthermore, the dissolved gases may diffuse into or out of the flowing fluid, promoting bubble nucleation, especially under temperature fluctuations and pressure changes. Even small bubbles can alter the microscale flow by introducing gas–liquid interfaces, modifying local velocity profiles, reducing effective cross-sectional area, and generating flow disturbances. Consequently, while the PDMS gas permeability enhances biological functionality, it may simultaneously compromise the reproducibility and quantitative accuracy of blood-flow measurements if evaporation and bubble formation are not regulated. Table 3 summarizes the typical permeability values of PDMS relative to different gases.

Table 3. Typical PDMS permeability ranges of different gases.

Gas	Typical Permeability in PDMS (Barrer)	Relevance	References
Oxygen	~600–800	Supports oxygenation of cultured cells	[14,15]
Carbon Dioxide	~3000–4000	Enables gas exchange and pH regulation	[14,15]
Nitrogen	~250–350	Dissolved-gas concentrations changes and bubble nucleation	[14]
Water vapor	High permeability (typically reported as vapor transmission rates rather than Barrer values)	Can cause evaporation and concentration changes	[16,17]

3.1.3. Mechanical Behavior

The elastomeric nature of PDMS allows it to deform under modest pressures while maintaining structural integrity. Reported elastic properties—including shear modulus and Young's modulus—vary widely across the literature depending on the mechanical test method [1], base-to-curing-agent ratio, and curing temperature [18]. This tunable elasticity enables fabrication of microchannels that mimic biological vessels, allowing studies of endothelial mechanotransduction, RBC deformability, and pressure-dependent flow resistance [19]. Simultaneously, excessive deformation under high flow rates and pressures alter channel geometry, hydraulic resistance, shear stress distribution, and flow stability. The low elastic modulus of PDMS, typically ranging from approximately 0.5 to 3 MPa depending on the curing ratio and manufacturing conditions, causes microchannel deformation under pressure-driven flow. Unlike rigid glass and silicon devices, PDMS channels undergo fluid–structure interactions in which the internal pressure expands the channel cross-section, thereby altering the hydraulic characteristics of the system. Consequently, the actual channel dimensions may differ from the nominal geometry used during the device design and the experimental analysis. The channel deformation affects the hydraulic resistance. For a rectangular microchannel, the hydraulic resistance is dependent on channel height, scaling approximately with h^{-3} under low-aspect-ratio conditions. Therefore, even modest pressure-induced increases in channel height can considerably reduce the flow resistance. As a result, the pressure–flow-rate relationship becomes nonlinear, deviating from the classical Hagen–Poiseuille prediction [20] for rigid conduits. Gervais et al. [21] demonstrated that compliant PDMS channels exhibit measurable increases in flow rate compared with rigid-channel predictions as pressure rises, owing to pressure-dependent expansion of the channel cross-section. Similar observations have been reported in subsequent experimental and numerical investigations of flexible microfluidic systems. Channel geometry plays a major role in determining the magnitude of the deformation. Wide channels generally deform more than narrow channels because the unsupported ceiling experiences greater bending. Likewise, channels with thin PDMS roof layers have considerably larger deflections than those fabricated with thicker walls. Pressure-induced deformation becomes particularly significant in large-aspect-ratio channels, where channel-height increases exceeding 10% have been reported at pressures above approximately 5 kPa, while deformations greater than 100% have been observed under pressures approaching 50 kPa for highly compliant geometries. These findings highlight the strong dependence of channel expansion on both geometry and operating pressure. Wall deformation also influences WSS as for a given flow rate, channel expansion increases the flow area and reduces velocity gradients near the walls, leading to lower shear stresses than those predicted using undeformed dimensions. Conversely, when a constant pressure drop is imposed, deformation modifies both flow rate and velocity distribution, producing spatially varying shear conditions along the channel length. Such deviations can lead to inaccurate estimation of critical hemodynamic parameters associated with RBC deformation, platelet activation, leukocyte adhesion, and thrombus formation. The effect is particularly relevant for blood because the blood rheology is highly shear dependent. Errors in shear-stress estimation propagate to apparent viscosity measurements, cell-free layer (CFL) characterization, and assessments of shear-thinning behavior. Consequently, studies employing PDMS microfluidics should account for pressure-dependent geometry changes through experimental calibration, fluid–structure interaction modeling, and exploration of stiffer materials and reinforced channels. Wall compliance can substantially alter the hemodynamic flow fields by modifying local velocity distributions, vortex structures, and WSS. The experimental studies conducted in compliant vascular models [22] have demonstrated that the wall deformation may generate measurable differences in pulsatile flow behavior compared with the

rigid-wall assumptions, highlighting the importance of the fluid–structure interactions in hemodynamic investigations. Table 4 summarizes recent findings on PDMS microchannels wall deformation in microfluidic devices.

Table 4. Findings on PDMS microchannels wall deformation in microfluidic devices.

Main Findings	Relevance	References
Demonstrated nonlinear pressure–flow behavior caused by PDMS wall deformation	Hydraulic resistance decreases as channels expand	[21]
Showed strong coupling between applied pressure and channel geometry in flexible PDMS microchannels	FSI effects become significant at elevated pressures	[23]
Developed theoretical models describing pressure-driven flow in deformable PDMS channels	Predicts pressure-dependent resistance and wall deformation	[24]
Reported deformation > 10% above 5 kPa and >100% at 50 kPa in large-aspect-ratio channels	Quantifies magnitude of measurement errors in compliant channels	[25]

3.1.4. Biocompatibility

PDMS is a biocompatible material, supporting short-term contact with blood and various cell types without inducing significant cytotoxicity [26]. Its chemical inertness and low protein reactivity make it suitable for hemocompatible applications, including platelet-adhesion assays and leukocyte-trafficking studies [27]. However, PDMS absorbs proteins and hydrophobic molecules, altering surface chemistry and influencing cell behavior [28]. Protein adsorption modifies near-wall boundary conditions, affecting slip length, viscosity, and adhesion. For long-term culture and sensitive biochemical assays, surface treatments and coatings are required to maintain consistent biological performance.

3.1.5. Chemical Composition and Curing Chemistry

The PDMS is a silicone-based polymer composed of repeating –Si$(CH_3)_2$–O– units. Commercial formulations consist of a vinyl-terminated PDMS base and a curing agent with cross-linker and platinum catalyst [29]. Curing proceeds through hydrosilylation, forming a three-dimensional elastomeric network. The degree of cross-linking—and thus the resulting chemical, mechanical, and transport properties—can be tuned by adjusting the base-to-curing-agent ratio and curing temperature and time.

3.1.6. Wettability

The PDMS is hydrophobic, exhibiting a water contact angle of approximately 110° [30], which hinders initial wetting of microchannels, promotes bubble entrapment, and influences blood–surface interactions through protein adsorption and biofouling. Oxygen–plasma treatment renders the surface hydrophilic by generating silanol groups, improving wettability and enabling irreversible bonding to glass or other PDMS layers [31,32]. The hydrophobicity also facilitates the absorption of hydrophobic drugs and biomolecules, posing a limitation for quantitative blood assays. Also, the wettability governs the boundary-condition behavior, capillary forces, and stability of multiphase interfaces, making surface modification essential for blood-flow measurements. Table 5 summarizes the properties of PDMS microfluidic devices for blood-flow investigations.

Table 5. Properties of the PDMS microfluidic devices for blood-flow investigation.

Property	Type of Devices	Benefits	Disadvantages	Impact on Experimental Accuracy	Mitigation	References
Optical Transparency	Flow cytometry chips Endothelialized channels Droplet assays	Enables high-resolution imaging Compatible with fluorescence microscopy	Autofluorescence at some wavelengths	High—affects imaging-based quantification	Low-autofluorescence PDMS Glass-PDMS hybrids	[33]
Elasticity/Softness	Shear-stress studies Vessel-mimicking channels Deformability assays	Mimics tissue mechanics Allows reversible deformation	Not physiologically identical to real vessels Deforms under pressure	Medium—channel deformation changes shear stress	Increase crosslinker ratio Hybrid PDMS–glass	[34]
Hydrophobicity	Droplet generators Plasma separation Cell adhesion studies	Stable droplet formation Reduces nonspecific wetting	Poor wetting for aqueous blood Protein adsorption increases fouling	High—affects flow stability and cell adhesion	Plasma treatment PEG-coating	[35]
Protein Adsorption	Coagulation assays Platelet studies Immunocapture devices	Useful for immobilizing antibodies	Alters blood protein Promotes clotting and fouling	High—can bias coagulation or adhesion results	PEGylation Parylene coating	[36]
Biocompatibility	Endothelialized chips Long-term perfusion	Cell-friendly Non-toxic after curing	Uncured oligomers leach into samples	Medium—affects cell viability	UV curing Barrier coatings	[37]
Chemical Absorption	Drug-testing chips Pharmacokinetics studies	None	Absorbs hydrophobic drugs Alters concentration	Very High—invalidates drug-response curves	Parylene-C, sol–gel coatings COC/PMMA hybrids	[38]
Thermal Stability	PCR-on-chip Temperature-controlled assays	Stable up to ~200 °C Good for thermal cycling	Expands with temperature Softens at high heat	Medium—affects channel geometry	Glass–PDMS hybrids External temperature control	[39]
Ease of Fabrication	Straight channels Droplet devices	Rapid prototyping Low cost	Limited to 2.5D geometries	Low–Medium—affects device complexity	3D printing and multilayer PDMS	[40]
Air Bubble Susceptibility	All blood-flow devices Narrow channels	None	Air bubbles disrupt flow Cause clotting	High—bubbles invalidate experiments	PDMS degassing Bubble traps Hydrophilic coatings	[41]
Mechanical Robustness	High-pressure flow Stenosis models	Flexible and durable Withstands moderate pressure	Deforms under high pressure Unsuitable for arterial-level pressures	Medium—affects shear stress accuracy	Reinforcement with glass Using thicker PDMS layers	[42]

3.2. Fabrication Techniques of the PDMS

3.2.1. Soft Lithography

Soft lithography begins with the fabrication of a master mold using standard photolithography, typically employing SU-8, an epoxy-based negative photoresist well suited for producing high-aspect-ratio microchannel structures with excellent mechanical stability. A silicon wafer is spin-coated with SU-8, where the rotation speed determines the final film thickness and thus the height of the microchannels. Different SU-8 formulations permit thicknesses ranging from a few micrometers to several hundred micrometers, enabling control of channel depth—an essential parameter in microfluidic blood-flow studies. After coating, the wafer undergoes soft-bake to evaporate solvents and stabilize the film. A photomask containing the microchannel layout is then aligned over the SU-8 layer and exposed to ultraviolet light. As a negative photoresist, SU-8 polymerizes and crosslinks

in the exposed regions, forming a chemically and mechanically resistant structure. A post-exposure bake completes the crosslinking. During development, the unexposed SU-8 dissolves, leaving a three-dimensional relief pattern with vertical sidewalls and smooth surfaces—features that make SU-8 suitable for microfluidic mold fabrication. The resulting SU-8 master serves as the template for PDMS casting. Liquid PDMS is poured over the master, degassed, and cured, replicating the microchannel geometry. The robustness of SU-8 allows repeated PDMS castings without quality degradation, ensuring reproducibility across experiments. Smooth SU-8 sidewalls minimize flow disturbances, which is critical for hemodynamic studies where channel height, width, and curvature influence flow regimes, shear profiles, and near-wall interactions. In these confined geometries, the characteristic length scales are typically on the order of tens-to-hundreds of micrometers. Together with the moderate flow velocities usually imposed in blood microfluidic studies, these dimensions often result in low Reynolds numbers and predominantly laminar flow conditions. However, the Reynolds number varies depending on the channel geometry, flow rate, and fluid properties, and values superior to one are reported for larger microchannels and high-throughput devices, while remaining within the laminar regime. SU-8-based soft lithography provides the geometric precision required to investigate microcirculatory phenomena including plasma skimming and shear-dependent viscosity in the low-Reynolds-number microfluidic systems [42].

3.2.2. Replica Molding

Replica molding is the core of PDMS microfabrication [43]. Liquid PDMS prepolymer is poured over the photolithographically patterned master and degassed to remove trapped air bubbles, ensuring uniform filling. The polymer is then cured at elevated temperatures to form an elastomeric solid that captures the mold geometry. Once cured, the PDMS layer is peeled from the master, producing a negative replica of the initial configuration. This technique enables fast and cost-effective production of PDMS microfluidics [44], and the master mold can be reused multiple times, making replica molding ideal for iterative prototyping.

3.2.3. Oxygen Plasma and Chemical Bonding

After molding, the PDMS replica must be bonded to another surface, typically glass or another PDMS layer, to form enclosed microchannels. The oxygen–plasma bonding is the most used method: plasma treatment generates silanol groups on the PDMS surface, which form covalent Si–O–Si bonds upon contact with another activated surface, creating an irreversible seal [45]. This bonding provides strong, leak-free interfaces suitable for high-pressure blood-flow experiments and ensures stable boundary conditions during shear-dependent rheological measurements. Alternative bonding strategies include silane coupling agents and UV-activated adhesives when the plasma bonding is not feasible.

3.2.4. Multilayer, 3D Printing, and Other Additive Manufacturing Techniques

The PDMS compatibility with layer-by-layer assembly makes it suitable for constructing multilayer and three-dimensional microfluidic systems [46]. Multilayer soft lithography enables the incorporation of valves, pumps, and control elements by aligning and bonding multiple PDMS layers with embedded microstructures [47]. This configuration supports the flow routing and the modulation of shear stress, which are valuable for studying blood-cell interactions, endothelial mechanotransduction, and vascular physiology. Three-dimensional PDMS and hybrid microfluidic devices can also be fabricated using techniques like sacrificial molding [48], laser processing [49], embedded 3D-printed templates [50], and other additive-manufacturing techniques [51]. These approaches allow construction of biomimetic vascular networks with curved, branching, and interconnected geometries

that resemble in vivo microcirculation and enable bifurcation-driven cell sorting, curvature-induced secondary flows, and heterogeneous shear fields, which are fundamental topics in the microscale hemodynamics. Figure 2 shows the roll-to-roll room temperate additive manufacturing for PDMS platforms.

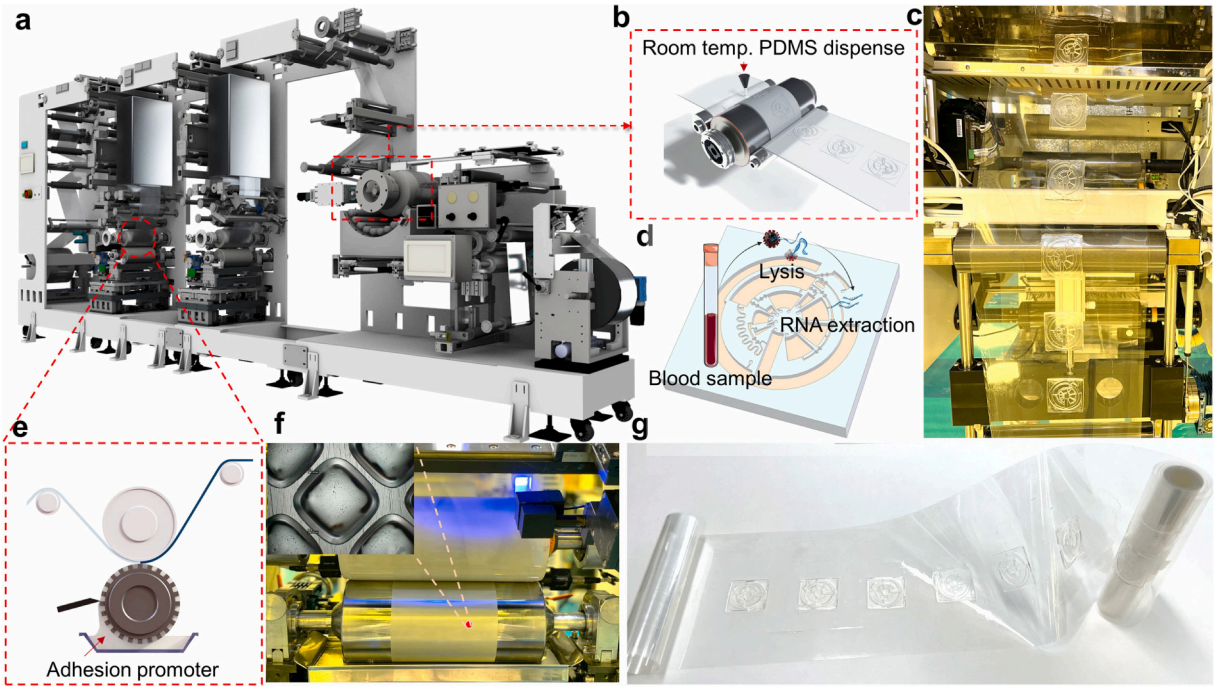

Figure 2. Room-temperature roll-to-roll imprinted PDMS centrifugal device: (**a**) roll-to-roll additive manufacturing platform, (**b**) roll-to-roll imprint, (**c**) rewinder, (**d**) on-chip isolation of RNA from whole blood, (**e**,**f**) gravure coating, and (**g**) production of PDMS centrifugal devices onto a PET substrate [52].

Despite its versatility, the PDMS molding from 3D-printed masters is hindered by three major issues: surface roughness, demolding difficulty, and chemical diffusion from the printed structure into the PDMS. Surface roughness arises from the layer-by-layer fabrication of Stereolithography (SLA), Digital Light Processing (DLP), and Fused Deposition Modeling (FDM) printers, which—even at high resolutions of 25–50 µm in the XY plane and 10–25 µm in the Z direction—produce micro-terraces that replicate directly into PDMS. Additional roughness originates from resin shrinkage during photopolymerization, generating micro-waviness, and from post-processing defects such as pits and scratches introduced during support removal. These imperfections increase hydrodynamic resistance in the PDMS microchannels, degrade the optical clarity required for PIV (Particle Image Velocimetry) and PTV (Particle Tracking Velocimetry) and fluorescence microscopy, reduce the plasma-bonding quality to glass, and alter the wettability relevant to capillary flows and droplet microfluidics. Demolding is also problematic because PDMS adheres to many photopolymer resins. This adhesion results from the mechanical interlocking with rough and undercut surfaces, affinity between PDMS and residual acrylates, and geometric constraints like deep channels and sharp corners that elevate peel forces. The consequences include tearing of thin PDMS features and distortion caused by stretching during demolding. Chemical diffusion from the 3D-printed mold into PDMS represents an additional concern, particularly for biocompatibility and optical or mechanical stability. SLA/DLP resins contain unreacted monomers, photoinitiators, oligomers, and plasticizers that migrate into PDMS during curing—especially between 60 and 80 °C—because PDMS is permeable to organic molecules. This diffusion can lead to yellowing and clouding, inhibition of PDMS

crosslinking, and changes in mechanical properties. These problems are replicated because PDMS has low pre-curing viscosity, allowing infiltration into microscopic defects, high compliance, enabling tight conformity to mold geometry, strong interfacial adhesion to many polymers, and high permeability to organic molecules. Mitigation strategies include applying post-print resin coatings such as UV-curable gloss layers, performing chemical or mechanical polishing, using higher-resolution printing methods such as advanced DLP or two-photon polymerization, applying mold-release agents and fluorinated silanes, designing molds with draft angles, curing PDMS at lower temperatures, post-curing printed molds to reduce residual monomers, extended UV curing, applying barrier coatings including Parylene-C and epoxy, and using thermoplastic molds when the chemical purity is essential.

3.2.5. Rapid Prototyping

The soft lithography technique supports workflows in which photomasks, master molds, and PDMS replicas can be fabricated quickly. This prototyping capability accelerates the experimental development by enabling variation of channel geometries, boundary conditions, and flow configurations with cost effectiveness. For blood-flow analysis, the rapid prototyping is valuable because the microscale hemodynamics are sensitive to the channel dimensions and confinement ratios. Moreover, the iterative fabrication allows for the tailoring of microchannels to cell types, disease models, and flow regimes—whether optimizing shear-rate distributions for RBC deformability studies, adjusting bifurcation angles for margination experiments, or tuning channel height to probe shear thinning under physiological conditions [53]. Table 6 summarizes PDMS and hybrid manufacturing techniques for blood-flow devices.

Table 6. Manufacturing techniques for PDMS and hybrid microfluidic blood-flow devices.

Manufacturing Technique	Benefits	Disadvantages	Complexity/Cost	Type of Devices	Applications	References
Soft Lithography	High precision Smooth channel walls	Requires cleanroom for master mold 2.5D geometries	Moderate–High	Straight channels Bifurcations Viscometers Droplet generators Endothelialized channels	Hemodynamics Shear-stress studies Droplet blood assays	[53]
Replica Molding	Fast prototyping Low material cost	Bonding defects possible PDMS swelling affects accuracy	Low–Moderate	Simple vascular models Plasma separators	Blood rheology Plasma extraction Point-of-care diagnostics	[54]
3D Printing and PDMS Casting	Complex 3D geometries Rapid iteration	Surface roughness from 3D prints Limited resolution for capillary-scale channels	Low–Moderate	Aneurysm models Stenosis models	Vascular pathology modeling Device testing	[55]
Direct 3D Printing of Microfluidics	True 3D vascular networks Multi-material options	Cytotoxicity of resins Lower gas permeability than PDMS	Moderate–High	Organ-on-chip Complex vascular networks Perfusion chambers	Tumor vasculature studies Drug testing Organ-mimicking systems	[56]
Hybrid PDMS–Hydrogel	Biomimetic ECM Tunable stiffness	Hydrogels degrade Fabrication more delicate	Moderate	Endothelialized networks Angiogenesis chips Tumor-vascular models	Angiogenesis Cancer metastasis	[57]
Laser Ablation	Rapid prototyping No molds required	Rough channel walls Simple geometries	Low–Moderate	Flow-focusing devices Viscometers	Quick prototyping Low-cost diagnostics	[58]

Table 6. *Cont.*

Manufacturing Technique	Benefits	Disadvantages	Complexity/Cost	Type of Devices	Applications	References
Injection Molding	Durability Chemical resistance	High upfront mold cost Less flexible than PDMS	High initial Low per-unit	Commercial blood-analysis cartridges Plasma separators	Point-of-care diagnostics Clinical consumables	[59]
Micro-Milling and Hot Embossing	Replication fidelity Compatible with biocompatible plastics	Specialized equipment 2D structures	Moderate–High	Capillary networks Disposable chips	Clinical diagnostics Blood filtration	[60]
PDMS–Glass Hybrid Bonding	Optical clarity Stable for blood assays	Plasma cleaner Bonding defects	Moderate	Flow cytometry chips Optical detection devices	Cell counting Imaging-based blood analysis	[61]
PDMS and Silicon Hybrid Fabrication	Precision Integrates sensors and MEMS	Expensive Cleanroom	High	Electrochemical sensors MEMS-integrated blood chips	Impedance cytometry Biosensing	[62]

3.3. Blood-Flow Microfluidic Principles

3.3.1. Laminar Flow

In microfluidic channels, fluid motion is overwhelmingly dominated by laminar flow, a direct consequence of the small characteristic dimensions and low velocities typical of these systems. The microvascular and microfluidic blood flows are generally characterized by low Reynolds numbers due to the small characteristic dimensions involved. Under these conditions, viscous forces dominate over inertial effects, promoting stable laminar flow. Nonetheless, the Reynolds number is not an intrinsic property of microfluidic systems and should not be assumed a priori. Its value depends on channel geometry, flow velocity, and fluid density and viscosity. Consequently, the Reynolds number may range from well below unity to several tens in microfluidic devices, while the flow often remains laminar since the transition to turbulence occurs at substantially higher Reynolds numbers. Moreover, the velocity profiles are predictable, often parabolic in simple geometries, and mixing occurs through molecular diffusion rather than turbulence-driven advection. Laminar regime is advantageous for microscale blood-flow studies because it enables control of shear rates and reproducible conditions that mimic those in capillaries and small vessels [63]. However, the laminar blood flow in microchannels is more complex than in Newtonian fluids due to the non-Newtonian and multiphase nature of blood. The RBCs, leukocytes, platelets, and plasma interact with the channel walls, producing flow behaviors that deviate from classical laminar predictions. One consequence of laminarity is the emergence of well-defined shear-rate gradients, which influence RBC deformation, aggregation, and orientation. At low shear rates, RBCs may form rouleaux, increasing viscosity and at moderate shear rates, they transit to tank-treading and tumbling modes; and at high shear rates, they align with the flow. These transitions can be mapped onto laminar shear-rate distribution, enabling studies of cell mechanics and hemorheological transitions. Furthermore, the laminar-flow conditions encountered in microfluidic devices facilitate the observation and quantification of cell margination. The margination does not arise from laminar flow itself, but rather from hydrodynamic interactions among blood cells under low-Reynolds-number conditions. Due to their high deformability, the RBCs preferentially migrate toward the channel center where shear-induced deformation is minimized. Repeated collisions between the RBCs and the stiffer cellular components displace the platelets and leukocytes toward the near-wall region, where they accumulate within or adjacent to the CFL. This segregation process is enhanced by confinement and shear-rate gradients and plays a key role in hemostasis, thrombosis, and inflammatory responses. The stable and predictable velocity fields associated with

laminar microchannel flows enable these migration dynamics to be visualized and quantified with high spatiotemporal resolution. From a fluid-mechanical perspective, margination results from a combination of deformability-induced RBC migration, wall-induced lift forces, and heterogeneous particle collisions. As deformable RBCs migrate away from the wall, a CFL develops near the channel boundaries. Less deformable particles, such as platelets and leukocytes, are subsequently transported into this region through collision-driven diffusion, increasing their probability of near-wall localization. Classical single-phase laminar-flow models cannot predict this behavior because margination emerges from multiphase interactions between suspended cells and the surrounding plasma. This segregation arises from the hydrodynamic lift forces and particle–wall interactions that are only stable in low-Reynolds-number environments. Microfluidic channels enable to quantify margination dynamics, platelet–wall collision frequencies, and near Wall Shear Stress (WSS) under confinement. Another feature of laminar microflows is the absence of turbulence, allowing for the formation of multiphase interfaces. This stability is essential for studying plasma skimming at bifurcations, RBC partitioning in asymmetric geometries, and development of CFLs near the channel walls. Laminar regime provides the environment for PTV, micro-PIV, and optical flow methods, which require stable flow to resolve velocity gradients and cell trajectories. The compatibility with non-Newtonian blood behavior makes the laminar flow fundamental to the study of microcirculatory phenomena including cell margination, plasma skimming, shear-dependent viscosity, and RBC biomechanics. Although many microfluidic systems operate within linear low-Reynolds-number regimes, recent studies have highlighted the emergence of nonlinear phenomena resulting from particle–particle interactions, deformable boundaries, multiphase transport, and geometry-induced instabilities. Such effects are particularly relevant for blood, which behaves as a concentrated suspension of deformable cells and therefore exhibits rheological responses that depart from classical linear microfluidic assumptions [64].

3.3.2. Shear Stress

Shear stress is a fundamental parameter governing blood-cell behavior, hemorheology, and vascular physiology. In microfluidic channels, the WSS is defined by Equation (1) [65]:

$$\tau_w = \mu \left(\frac{du}{dy} \right)_{y=0} \quad (1)$$

where $\frac{du}{dy}$ is the velocity gradient at the channel wall. Equation (1) corresponds to the classical Newtonian definition of WSS, where the viscosity is assumed constant and independent of the shear rate. For blood, this approximation is appropriate at sufficiently high shear rates and in channels substantially larger than individual blood cells, where an effective viscosity can be defined. However, under low-shear conditions and when shear-dependent rheological effects become significant, the apparent viscosity varies with shear rate and constitutive descriptions, such as the Carreau–Yasuda, Cross, Casson, and Quemada models, may be required. Consequently, Equation (1) should be interpreted as a first-order approximation frequently employed in microfluidic blood-flow analysis rather than a universally valid description. Because microfluidic flows operate in the low-Reynolds-number regime, the velocity field is stable, allowing shear stress to be controlled through adjustments in flow rate, and channel height and width. This tunability enables investigation of shear-dependent phenomena including RBC deformation, platelet activation, leukocyte rolling, and endothelial mechanotransduction [66]. In rectangular PDMS microchannels, and for a given volumetric flow rate, reducing the channel height increases the velocity gradient near the wall, thereby increasing the shear stress. This geometric sensitivity allows to design microchannels replicating physiological shear ranges—from sub-capillary shear rates ($<10\ s^{-1}$) associated with RBC aggregation, to arterial-level shear ($>1000\ s^{-1}$) relevant

to platelet activation and thrombosis. The ability to impose uniform, heterogeneous, or time-varying shear profiles is essential for microvascular environments. RBCs transit from aggregation at low shear to tank treading or tumbling at moderate shear, and alignment at high shear. Platelets respond to shear gradients by activating, adhering to, or forming aggregates, while leukocytes modulate rolling velocity and adhesion strength based on local shear stress. The high surface-to-volume ratio of microchannels also enhances wall interactions, making surface chemistry, roughness, and wettability determinant factors of blood–material responses. The hydrophobic PDMS surfaces promote protein adsorption, altering near-wall viscosity and slip length. Surface roughness influences shear stress, platelet adhesion, and leukocyte capture. Coatings, plasma treatments, and hybrid materials play a central role in ensuring shear-dependent measurements. Microfluidic systems enable pulsatile, oscillatory, and ramped shear profiles that mimic physiological conditions such as cardiac pulsatility and inflammatory shear fluctuations. These controlled perturbations allow for the study of transient mechanobiological responses, including endothelial calcium signaling, cytoskeletal remodeling, and shear-induced changes in the RBC morphology.

3.3.3. Non-Newtonian Behavior

Human blood exhibits a complex rheological behavior that deviates from Newtonian fluids, particularly at low shear rates and under geometric confinement [67]. Its shear-thinning properties arise from two coupled microscopic mechanisms: shear-induced dissociation of RBC aggregates at low to moderate shear stresses at high shear stresses. This dual mechanism was established by Chien et al. [68], who demonstrated that rouleaux, linear or branched aggregates formed at low shear due to plasma macromolecules, break apart as shear stress increases. Chien et al. [69] observed the dynamics of RBC doublets under oscillatory shear, showing that aggregate breakup occurs through sliding, rolling, and partial separation. This dissociation reduces the viscosity in low-to-moderate shear regime. At higher shear stresses, the dominant mechanism shifts from the aggregate breakup to the cell deformability. In their work [68], they demonstrated that normal RBCs undergo deformation—elongation and alignment with the flow—when subjected to elevated shear. When the RBCs were chemically stiffened, the suspensions exhibited higher viscosity and almost no shear thinning, proving that membrane deformability is essential for the viscosity drop at high shear rates. These findings established that blood rheology cannot be understood without considering the nonlinear elastic response of RBC membrane. The analysis by Viallat and Abkarian [70] extends the framework of Chien et al. [68,69,71–73]. They describe RBCs as active particles whose shape, membrane tension, and cytoskeletal remodeling influence flow resistance. Their work details transitions between tumbling, rolling, swinging, and tank-treading regimes. By integrating microfluidic observations with theoretical modeling, Viallat and Abkarian show how RBC deformability governs blood rheology from capillary flows to large-artery hemodynamics. Together, Chien et al. [68,69,71–73] and Viallat and Abkarian [70] provide a unified interpretation of shear-thinning low-shear viscosity reduction arising from dissociation of RBC aggregates, whereas high-shear viscosity reduction is driven by RBC deformation and flow alignment. Confinement, wall proximity, and geometric heterogeneity generate non-uniform shear fields, producing spatially varying rheological regimes within a single microchannel. In PDMS microchannels, the combined effects of geometric confinement, high surface-to-volume ratio, and locally varying shear rates can produce several characteristic blood-flow phenomena, including rouleaux breakup near the walls, RBC tank-treading within the channel core, confinement-enhanced deformation, wall-induced lift forces, and nonlinear changes in apparent viscosity and flow resistance. Although these effects are commonly observed under low-Reynolds-number conditions, they are governed primarily by cell-scale hydrodynamics, confinement, and

shear-rate distributions rather than by Reynolds number alone. These effects suggest that blood rheology in confined geometries cannot be described by classical shear-rate–viscosity curves. Instead, a multiregime rheological map is required—one that links shear rate, confinement ratio, and wall proximity to the dominant microscopic mechanism (aggregation, deformation, or alignment). This framework is essential for interpreting measurements obtained in PDMS devices. Phenomena like the Fåhræus–Lindqvist effect [74], plasma skimming [75], and cell margination [76] emerge in microfluidics, making PDMS devices valuable for examining microcirculatory rheology under physiologically relevant conditions. However, these phenomena are not exclusive to PDMS channels as experiments performed in glass capillaries and tubes demonstrated the emergence of these effects under strong geometric confinement.

3.3.4. Applicability of Classical Flow Models to Blood Microflows

The selection of an appropriate blood-flow model depends primarily on the characteristic length scale of the system and the underlying phenomena being investigated. In many microfluidic devices operating at moderate to high shear rates and with channel dimensions substantially larger than individual erythrocytes, blood can be reasonably treated as a homogeneous Newtonian fluid characterized by an effective viscosity. Under these conditions, classical fluid-mechanical approaches are often sufficient for predicting bulk flow behavior, pressure losses, velocity profiles, and WSS. Despite the inherently complex rheology of blood, the Newtonian approximation becomes increasingly valid at shear rates exceeding approximately 100 s^{-1}, where rouleaux formation is significantly reduced and the apparent viscosity approaches a nearly constant value. Consequently, Poiseuille flow theory can provide reliable estimates of pressure drop and flow characteristics, particularly in microchannels with dimensions much larger than RBCs and at moderate hematocrit levels where confinement effects remain limited. However, the validity of this approximation diminishes at low shear rates, in strongly confined geometries, or in channels containing complex features such as bifurcations, contractions, and expansions. In such cases, RBC aggregation, deformation, migration, and the development of a CFL generate spatial variations in viscosity and non-uniform stress distributions that cannot be adequately described by classical Poiseuille theory [77]. Likewise, when channel dimensions become comparable to the characteristic size of RBCs, individual cell dynamics begin to influence macroscopic flow behavior, limiting the applicability of continuum models based on constant viscosity assumptions. For situations in which hematocrit-dependent rheology and RBC aggregation play a significant role, non-Newtonian continuum models provide a more realistic representation of blood flow. In this continuum-non-Newtonian regime, constitutive relations such as the Casson [78], Carreau-Yasuda [79], Quemada [80], and Cross [81] models are commonly employed to capture the shear-thinning behavior of blood. Accordingly, blood-flow modeling in microfluidic systems can be broadly classified into three regimes. In the continuum-Newtonian regime, blood behaves approximately as a Newtonian fluid, and classical analytical solutions yield reasonable predictions of flow behavior. In the continuum-non-Newtonian regime, shear-dependent constitutive models are required to account for variations in apparent viscosity. Finally, in the cell-resolved regime, where strong confinement and cell-scale interactions dominate, continuum descriptions become insufficient. Under these conditions, particle-based, immersed-boundary, and Fluid-Structure Interaction (FSI) approaches are necessary to accurately capture phenomena such as RBC deformation, cell aggregation, margination, plasma skimming, CFL formation, and microvascular occlusion.

3.3.5. Confinement Effects

Geometric confinement is one of the most influential factors governing microscale blood-flow behavior. When the characteristic channel dimension approaches the size of RBCs (≈8 μm), the flow transitions from a bulk suspension regime to a confined regime in which wall proximity, cell deformability, and hydrodynamic interactions dominate. The degree of confinement is quantified by the confinement ratio χ given by Equation (2) [82]:

$$\chi = \frac{d_{RBC}}{D_{channel}} \quad (2)$$

where d_{RBC} is the effective RBC diameter and $D_{channel}$ is the microchannel hydraulic diameter. As χ approaches one, blood exhibits rheological and transport behaviors that deviate from classical predictions. This definition assumes that RBCs can be represented using an effective characteristic diameter and that the channel cross-section is adequately described by a single hydraulic length scale. While useful for characterizing confinement, the parameter does not account for RBC deformability, orientation, and shape changes during flow, which may become significant under strong confinement conditions. Under strong confinement, the RBCs experience wall-induced lift forces that push them toward the channel centerline, contributing to the formation of a CFL near the walls. The CFL reduces viscosity and is central to the Fåhræus–Lindqvist effect, in which the blood viscosity decreases with decreasing vessel diameter [83]. Confinement also enhances plasma skimming at bifurcations [84], where asymmetric partitioning of RBCs and plasma leads to heterogeneous hematocrit distributions downstream. Recent studies have further demonstrated that the development of the CFL in bifurcating microchannels depends not only on cell deformability but also on the spacing between successive bifurcations. Rashidi et al. [85] showed that insufficient branch length prevents an equilibrium CFL, leading to asymmetric RBC partitioning downstream and altered microvascular transport behavior. The microfluidic systems enable the study of confinement effects because they allow precise control of channel height, width, curvature, and bifurcation geometry, enabling evaluation of how confinement modulates hemorheology. Confinement can be adjusted to probe transitions between tumbling, rolling, swinging, and tank-treading RBC regimes, revealing how cell shape and membrane tension influence flow resistance. Confinement also amplifies non-Newtonian behavior, causing shear thinning at lower shear rates than in bulk flow due to enhanced RBC deformation and rouleaux breakup. A framework in which the rheological state of confined blood can be mapped onto the following interacting parameters is as follows: χ determines the wall-induced lift forces and CFL thickness, shear rate that controls the balance between aggregation, deformation, and alignment, wall proximity (normalized distance) governs hydrodynamic interactions, RBC orientation, and margination dynamics. Within this parameters, distinct rheological regimes emerge: aggregation regime (low shear rate and moderate confinement); rouleaux formation, high viscosity, deformation regime (moderate shear rate and strong confinement); RBC elongation, tank-treading, and viscosity reduction, wall-interaction regime (high χ and near-wall proximity); margination, CFL formation, plasma skimming, and transition regime; mixed behaviors with heterogeneous viscosity. RBCs exhibit geometric focusing, aligning along streamlines in narrow channels, platelets experience enhanced near-wall accumulation, increasing the adhesion probability, and leukocytes display altered rolling velocities due to modified shear gradients. These effects are critical for understanding thrombosis, inflammation, and microvascular occlusion.

3.3.6. Microvascular Replication

PDMS microfluidic devices frequently replicate microvascular branching patterns and dimensions, typically spanning diameters from 5 to 100 μm [85]. These scales correspond to physiological microcirculation, where geometric confinement, bifurcation topology, and

curvature strongly modulate hemodynamics. The design of microchannels is guided by vascular-physiology scaling laws like Murray's law [86], which prescribes optimal branching ratios based on metabolic and hydrodynamic efficiency, and Poiseuille's law [87], which governs laminar flow resistance in cylindrical conduits. These principles allow for the constructing of networks that emulate microvasculature characteristics. Biomimetic geometries enable investigation of flow disturbances arising in curved pathways, bifurcations, and stenoses, which are critical sites for thrombosis, cell adhesion, and pathological flow patterns [88]. Reinhart et al. [89] developed PDMS networks that reproduce physiological bifurcation geometries, incorporating diameter ratios and branching angles derived from Murray's law. Their devices enabled studies of RBC partitioning, plasma skimming, and shear-stress heterogeneity. By varying parent-to-daughter vessel diameters, they quantified how microscale geometry governs hematocrit distribution and downstream oxygen-delivery potential—phenomena that cannot be captured in straight-channel microfluidics. They concluded that curvature and asymmetric bifurcations generate localized shear gradients and flow disturbances that influence endothelial interaction and onset of pathological flow patterns. Reinhart et al. [89] provided understanding of how microvascular architecture modulates microscale blood rheology. Fenech et al. [90] extended this approach by producing biomimetic PDMS networks with physiologically realistic branching ratios, stenotic constrictions, and curved pathways. Their work emphasized how microchannel geometry governs thrombosis initiation, platelet adhesion, and endothelial activation. By integrating stenoses and aneurysmal expansions into microfluidic networks, they recreated the pathological flow environments that mimic the in vivo microcirculation. These models revealed how disturbed flow, particularly at bifurcations and curved segments, creates recirculation zones and low-shear pockets that promote thrombus formation. Pries and Secomb [91] contributed to understanding microvascular geometry, RBC distribution, and plasma skimming as they described how vessel diameter, branching ratios, and network topology determine hematocrit heterogeneity and oxygen delivery. Their analysis of bifurcation hemodynamics, Fåhræus–Lindqvist effects, and cell-free-layer dynamics provided fundaments for interpreting microfluidic experiments. Popel and Johnson [92] emphasized how vessel geometry, branching configuration, and rheological properties interact to produce hemodynamic patterns. They highlighted the importance of curvature, bifurcation asymmetry, and diameter variation in shaping the RBC trajectories, shear-stress distributions, and cell–wall interactions. A framework that maps microvascular behavior onto the following interacting geometric parameters is as follows: diameter ratio (parent/daughter vessels) governs RBC partitioning, hematocrit heterogeneity, and plasma skimming, curvature and tortuosity control secondary flows, recirculation zones, and localized shear-stress pockets. Bifurcation asymmetry determines cell-free-layer redistribution, platelet margination, and endothelial mechanotransduction. PDMS microvascular networks offer capabilities that classical glass-capillary experiments cannot including rapid fabrication of complex, multi-scale vascular networks, control of geometric parameters, high-resolution optical access for PIV/PTV and cell tracking, and integration of pathological geometries (stenoses, aneurysms, tortuous segments). Vortex-based microfluidic architectures have also emerged as attractive platforms for particle and cell manipulation, demonstrating enhanced particle retention and separation performance through controlled recirculating flow structures. Such approaches may be adapted for blood-component sorting, circulating-cell isolation, and diagnostic applications [93]. These features position the PDMS microchannels as synthetic microvasculature, enabling them to isolate geometric effects on hemodynamics, which is something impossible in vivo.

4. PDMS Microfluidic Platforms for Blood-Flow Analysis

PDMS microfluidic platforms are widely used in blood-flow experiments dealing with the different blood-related topics. Figure 3 shows the distribution of literature works on blood-flow investigations.

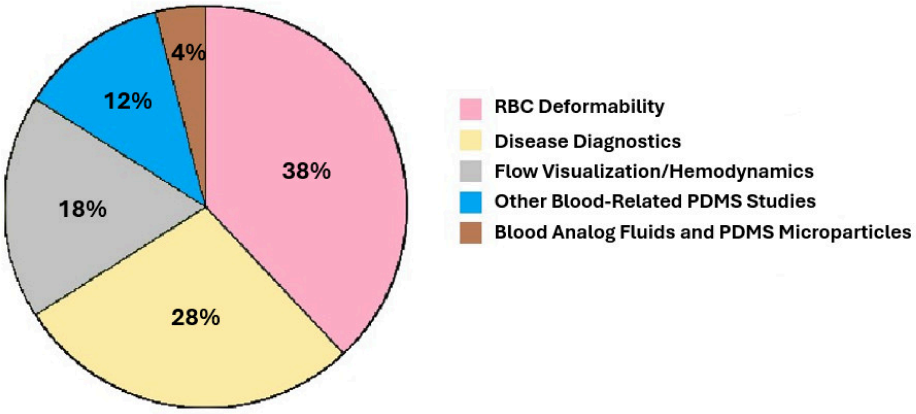

Figure 3. Theme distribution of blood-flow studies with PDMS microfluidics. This distribution is intended as an illustrative summary of the literature discussed in this review and does not represent a bibliometric analysis of all published studies in the field.

4.1. Straight Microchannels

Straight microchannels represent the foundational geometry in PDMS microfluidic platforms and serve for evaluating blood-flow behavior under controlled hydrodynamic conditions. Their simpleness enables regulation of channel dimensions, velocity fields, and shear-rate distributions, making them ideal for studying the hemodynamic phenomena that govern microcirculatory function [94].

4.1.1. RBC Deformability

RBC deformability is a determinant of microvascular perfusion, as erythrocytes must undergo substantial shape changes to traverse capillaries with diameters comparable to or smaller than their resting size [95]. Straight PDMS microchannels allow to impose shear stresses and confinement conditions, enabling the assessment of RBC elongation, membrane elasticity, and transit time [96]. These platforms enable the study of pathological states like sickle-cell disease and hereditary membrane disorders [97]. By tuning channel dimensions, straight microchannels mimic capillary-like constrictions, revealing how the altered deformability contributes to microvascular occlusion, impaired tissue perfusion, and abnormal flow resistance.

4.1.2. Plasma Skimming

Plasma skimming refers to the preferential partitioning of plasma and RBCs at microvascular bifurcations and flow-splitting geometries [98–100]. Due to the presence of a CFL adjacent to the channel walls, branches receiving a smaller fraction of the total flow tend to be enriched in plasma and depleted of RBCs, resulting in a reduced local hematocrit. Therefore, plasma skimming is fundamentally associated with channel bifurcations rather than straight microchannels. Nevertheless, phenomena occurring in straight channels, including RBC migration toward the channel centerline and the consequent formation of a CFL, provide the necessary preconditioning that enables plasma skimming when the flow subsequently encounters a bifurcation. In contrast, RBC margination, CFL formation, and platelet accumulation can be directly observed in straight microchannels. CFL formation

results from hydrodynamic lift forces and cell–cell interactions that drive deformable RBCs away from the walls. This redistribution of RBCs creates a near-wall region with reduced cell concentration. Platelets, owing to their smaller size and reduced deformability, can subsequently become enriched within this region, a phenomenon commonly referred to as platelet margination. Indeed, the platelet enrichment in the near-wall region has been experimentally observed in numerous microfluidic studies. This behavior is generally attributed to a combination of RBC-induced collisions, hydrodynamic interactions, and deformability-related migration mechanisms. While these processes are well established experimentally, the precise relative contributions of hydrodynamic interactions, collisions, cell deformability, and confinement effects remain active areas of investigation. Figure 4 shows a microsystem for plasma separation.

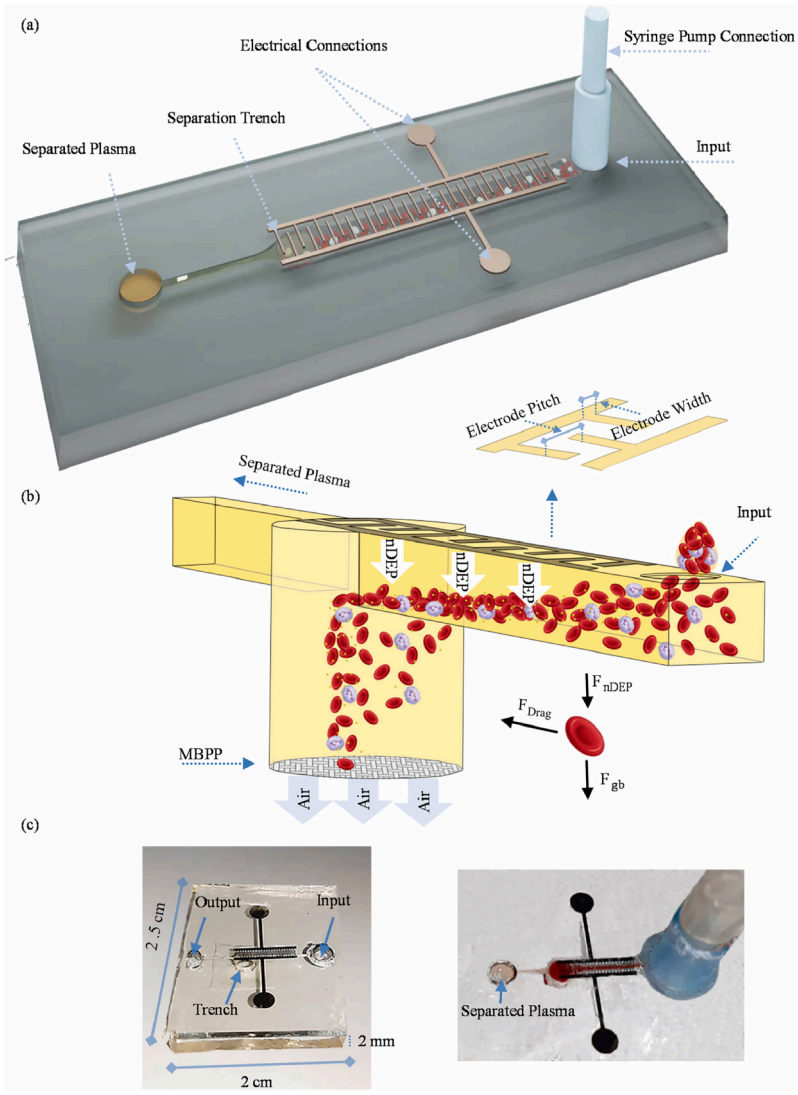

Figure 4. Microsystem for plasma separation: (**a**) different parts of the system, (**b**) electrodes and forces applied to blood cells inside the microsystem. The cells are deflected to the bottom of the channel by negative dielectrophoresis force and then directed into the separation trench sealed by the melt-blown polypropylene porous layer, and (**c**) microsystem for plasma separation [101].

Figure 5 shows a PDMS microchannel device assembled on a glass slide and a lead zirconate titanate (PZT) disk for blood plasma separation and fluorescence detection of biomarkers using acoustic microstreaming.

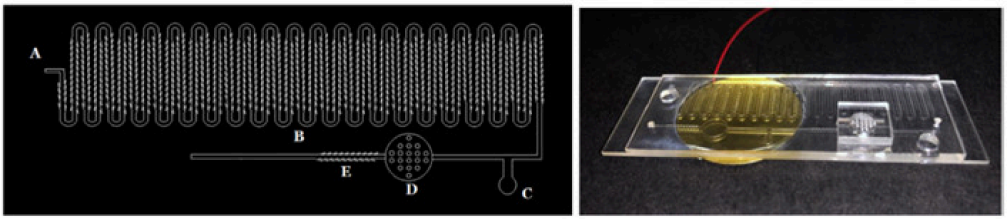

Figure 5. (**a**) PDMS microchanneled device: A—Inlet 1, B—Plasma separation microchannel with 40 serpentine turns, C—Inlet 2, D—Acoustic mixing chamber, and E—Detection channel and (**b**) device assembled on a glass slide of 75 mm × 25 mm and on a PZT disk (yellow circle) glued on the glass slide back [102].

4.1.3. Cell Margination

Cell margination—the lateral migration of blood cells toward or away from microchannel walls—plays a pivotal role in immune surveillance, platelet adhesion, and inflammation [103]. Straight PDMS microchannels enable to analyze margination dynamics by providing uniform shear fields and boundary conditions. These systems reveal how the RBC deformability, channel size, and flow velocity influence the segregation of leukocytes and platelets toward the vessel periphery [104]. Also, the PDMS devices incorporate endothelial layers and coatings to evaluate how wall interactions regulate margination [105]. Such studies understand pathological conditions in which margination is altered, including sepsis, thrombosis, and cardiovascular disease. Table 7 summarizes the PDMS straight microchannel vascular models.

Table 7. PDMS straight microchannel vascular models.

Type of Device	Applications	Studied Parameters	Benefits	Limitations	References
Simple Rectangular Straight Microchannels	Shear-stress mechanobiology Endothelial alignment	WSS Endothelial morphology Cell elongation	Controlled shear environment Mechanotransduction	Oversimplified geometry PDMS stiffness not physiological	[106]
Straight Microchannels with Variable Height/Width	Hemodynamics RBC deformability	RBC transit time Deformation index	Tuning of microvascular-like confinement Sickle-cell and malaria	PDMS swelling alters dimensions Limited 3D confinement realism	[107]
Endothelialized Straight Channels	Barrier function, inflammation Leukocyte adhesion	Permeability Leukocyte rolling/adhesion	Mimics vascular endothelium Immune-cell interaction	Endothelial phenotype drifts over time Requires careful coating	[108]
Straight Channels with Embedded Sensors	Real-time blood analysis Coagulation monitoring	Optical absorbance Clot formation kinetics	Continuous monitoring Integrates sensing and flow	Sensor integration increases complexity PDMS absorbs hydrophobic molecules	[109]
High-Shear Straight Channels	Platelet activation Thrombosis	Shear-induced activation Clot growth rate	Recreating arterial shear Antithrombotic drug testing	PDMS is non-thrombogenic unless coated Limited biochemical complexity	[110]

Table 7. *Cont.*

Type of Device	Applications	Studied Parameters	Benefits	Limitations	References
Low-Shear Straight Channels	Venous thrombosis Leukocyte behavior	Rolling velocity Adhesion strength	Venous inflammation Stable low-shear environment	Hard to mimic venous valve dynamics Limited oxygen gradients	[111]
Straight Microchannels with Porous Walls	Transendothelial migration Nutrient transport	Cell transmigration Barrier disruption	Controlled molecular exchange Immune-cell migration studies	Complex porous PDMS fabrication Pore size uniformity difficult	[112]
Straight Channels with Surface Patterning	Endothelial mechanosensing Endothelial Cell alignment	Cytoskeletal organization Focal adhesion formation Flow-topography coupling	Enhances physiological relevance Topographical cues studies	Pattern fidelity degrades with use Hard to mimic natural basement membrane	[113]
Straight Microchannels for Drug Perfusion Studies	Pharmacokinetics Endothelial drug response	Drug uptake Barrier permeability changes Cytotoxicity	Low reagent consumption Controlled exposure profiles	PDMS absorbs many drugs Surface treatments to reduce adsorption	[114]
Straight Microchannels for RBC/Platelet Mechanics	Hemorheology Vascular Occlusion	Deformability Aggregation Flow resistance	Single-cell biomechanics High-speed imaging	2D confinement limits physiological accuracy No active vessel contraction	[115]

4.2. Biomimetic Vascular Networks

Biomimetic vascular networks represent a breakthrough in PDMS microfluidics, enabling the recreation of microenvironments that capture the hemodynamic diversity of microcirculation. These platforms extend beyond straight channels by incorporating branching patterns, constrictions, curvature, and living endothelial layers. As a result, they enable the study of blood flow in conditions that resemble the in vivo physiology [116].

4.2.1. Capillary-like Networks

Capillary-like microfluidic networks are designed to emulate the dense, interconnected architecture of the microcirculation, where vessel diameters typically range from 5 to 10 µm. PDMS microfabrication enables precise control over channel dimensions, spacing, and branching topology, allowing for the creation of networks that mimic capillary beds, reticular structures, and tortuous microvascular pathways [117]. These systems support investigations of RBC transit, deformability, oxygen transport, and microvascular resistance under physiologically relevant confinement. Because the RBCs must deform to traverse capillary-scale channels, capillary-like networks provide a platform for quantifying transit time, shape transitions, membrane tension, and flow-induced deformation modes. Their optical transparency allows for high-resolution imaging of cell–cell and cell–wall interactions within geometries that approximate in vivo environment. These networks can study pathological microcirculatory dysfunction, including impaired perfusion in diabetes, malaria-induced sequestration, and sickle-cell-related vaso-occlusion [118]. Capillary-like networks reveal physics that emerge only under extreme confinement and controlled microvascular geometries. A capillary flow framework that maps microcirculatory behavior onto the following interacting parameters is as follows: confinement ratio ($\chi = d_{RBC}/D_{channel}$) governs RBC deformation, CFL thickness, and viscosity, branching density controls hematocrit redistribution, plasma skimming, and oxygen-delivery heterogeneity, tortuosity and curvature modulate secondary flows, recirculation zones, and shear-stress pockets. This framework enables interpretation of microfluidic blood-flow research, enabling the predicting of how

capillary geometry modulates rheology, transport, and cell biomechanics. The capillary PDMS networks offer capabilities that classical glass-capillary experiments cannot like rapid fabrication of multi-scale vascular networks, control of geometric parameters, optical access for PIV/PTV and cell-tracking, and integration of pathological geometries. These features enable PDMS capillary networks to isolate geometric effects on hemodynamics, which is something impossible in vivo. The microfluidic studies have revealed that capillary geometry induces rheological bifurcations, where small changes in diameter and curvature produce abrupt transitions in viscosity, RBC orientation, CFL thickness, and endothelial mechanotransduction. Figure 6 shows a capillary-driven device using surfactant-added poly(dimethylsiloxane) for plasma extraction.

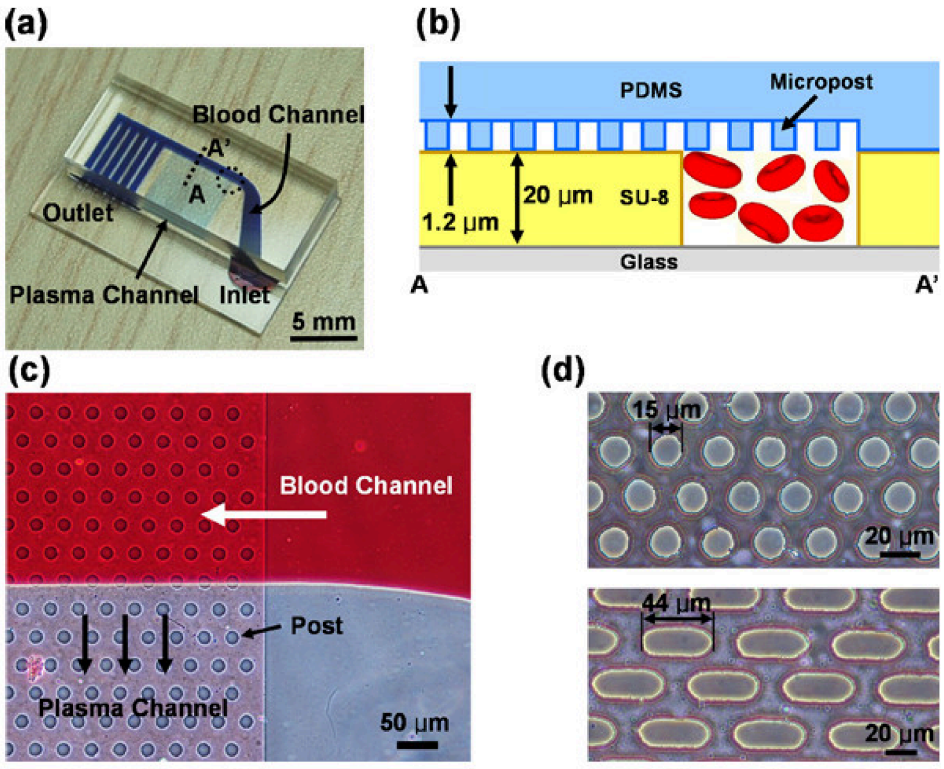

Figure 6. (**a**) Photograph of the device; (**b**) cross-section between blood and plasma channels; (**c**) micrograph of the device (dotted circle in panel (**a**)); (**d**) two types of post shapes used in the plasma channel (top: circular, bottom: ellipsoidal) [119].

4.2.2. Bifurcations, Stenoses, and Aneurysm Models

PDMS microfluidics can replicate vascular geometries that correspond to the most hemodynamically disturbed regions of microcirculation, including bifurcations, stenotic segments, and aneurysmal expansions [120]. These geometries are central to understanding how structural abnormalities modulate blood-flow physics, cellular transport, and vascular pathology. Also, the bifurcations are sites where the blood-flow partitioning, plasma skimming, and cell distribution occur—phenomena essential for microvascular hematocrit regulation and leukocyte trafficking [121]. The PDMS bifurcation models allow for the investigation of RBC partitioning driven by asymmetric shear fields, plasma skimming governed by daughter-branch diameter ratios, cell-free-layer redistribution at branching points, and leukocyte and platelet margination influenced by bifurcation geometry. These models provide environments for quantifying how branching angle, diameter ratio, and flow asymmetry shape the microvascular transport. Stenotic microchannels recreate narrowed vessel segments that generate elevated shear stress and disturbed flow patterns [122]. These

models reveal high-shear zones that promote platelet activation, flow separation regions that enhance thrombus nucleation, and RBC deformation and orientation changes under shear. Stenosis models allow to study atherosclerotic hemodynamics, where shear-stress gradients and recirculation zones drive endothelial dysfunction and plaque progression. Aneurysm-like expansions produce regions of recirculation, vortex formation, and low shear [123]. PDMS aneurysm models enable the investigation of vortex dynamics and flow instability in low-shear pockets, clot initiation driven by prolonged residence time, endothelial mechanotransduction failure in disturbed flow, and platelet aggregation in recirculation zones. Studies performed in simplified aneurysm geometries have shown that vascular cavities generate complex recirculation zones, secondary flows, and transient vortical structures, emphasizing the importance of accurately reproducing physiological geometries when investigating blood-flow dynamics in microfluidic platforms [124].

4.2.3. Endothelialized PDMS Channels

Endothelialized microfluidic channels represent a step toward physiological relevance by incorporating living endothelial cells along the channel walls. The gas permeability and optical transparency of PDMS make it suitable for supporting endothelial monolayers under controlled shear stress [125]. These systems reproduce vascular biology, including barrier function, mechanotransduction, and inflammatory signaling [126]. Endothelialized channels enable studies of leukocyte rolling and adhesion, leukocyte–endothelium interactions, and impact of biochemical gradients on vascular behavior [127]. They also serve as components of organ-on-chip and vascular-on-chip platforms, where endothelial function is integrated with other tissue types to model disease processes and drug responses [127]. Endothelialized PDMS channels allow for the construction of mechanotransduction maps linking shear stress and biochemical environment to endothelial responses including cytoskeletal remodeling, junctional integrity, and inflammatory activation. The endothelialized PDMS channels offer shear-stress control for mechanobiology studies, integration with immune cells for leukocyte-adhesion assays, compatibility with biochemical gradients for inflammation modeling, and rapid prototyping of disease-specific geometries (stenosis, aneurysm, and bifurcation). Table 8 summarizes the PDMS biomimetic vascular network devices.

Table 8. PDMS biomimetic vascular network devices.

Type of Device	Applications	Studied Parameters	Benefits	Limitations	References
Straight Microchannel Vascular Models	Shear-stress and flow studies Endothelial biology	WSS Endothelial alignment	Controlled flow Simple fabrication	Limited physiological realism No branching or curvature	[128]
Branched/Bifurcating Vascular Networks	Hemodynamics Atherosclerosis	Platelet adhesion Local shear gradients	Mimics arterial bifurcations Disturbed flow studies	PDMS stiffness not fully physiological Limited 3D geometry	[129]
Tortuosity/Curved Vessel Models	Aging vasculature Tumor vasculature	RBC deformation Flow resistance	Pathological vessel shapes Cancer microcirculation studies	Hard to reproduce complex 3D tortuosity PDMS swelling affects geometry	[130]
Microvascular Capillary-Like Networks	Microcirculation Oxygen transport	RBC transit time Capillary occlusion	Mimic capillary beds Single-cell flow	Often 2D Limited extracellular matrix integration	[131]

Table 8. *Cont.*

Type of Device	Applications	Studied Parameters	Benefits	Limitations	References
Endothelialized Vascular Networks	Barrier function Inflammation	Leukocyte adhesion Transendothelial migration	Physiologically relevant barrier Immune-cell interaction	Endothelial phenotype drifts over time Complex cell culture	[132]
Vascular Networks with Embedded ECM	Angiogenesis Thrombosis	ECM remodeling Cell–matrix interactions	Realistic microenvironment 3D cell migration	Complex fabrication Hydrogel stability varies	[133]
Stenosis/Constriction Models	Atherosclerosis Thrombosis Embolism	Shear gradients Clot formation dynamics	High-risk vascular geometries Drug testing	PDMS is non-thrombogenic unless coated Limited biochemical complexity	[134]
Aneurysm-Mimicking PDMS Models	Cerebrovascular research Rupture risk	WSS oscillations Flow vortices	Aneurysm hemodynamics studies Device testing	PDMS elasticity differs from real vessels No active smooth muscle	[135]
Vascular Networks with Perivascular Cells	Vessel maturation Vascular remodeling	Contractility Barrier reinforcement	More complete vessel physiology Vasoconstriction studies	Co-culture stability is challenging Limited long-term viability	[136]
Tumor-Vasculature-on-Chip	Cancer metastasis Drug penetration	Tumor-endothelial interactions Permeability changes	Mimics leaky tumor vessels Anti-angiogenic drug testing	Tumor heterogeneity difficult to reproduce PDMS absorbs hydrophobic drugs	[137]
Thrombosis-on-Chip Vascular Networks	Platelet function Coagulation Antithrombotic drug screening	Clot growth rate Fibrin formation	Flow and shear control	Thrombosis-on-Chip Vascular Networks	[138]

4.3. Specialized Devices

Specialized PDMS microfluidic devices broaden the analytical capabilities of blood-flow research by enabling controlled compartmentalization, precise rheological measurements, selective cell manipulation, and high-throughput single-cell analysis [139]. These platforms exploit geometric flexibility, optical accessibility, and rapid prototyping of PDMS to incorporate complex flow fields and multiphase interfaces, extending beyond conventional straight-channel assays. Although the microfluidic techniques discussed in this section can be implemented using a variety of materials, including glass, silicon, PMMA, cyclic olefin copolymers (COC), and other thermoplastics, many reported blood-flow studies employ PDMS because of its optical transparency, ease of fabrication through soft lithography, gas permeability, and rapid prototyping capability. Nevertheless, the performance of these platforms often depends on the underlying microfluidic design rather than exclusively on PDMS as the structural material. Therefore, throughout this section, emphasis is placed on studies that utilize PDMS devices while also acknowledging that equivalent approaches may be implemented using alternative materials. Figure 7 presents a wrist-wearable blood-flow meter by biomimetically structured conductive PDMS composite.

Specialized PDMS devices are designed to isolate the physical mechanisms like shear-rate gradients, and confinement transitions, making them very suitable for studying fluid-mechanical phenomena in blood. They enable controlled perturbations (oscillatory shear, pulsatile flow), localized confinement transitions (sudden expansions, contractions, nozzles), precise multiphase interfaces (droplet formation, plasma–cell separation), single-cell hydrodynamic manipulation (trapping, sorting, deformation), and integrated rheometry (pressure-drop measurement, viscosity, viscoelastic response).

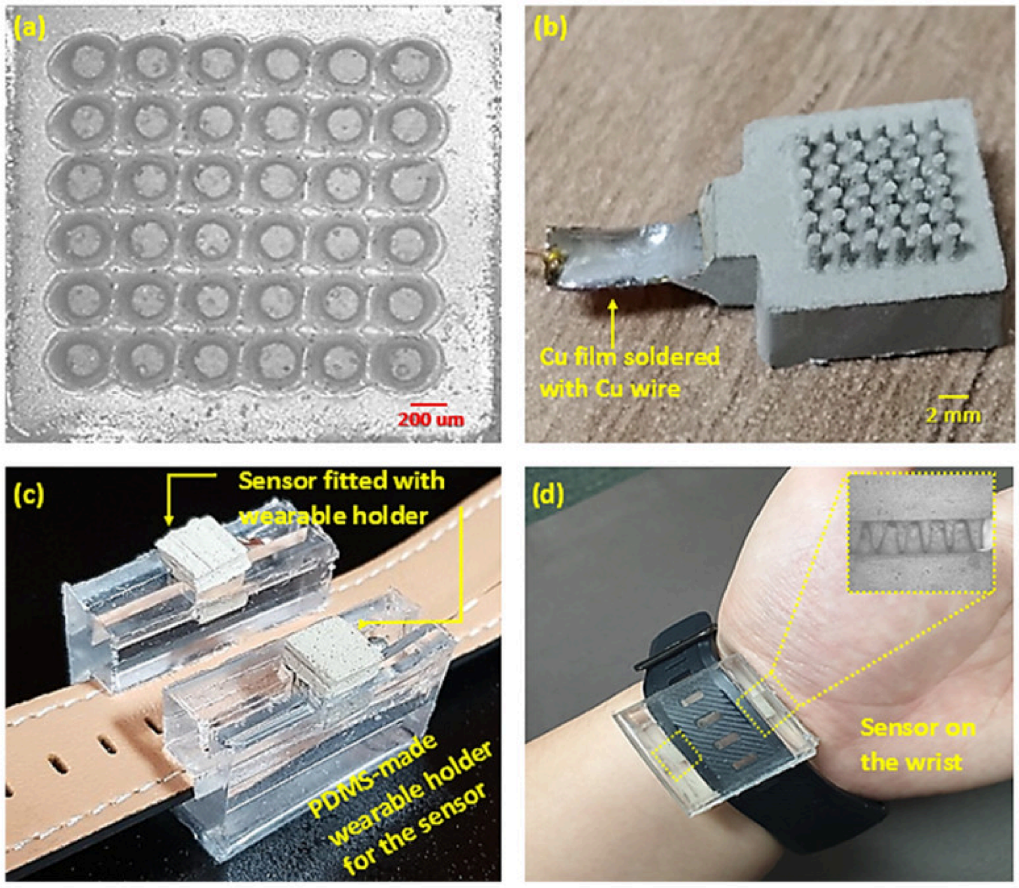

Figure 7. PDMS wrist pulse sensor: (**a**) microscopic top view, and (**b**) side view of the biomimetic sensor layers. Fixation mechanism of the double-layered sensor with (**c**) PDMS wearable holder, and (**d**) watch band. Two sensors were fixed with the wristband to detect pulse signals at different places on the wrist. The wrist-mounted, double-layered sensor is shown inset [140].

4.3.1. Droplet-Based Blood Assays

Droplet microfluidics use immiscible fluids to generate discrete picoliter-to-nanoliter droplets that act as isolated reaction chambers. Numerous droplet-based blood assays have been implemented in PDMS microfluidic devices owing to the ease with which complex flow-focusing and T-junction geometries [141] can be fabricated using soft lithography. The optical transparency of PDMS additionally facilitates real-time imaging of droplet formation and blood-cell behavior. However, droplet microfluidics is not inherently dependent on PDMS and is increasingly being implemented in thermoplastic and glass devices for commercial and large-scale production. In blood analysis, droplet systems enable encapsulation of individual cells, plasma fractions, and biochemical reagents, allowing the screening of cellular responses, enzyme activities, and biomarker concentrations [142]. The compartmentalization inherent to droplet microfluidics [143] reduces cross-contamination and reagent consumption, making it ideal for single-cell assays, and rare-cell detection [144]. PDMS droplet platforms also support studies of cell heterogeneity, immune activation, and drug response at unmatched resolution [145]. Droplet-based systems examine blood flow at liquid–liquid interfaces like RBC deformation inside confined droplets and plasma–cell partitioning under multiphase shear. Biomarker detection can be also found by using PDMS devices like the one in Figure 8, which shows PDMS porous microneedles used in microfluidic devices for biomarker detection.

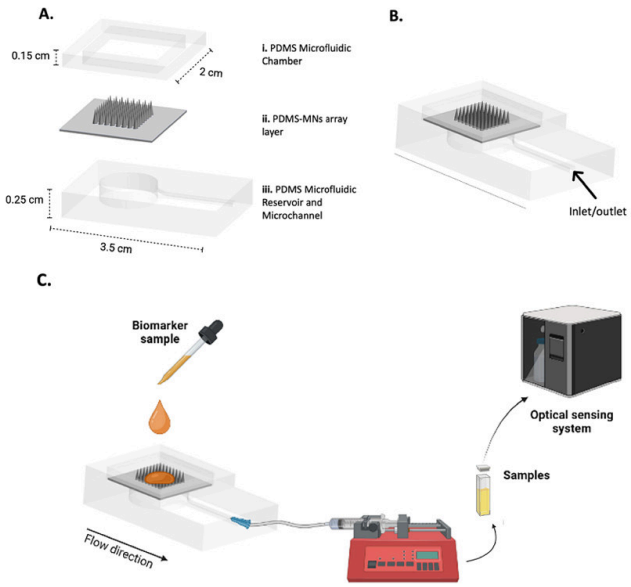

Figure 8. PDMS microfluidic device: (**A**) device prototype layers: i. PDMS chamber, ii. PDMS-microneedles array layer, iii. PDMS chamber and microchannel, (**B**) bonded layers, and (**C**) setup for collection and detection of albumin concentration [146].

The compartmentalization inherent to droplet microfluidics minimizes the cross-contamination and reduces reagent consumption, making it ideal for single-cell assays, digital PCR, and rare-cell detection [147]. PDMS platforms also support studies of cell heterogeneity, immune activation, and drug response with elevated resolution [148]. Figure 9 shows a size-adjustable PDMS droplet microfluidic system using an on-chip microfluidic peristaltic pump.

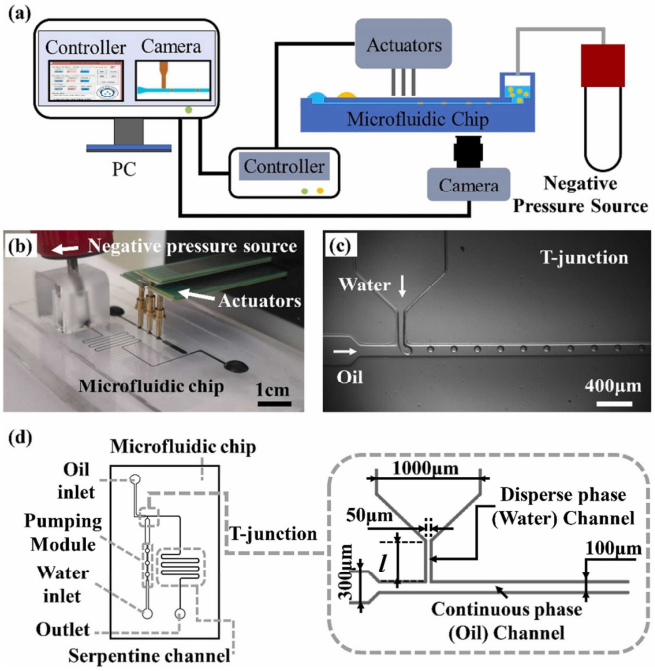

Figure 9. (**a**) Setup for size-tunable droplet generation: control system, microfluidic chip, actuators to compose the peristaltic micropump with part of the chip, charge coupled device monitor system and negative pressure source, (**b**) droplet microfluidic system (**c**) droplet generation on the chip, (**d**) design of the chip-oil inlet, water inlet and one outlet on the chip. The micropump controlled the water flowing, and the T-junction structure generated the droplets [149].

4.3.2. Microfluidic Viscometers

Microfluidic viscometers exploit laminar flow in PDMS channels to measure rheological properties of blood and plasma. Common designs include constriction–expansion geometries, parallel-channel configurations, and co-flow systems that compare the sample flow to a reference fluid [150]. Because blood exhibits shear thinning and non-Newtonian behavior, microfluidic viscometers allow for the characterization of viscosity across different shear rates using minimal sample volumes. These devices are valuable for studying disease-related changes in blood rheology, including increased viscosity in diabetes, inflammation, and hypercoagulable states [150]. Microfluidic viscometers enable rheological characterization under confinement, revealing viscosity and deformation transitions that cannot be captured in bulk rheometers. PDMS-based viscometers benefit from rapid prototyping and straightforward integration of pressure sensors and optical measurement systems. Nevertheless, because PDMS is mechanically compliant, channel deformation may alter hydraulic resistance and introduce measurement uncertainties. For this reason, glass and rigid thermoplastic devices are frequently preferred when highly accurate quantitative viscosity measurements are required.

4.3.3. Cell-Sorting and Separation Devices

PDMS microfluidic systems support a wide range of passive and active cell-sorting strategies that leverage differences in cell size, deformability, density, and hydrodynamic behavior [151]. These platforms exploit fluid mechanics to achieve label-free separation. Passive methods—including deterministic lateral displacement (DLD), inertial focusing, and pinched-flow fractionation—use channel geometry and intrinsic flow patterns to separate cells without external actuation. DLD is versatile due to its high resolution, throughput, and size selectivity. In DLD devices, a staggered array of micropillars separates particles based on a critical diameter: particles smaller than this threshold follow the main flow, while larger particles undergo lateral displacement. Studies have examined factors influencing DLD performance. Zhang et al. [151] showed that micropillar shape determines local velocity distribution, while gap size and array period define the critical-radius bandwidth. They proposed an expression for critical radius for various pillar geometries. Subsequent works explored I-shaped [152], L-shaped [153], and diamond-inspired pillar configurations [154,155] that mitigate clogging and improve separation. Most numerical studies treat particles as point masses, neglecting fluid–particle coupling. Exceptions include Chen et al. [156] and Zhang et al. [151], who incorporated bidirectional coupling, finite-size particles, deformability, and full 3D simulations. Inertial focusing relies on size-dependent inertial forces acting on suspended particles, as explored by Qian et al. [157]. Within confined microchannels, the interplay between inertial and viscous forces drives particles toward distinct equilibrium positions. Channel geometry and particle dimensions influence migration, producing lateral focusing in straight channels [158,159], Dean-flow-induced secondary motion in spiral and serpentine channels [160,161]. Spiral inertial devices require additional computational and experimental work to clarify how channel dimensions, cell type, and cross-sectional morphology govern focusing efficiency. These methods are suitable for isolating circulating tumor cells [162,163] and separating plasma from whole blood [164]. Active sorting applies external fields—including dielectrophoresis, magnetophoresis, and acoustophoresis—to achieve higher precision and selectivity. PDMS is compatible with embedded electrodes, magnetic elements, and acoustic transducers, enabling multifunctional separation platforms for clinical applications [165]. Acoustophoresis uses ultrasound waves to exert forces dependent on particle size, density, and deformability [166]. Recovery rates of 83% for circulating tumor cells at throughputs of 10^3 cells have been reported [167]. Dielectrophoresis manipulates cells according to dielectric properties

under non-uniform electric fields. Collection efficiencies up to 92% (human mesenchymal stem cells) and 67% (osteoblasts), with purities up to 84% and 87%, have been demonstrated [168]. Magnetophoresis uses magnetic fields to separate magnetically labeled or intrinsically magnetic cells. Applications include removal of malaria-infected cells [169] and label-free separation of RBCs and White Blood Cells (WBCs) based on magnetic susceptibility [170]. PDMS has been widely used for proof-of-concept cell-sorting devices because it enables the rapid fabrication of intricate channel architectures and integration of pneumatic control elements. However, the cell-sorting mechanisms themselves, whether based on size, deformability, inertial effects, and hydrodynamic interactions, are generally independent of the substrate material and can be implemented in alternative microfabrication platforms.

4.3.4. Microfluidic Flow Cytometry

Microfluidic flow cytometry miniaturizes the principles of conventional flow cytometry into PDMS platforms offering reduced sample consumption and seamless integration with upstream modules [171]. These systems rely on hydrodynamic focusing to align cells into a single-file stream, enabling optical interrogation as individual cells pass through a detection region. Microfluidic flow-cytometry platforms are frequently fabricated from PDMS because its optical transparency facilitates high-sensitivity fluorescence detection, while its fabrication flexibility allows the incorporation of waveguides, microlenses, and photodetectors [172]. This integration transforms PDMS devices into cytometry platforms for point-of-care diagnostics, analyzing small sample volumes, and combining cell sorting and analysis within a single device [173]. Nevertheless, the underlying hydrodynamic focusing and detection principles are not unique to PDMS, and commercial systems increasingly employ thermoplastic materials that offer improved manufacturability and long-term stability. Microfluidic flow cytometry is governed by viscous forces, channel geometry, and particle–fluid interactions. Hydrodynamic focusing generates a stable core stream by balancing sheath-flow momentum with sample-flow inertia. This controlled flow enables interrogation of cell deformability, morphology, and mechanical properties by coupling optical detection with microchannel-induced deformation. As cells traverse constrictions and extensional-flow regions, their shape changes encode information about membrane elasticity, cytoskeletal integrity, and pathological stiffening. Microfluidic flow cytometry introduces capabilities that conventional cytometers cannot achieve like geometry-induced biomechanical interrogation, constrictions, nozzles, and tapered channels generate deformation modes linked to disease states, sheath-flow-controlled velocity fields as precise velocity regulation allows mapping of cell transit time, rotational dynamics, and orientation under laminar flow, and integration with upstream sorting modules PDMS devices can combine DLD sorting, inertial focusing, or acoustophoresis with downstream cytometric analysis. By integrating deformation zones with optical interrogation, the PDMS cytometers enable high-throughput cytometry, where each cell mechanical response is quantified at kilohertz rates. This provides stiffness-based classification of RBCs, deformability identification of leukocyte activation, and screening of drug-induced mechanical changes. Table 9 summarizes specialized PDMS microfluidic devices.

Table 9. Specialized PDMS microfluidic devices for blood-flow applications.

Type of Device	Manufacturing Complexity	Benefits	Limitations	Applications	References
Droplet-Based Blood Assay Chips	Moderate–High	Enables compartmentalized reactions Low reagent consumption	Surfactant compatibility issues Droplet stability sensitive to flow fluctuations	Digital PCR Single-cell assays Immunoassays	[174]
Viscometers	Low–Moderate	Viscosity measurement Whole blood rheology	Sensitive to temperature PDMS absorption affects the analytes	Hemorheology anemia screening Coagulation monitoring	[175]
Cell Sorting and Separation	Moderate–High	Label-free separation Gentle on cells	Fabrication precision Clogging with whole blood	CTC isolation WBC/RBC separation Platelet enrichment	[176]
Flow Cytometry Chips	High	Portable cytometry Fluorescence detection	Lower sensitivity than benchtop cytometers Complex fabrication	Point-of-care cytometry Blood cell counting	[177]
Blood Plasma Separation Chips	Low–Moderate	Rapid plasma extraction No centrifuge	Filter clogging Limited throughput	Point-of-care diagnostics Biomarker detection	[178]
Microfluidic Coagulation Chips	Moderate	Rapid coagulation testing Portable and low-volume	Sensitive to temperature and surface chemistry	Anticoagulation monitoring Emergency diagnostics	[179]
Organ-on-Chip Blood-Flow Models	High	Physiologically relevant flow Enables endothelial studies	Expensive and labor intensive Cell culture expertise	Drug testing Thrombosis research	[180]
Shear-Stress Controlled Microchannels	Low–Moderate	Shear stress control Blood cell mechanics	Limited to simple geometries	RBC deformability Point-of-care diagnostics	[181]
Microfluidic Immunoassay	Moderate–High	High specificity Captures rare cells	Surface fouling Antibody coating	Cancer diagnostics Rare-cell isolation	[182]
Acoustic Blood Cell Manipulation Chips	High	Label-free, gentle manipulation Continuous separation	Complex fabrication Requires external electronics	Cell sorting Plasma separation	[183]

5. Biological and Biophysical Studies

5.1. Red Blood Cell Mechanics

RBC mechanics play a central role in determining microvascular perfusion, oxygen delivery, and overall hemodynamic function [184]. The PDMS microfluidic platforms give conditioning for examining the RBC behavior at single-cell and population levels, enabling the analysis of deformability, aggregation, and pathological mechanical alterations [185].

5.1.1. Deformability

RBC deformability is a multifactorial mechanical and biochemical phenomenon governed by membrane viscoelasticity, cytoskeletal architecture, intracellular viscosity, and surrounding hydrodynamics. The biconcave RBC shape is maintained by a composite membrane consisting of a lipid bilayer coupled to a spectrin–actin cytoskeleton, providing shear elasticity, bending resistance, and the ability to undergo large deformations without rupture. The local shear rate on an RBC is given by Equation (3) [77]:

$$\dot{\gamma} = \frac{du}{dy} \quad (3)$$

RBC deformation is quantified using the Deformation Index (DI) expressed by Equation (4) [77]:

$$DI = \frac{L - W}{L + W} \tag{4}$$

where L and W are the major and minor axes of the deformed cell. Higher DI values indicate greater elongation. The membrane shear modulus G_s and bending modulus k_b govern resistance to deformation given by Equation (5) [77]:

$$\sigma_{mem} = G_s\,\epsilon + k_b\,\nabla^2\theta \tag{5}$$

where ε is the membrane strain and θ is the curvature. Intracellular viscosity μ_{int} modulates tank-treading frequency according to $f_{tt} \propto \frac{\tau}{\mu_{int}}$. Depending on viscosity ratio, membrane elasticity, and confinement, RBCs exhibit tumbling, swinging, full and intermittent tank treading, and different shapes. In confined microchannels approaching capillary dimensions, RBCs display deformation modes driven by wall interactions, lubrication forces, and entrance effects, often flattening or folding in ways not observed in bulk shear flow. PDMS microchannels enable the construction of a deformation phase map linking shear rate $\dot{\gamma}$, confinement ratio $\chi = d_{\text{RBC}}/D_{\text{channel}}$, viscosity ratio $\lambda = \mu_{\text{int}}/\mu_{\text{ext}}$, and membrane shear modulus G_s, to distinguish the deformation regimes. This provides a framework for predicting perfusion failure in sickle-cell anemia, malaria, diabetes, and hereditary membrane disorders.

5.1.2. Aggregation and Rouleaux Formation

RBC aggregation, including rouleaux formation, influences blood viscosity and microvascular resistance at low shear rates [186]. The PDMS microfluidic systems provide stable laminar flows in which shear rate, hematocrit, and plasma protein composition are controlled [187]. These platforms allow real-time observation of rouleaux formation, breakup, and reformation under varying hemodynamic conditions [188]. Aggregation occurs when adhesive forces exceed hydrodynamic disruptive forces, the latter given by Equation (6) [189]:

$$\mathrm{F_{hyd}} \approx 6\pi\mu a^2\dot{\gamma} \tag{6}$$

With α, the characteristic RBC radius. Microfluidic studies often quantify aggregation using Equation (7) [190]:

$$AG = \frac{I_{agg} - I_{base}}{I_{base}} \tag{7}$$

where I_{agg} is the optical intensity during aggregation and $\mathrm{I_{base}}$ is the baseline intensity. At low shear rates, rouleaux formation increases apparent viscosity given by Equation (8) [191]:

$$\mu_{app} = \mu_{plasma}(1 + k\,H_t\,A) \tag{8}$$

where H_t is hematocrit and A is aggregation strength. As shear increases, rouleaux break apart, reducing viscosity. PDMS channels allow for the measurement of aggregation kinetics using Equation (9) [192]:

$$\frac{dA}{dt} = k_{form} - k_{break}\dot{\gamma} \tag{9}$$

revealing how plasma proteins (fibrinogen, immunoglobulins), hematocrit, and confinement determine aggregation dynamics. The microfluidic aggregation studies are essential for understanding inflammatory diseases, hyperfibrinogenemia, and sepsis-induced rheological changes.

5.1.3. Pathological RBC Behavior

PDMS microfluidic platforms have become indispensable for studying pathological RBC mechanics in diseases where cell deformability, morphology, and membrane integrity are altered [193]. These systems impose shear stresses, confinement, and oxygen tension, enabling the analysis of how diseased RBCs disrupt microvascular perfusion. In sickle-cell disease, hemoglobin S polymerizes under low oxygen tension, producing rigid RBCs that obstruct microvessels and trigger vaso-occlusive crises [194]. PDMS channels with capillary dimensions and stenotic geometries allow for the observation of sickled RBC transit time, occlusion dynamics, jamming transitions, adhesion to endothelial layers, and oxygen-dependent shape transitions [195]. The resistance of sickled RBCs can be expressed through an elevated effective shear modulus G_s^{SCD}, which increases the critical shear stress required for deformation given by Equation (10) [196]:

$$\tau_{crit}^{SCD} = G_s^{SCD}\,\epsilon_{yield} \tag{10}$$

Malaria-infected RBCs (iRBCs) exhibit increased stiffness due to parasite-induced cytoskeletal remodeling and cytoadherence [197]. The PDMS microchannels enable quantification of increased membrane shear modulus, reduced Deformation Index (DI), and adhesion to endothelialized surfaces. The deformability reduction is given by Equation (11) [95]:

$$DI_{iRBC} = \frac{L - W}{L + W} \tag{11}$$

and the increased membrane tension T_{mem} can be modeled by Equation (12) [198]:

$$T_{mem}^{iRBC} = T_0 + \Delta T_{parasite} \tag{12}$$

PDMS microfluidics have also been applied to RBCs affected by hereditary spherocytosis, elliptocytosis, diabetes-induced stiffening, and enzymatic deficiencies. These conditions alter intracellular viscosity μ_{int}, membrane elasticity, and cytoskeletal stability. The increased intracellular viscosity reduces the tank-treading frequency. PDMS platforms reveal new physics of pathological occlusion that are not captured in bulk rheology:

1. Critical Occlusion Number: Number describing the transition from free flow to occlusion given by $Oc = \frac{N_{cells} d_{cell}}{D_{channel} L_{channel}}$, where occlusion occurs when $O_c > O_{ccrit}$. This parameter is proposed as a conceptual metric describing the combined influence of cell accumulation and geometric confinement on the onset of channel obstruction. Larger values indicate a greater tendency for flow blockage due to increased cell occupancy within confined microchannels. Although not intended as a predictive model, the concept is consistent with previous studies highlighting the existence of critical transitions between unobstructed and occluded flow states. For example, Belyaev et al. [199] demonstrated that the microvascular thrombosis displays a threshold behavior governed by a critical injury length, above which complete vessel occlusion may occur. Also, Man et al. [200] introduced an occlusion index as a measure of microvascular blockage resulting from impaired RBC deformability. In this context, the proposed Critical Occlusion Number should be regarded as a framework to qualitatively capture the interplay between cellular loading and channel geometry rather than to predict occlusion quantitatively. Consequently, its applicability across the different pathological conditions, channel geometries, hematocrit levels, and flow regimes remains to be investigated and validated through dedicated experimental and computational studies.
2. Pathological Jamming Transition [95]: Diseased RBCs exhibit a jamming threshold at lower hematocrit $H_t^{path} < H_t^{healthy}$ due to increased stiffness and adhesion.

3. Confinement-Amplified Pathology: Pathological RBCs show nonlinear increases in flow resistance under confinement $R_{flow}^{path}(\chi) \propto \chi^n$, $n > 2$, where $\chi = d_{\mathrm{RBC}}/D_{\mathrm{channel}}$.

PDMS microfluidics enable pathological RBC studies like oxygen-controlled sickling assays, endothelialized adhesion studies, stenosis-induced occlusion modeling, and single-cell deformability phenotyping. Figure 10 presents the distribution of literature works concerning blood-related diseases using PDMS devices.

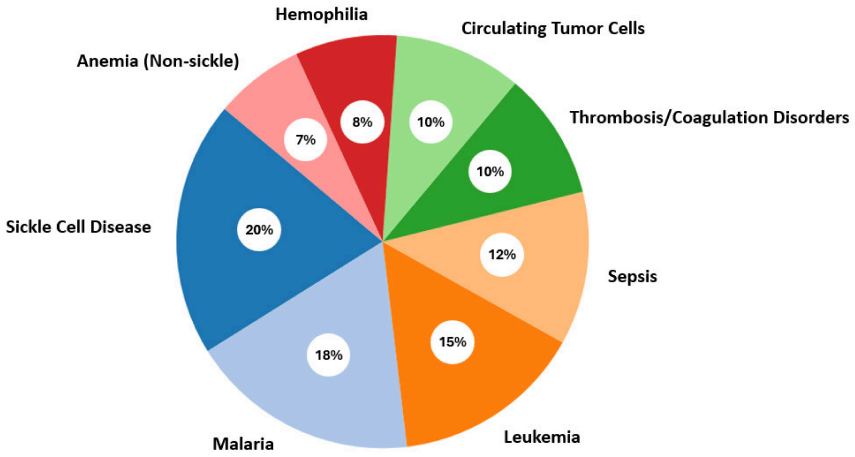

Figure 10. Distribution of works on blood-related diseases using PDMS microfluidic devices. This distribution is intended as an illustrative summary of the literature discussed in this review and does not represent a bibliometric analysis of all published studies in the field.

5.2. Platelet Adhesion and Thrombosis

Platelet adhesion and thrombosis are central to hemostasis and pathological clot formation—processes exquisitely sensitive to local hemodynamics, shear-stress gradients, and microvascular geometry [200]. PDMS microfluidic platforms allow for the study of these phenomena under controlled flow conditions, enabling quantitative analysis of platelet activation, coagulation dynamics, and thrombus development [201]. Their optical transparency and compatibility with real-time imaging make PDMS devices indispensable for examining the interplay between shear forces, biochemical cues, and cellular interactions that drive thrombosis [202].

5.2.1. Shear-Dependent Platelet Activation

The platelets are sensitive to shear stress, with activation thresholds that vary across venous, arterial, and pathological flow regimes. PDMS microfluidic channels allow to impose shear rates ranging from venous between 1 and 10 dyn/cm^2 to arterial above 70 dyn/cm^2 and even the extreme shear conditions found in stenotic vessels [203]. Platelet activation probability P_{act} increases sharply when shear exceeds a critical threshold τ_{crit} $P_{act} \propto \begin{cases} 0, & \tau_w < \tau_{crit} \\ (\tau_w - \tau_{crit}), & \tau_w \geq \tau_{crit}. \end{cases}$ Under pathological high shear, von Willebrand factor (vWF) undergoes force-induced elongation, exposing binding sites for platelet GPIbα. The elongation can be approximated by Equation (13) [204]:

$$L_{vWF}(\tau) = L_0(1 + \alpha\tau) \tag{13}$$

where α is a force-sensitivity coefficient. PDMS platforms allow real-time visualization of platelet shape change, granule release, integrin activation, adhesion to collagen and vWF-coated surfaces [205], vWF-mediated tethering under stenotic shear [206]. Microfluidic channels enable construction of shear-gradient activation maps, linking local shear stress,

shear-rate heterogeneity, vWF elongation, and platelet adhesion probability. This provides a mechanistic framework for understanding platelet hyperreactivity in cardiovascular disease.

5.2.2. Coagulation Cascade Modeling

The coagulation cascade is a network of enzymatic reactions strongly influenced by the flow-mediated transport of clotting factors [207]. PDMS microfluidic devices enable the introduction of procoagulant stimuli (tissue factor, thrombin, activated platelets), while monitoring fibrin generation, factor diffusion, and thrombin propagation [1]. The concentration of a clotting factor concentration C evolves according to Equation (14) [208]:

$$\frac{\partial C}{\partial t} + u \cdot \nabla C = D\nabla^2 C + R(C) \tag{14}$$

where u is the velocity field, D is the diffusion coefficient, $R(C)$ is the reaction term (enzyme kinetics). Thrombin propagation speed v_{thr} depends on reaction rate k and diffusion D by Equation (15) [209]:

$$v_{thr} \approx 2\sqrt{kD} \tag{15}$$

Equation (15) represents an idealized reaction-diffusion estimate for the propagation velocity of a biochemical activation front. Its derivation assumes homogeneous media, isotropic diffusion, and simplified reaction kinetics. In the thrombus formation, additional phenomena including advection, platelet transport, endothelial interactions, and nonlinear coagulation cascades influence the propagation dynamics. Therefore, Equation (15) should be interpreted as a conceptual scaling relationship rather than a model of thrombin transport under physiological conditions. PDMS devices support surface-triggered coagulation (collagen, tissue factor) and flow-triggered coagulation (activated platelets, thrombin injection). These platforms serve to evaluate anticoagulant therapies, patient-specific coagulopathies, and clot initiation and propagation [210–214]. Figure 11 shows deformable U-shaped microelectrodes of carbon-PDMS for blood coagulation tests.

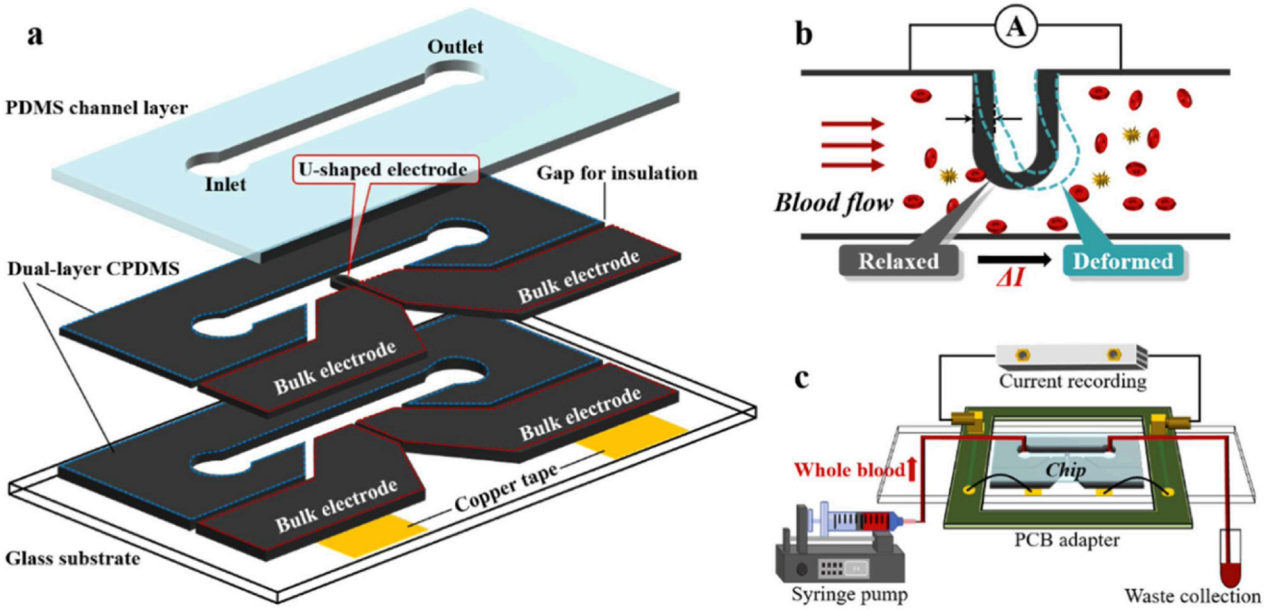

Figure 11. (**a**) PDMS composite device, blue dashed line: passive region, red dashed line: active region, (**b**) working principle, (**c**) setup [214].

5.2.3. Thrombus Formation Under Flow

Thrombus formation involves platelet adhesion, aggregation, fibrin deposition, and clot stabilization. PDMS microfluidic systems allow for the observation of thrombus de-

velopment under controlled flow conditions, enabling the determination of growth rate, stability, porosity, and embolization [210]. The thrombus height $h(t)$ follows a sigmoidal growth curve according to Equation (16) [215]:

$$h(t) = \frac{h_{max}}{1 + e^{-k(t-t_0)}} \tag{16}$$

where h_{max} is the maximum thrombus height, k is the growth rate constant, and t_0 is the onset time. Thrombus stability S decreases with increasing shear stress according to Equation (17) [216]:

$$S(\tau) = S_0 e^{-\beta\tau} \tag{17}$$

where β is a shear-sensitivity parameter. By incorporating stenotic geometries, bifurcations, and aneurysm-like expansions, the PDMS devices replicate disturbed flow patterns that promote thrombosis [202]. These geometries generate recirculation zones, low-shear pockets, high-shear gradients, and vortex-driven platelet accumulation. Microfluidic imaging enables construction of thrombus architecture maps, linking shear stress, platelet density, fibrin network porosity, and embolization probability.

5.3. Leukocyte Dynamics

The leukocyte dynamics are central to immune surveillance, inflammation, and vascular homeostasis [217]. Their behavior in microcirculation emerges from an interplay between hemodynamic forces, endothelial signaling, and cell–cell interactions. PDMS microfluidics provide physiologically relevant environments for dissecting these processes, thanks to their optical transparency and compatibility with endothelialization [218].

5.3.1. Rolling and Adhesion

Leukocyte rolling and adhesion constitute the initial stages of the inflammatory response, enabling immune cells to survey the endothelium and respond to sites of injury or infection [219]. PDMS microfluidic channels allow for the control of shear stress, ligand presentation, and endothelial activation state [220], supporting visualization of selectin-mediated rolling, integrin activation, firm adhesion, and spreading and arrest. The adhesive bond force between leukocyte receptors and endothelial ligands (selectins) can be modeled by Equation (18) [221]:

$$F_{bond} = N_b f_b \tag{18}$$

where N_b is the number of active bonds and f_b is the force per bond. Rolling occurs when $F_{drag} \approx F_{bond}$. The leukocyte rolling velocity V_r decreases with increasing bond formation rate. The PDMS channels allow for the modulation of shear stress, ligand density (P-selectin, E-selectin), and endothelial activation (TNF-α, IL-1β). These platforms reveal how cytokine stimulation, glycocalyx degradation, and altered leukocyte mechanics affect rolling velocity and adhesion strength [222].

5.3.2. Immune Cell Trafficking

Immune cell trafficking involves complex migratory behaviors as leukocytes navigate vascular and interstitial environments [223]. The PDMS microfluidics create chemokine gradients and bifurcated pathways mimicking the constraints of microvasculature and surrounding tissues [224]. These platforms assess chemotaxis (migration guided by soluble gradients), haptotaxis (migration guided by substrate-bound cues), durotaxis (migration guided by stiffness gradients), rheotaxis (migration guided by flow direction), and mechanotaxis (migration guided by mechanical forces) [225]. They also support neutrophil swarm-

ing, monocyte recruitment, and lymphocyte trafficking studies [226]. Leukocyte migration velocity V_m under a chemokine gradient ∇C can be expressed by Equation (19) [227]:

$$V_m = \chi_c \nabla C \tag{19}$$

where χ_c is chemotactic sensitivity. Under flow, leukocytes experience a hydrodynamic torque given by Equation (20) [228]:

$$\tau_h = \eta a^3 \dot{\gamma} \tag{20}$$

where η is the viscosity, α is the cell radius, and $\dot{\gamma}$ is the shear rate. This torque aligns the cells with the flow direction, producing rheotactic migration. In narrow PDMS channels, the confinement modifies the leukocyte shape and migration speed. The effective friction coefficient is given by Equation (21) [229]:

$$\zeta_{\text{conf}} = \zeta_0(1 + \alpha\chi) \tag{21}$$

where $\chi = d_{\text{cell}}/D_{\text{channel}}$ is the confinement ratio. PDMS platforms enable the construction of migration maps linking chemokine gradients and flow fields to migration modes (chemotaxis, durotaxis, rheotaxis, mechanotaxis). Figure 12 presents a hydrophilic PDMS microfluidic capillary platform for point-of-care immunoassays.

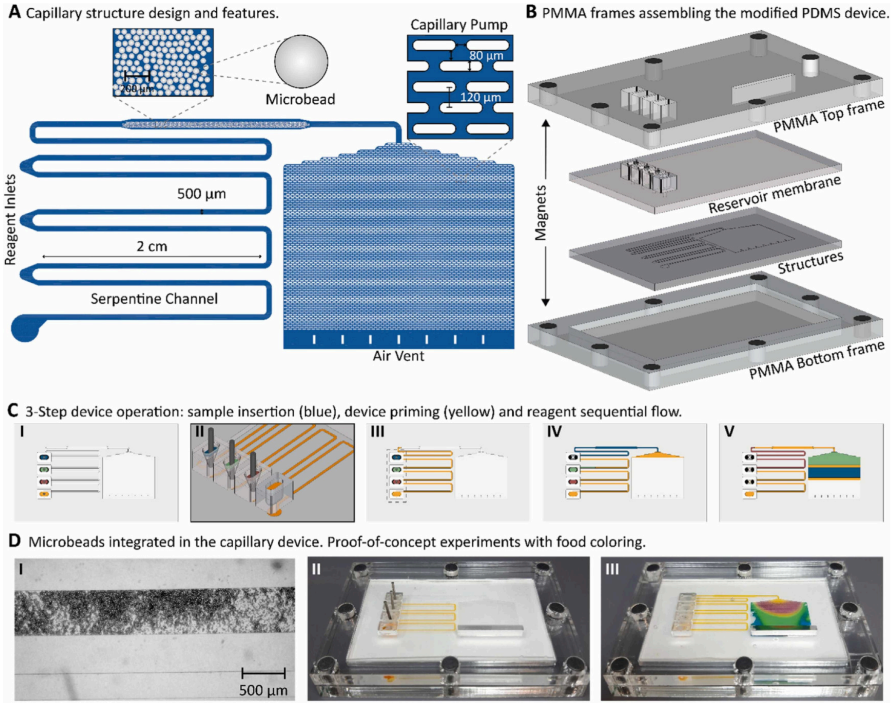

Figure 12. Device assembly, features, and working principles: (**A**) capillary structure design-serpentine channel, reagent inlets, microbead chamber, capillary pump, and air vent; (**B**) PMMA frames with integrated magnets assisting device sealing: (**C**) reservoirs filling (**I**); device priming (**II**,**III**); and sequential entry of the content of the other reservoirs (**IV**,**V**): and (**D**) Microbeads (**I**) proof-of-concept with food coloring (**II**,**III**) [182].

5.3.3. Inflammation Models

The PDMS microfluidic systems offer a platform for constructing in-vitro inflammation models that capture the interaction between blood and endothelial cells, and inflammatory mediators [230,231]. Endothelialized PDMS channels are stimulated with cytokines like TNF-α and IL-1β, inducing expression of adhesion molecules (E-selectin, ICAM-1, VCAM-1) and replicating inflamed vascular environments [232]. These systems enable the observation

of leukocyte recruitment, rolling, adhesion, and transmigration under controlled flow [233]. Advanced models incorporate co-cultures of endothelial cells, immune cells, and tissue-specific cells to recreate organ-specific inflammatory responses. PDMS inflammation models are used to study sepsis [234], atherosclerosis [235], and microvascular dysfunction [236]. Endothelial activation under cytokine stimulation is described by the upregulation kinetics of adhesion molecules. For a given adhesion molecule concentration $A(t)$ is given by Equation (22) [237]:

$$\frac{dA}{dt} = k_{on}C_{cytokine} - k_{off}A \tag{22}$$

where k_{on} is the activation rate constant, k_{off} is the decay/internalization rate, C_{cytokine} is the cytokine concentration (TNF-α, IL-1β). This captures how inflammatory signaling increases leukocyte-binding capacity over time. The adhesion probability P_{adh} scales with adhesion molecule density and hydrodynamic drag $P_{adh} \propto \frac{A(t)}{F_{drag}}$. Where α is the leukocyte radius, μ the viscosity, and U the local velocity. Leukocyte transmigration across endothelial layers involves adhesive bond formation, cytoskeletal remodeling, and migration through endothelial junctions. The transmigration velocity V_{trans} is given by Equation (23) [238]:

$$V_{trans} = \chi_{chem}\nabla C + \chi_{mech}\nabla\sigma \tag{23}$$

where χ_{chem} is the chemotactic sensitivity, χ_{mech} is the mechanotactic sensitivity, ∇C is the chemokine gradient, and $\nabla\sigma$ is the mechanical stress gradient across the endothelium. Equation (23) represents a simplified phenomenological description of leukocyte transmigration driven by both biochemical and mechanical cues. The first term accounts for chemotaxis, whereby leukocytes migrate along chemokine concentration gradients, while the second term describes mechanotactic responses induced by gradients in mechanical stress. The model assumes a linear relationship between the migration velocity and the driving gradients and neglects more complex processes like receptor saturation, intracellular signaling pathways, cell polarization, and dynamic interactions with the endothelial cells. Consequently, Equation (23) should be interpreted as a conceptual framework for coupled chemo-mechanical migration rather than a universal model of leukocyte transmigration. PDMS devices allow the precise control of both gradients, enabling mechanistic dissection of transmigration pathways. PDMS inflammation models incorporate endothelial cells from vascular beds (lung, brain, liver), immune cells (neutrophils, monocytes, lymphocytes), tissue stromal cells, and extracellular matrix components. This enables organ inflammation modeling, including lung-on-chip for sepsis-induced neutrophil infiltration, artery-on-chip for atherosclerotic plaque inflammation, and blood–brain barrier-on-chip for neuroinflammation. These models reveal how geometry, shear stress, and biochemical gradients regulate inflammatory responses. Inflammation assays allow the extraction of quantitative metrics including rolling velocity, adhesion density given by Equation (24) [239]:

$$\rho_{adh} = \frac{N_{cells}}{A_{surface}} \tag{24}$$

Transmigration rate expressed by Equation (25) [240]:

$$R_{trans} = \frac{N_{trans}}{t} \tag{25}$$

And endothelial permeability given by Equation (26) [241]:

$$P = \frac{J}{\Delta C} \tag{26}$$

Endothelial permeability is commonly used as a quantitative indicator of barrier integrity in microvascular and organ-on-chip models. Equation (26) provides a simplified

description relating solute transport across the endothelial layer to the concentration gradient driving diffusion. Although this formulation is useful for comparing endothelial barrier function under different experimental conditions, it represents a phenomenological approximation based on transport theory and does not explicitly account for the complex biological mechanisms governing transendothelial transport. Factors like intercellular junction remodeling, endothelial glycocalyx structure, cell heterogeneity, and flow-induced mechanotransduction can significantly influence permeability measurements. Therefore, the permeability coefficient obtained from Equation (26) should be interpreted as an effective or apparent parameter reflecting the transport properties of the endothelial barrier under the specific experimental conditions employed.

6. Limitations of PDMS

The hydrophobicity of PDMS presents substantial challenges for microfluidic applications involving blood [242]. With a water contact angle of approximately 110° [243], PDMS resists uniform wetting, leading to unreliable channel priming and unstable flow conditions. This hydrophobicity affects capillary filling, bubble nucleation, and shear-profile stability. The difficulty in wetting PDMS channels arises from the unfavorable capillary pressure given by Equation (27) [244]:

$$\Delta P_{cap} = \frac{2\gamma cos\theta}{r} \tag{27}$$

where γ = surface tension, $\theta \approx 110°$ = PDMS contact angle, and r = hydraulic radius. Because $\cos\theta < 0$, the capillary pressure opposes filling, causing incomplete channel priming, irregular meniscus progression, and stagnant "dead zones" [245]. These issues are pronounced in small cross-section channels, where capillary forces dominate. Poor wetting allows air pockets to persist during priming in narrow or high-aspect-ratio geometries. PDMS gas permeability enhances the problem as trapped air diffuses into the channel over time, generating microbubbles during long-term experiments [246], which may lead to disruption of laminar flow, shear-stress spikes, and cell damage [247], unwanted platelet and leukocyte activation due to rapid shear fluctuations. Bubble formation is problematic in stable shear assays, such as platelet adhesion, and leukocyte rolling [248]. In the absence of wetting defects, and gas inclusions, the velocity field in a microchannel can be approximated by the classical fully developed laminar-flow profile represented by Equation (28) [249].

$$u(y) = u_{max}\left(1 - \left(\frac{y}{R}\right)^2\right) \tag{28}$$

Bubble intrusion, partial wetting, and trapped gas pockets cause deviations from this ideal velocity distribution by reducing the available flow cross-section and introducing localized flow recirculation and acceleration regions. Consequently, the actual velocity field may differ from the profile predicted by Equation (28), resulting in non-uniform shear-rate distributions and increased uncertainty in flow measurements. Also, the shear gradients compromise flow stability, cell distribution uniformity, and reproducibility of hemodynamic measurements [250]. Platelet adhesion assays are sensitive to shear variations, and leukocyte rolling dynamics require stable flow conditions to ensure accurate quantification [251]. On the other hand, the PDMS tendency to absorb/adsorb biomolecules perturbs mass transport, surface interactions, and biochemical stability, thereby compromising the accuracy of assays involving blood cells and plasma proteins. PDMS is a porous silicone elastomer with affinity for hydrophobic compounds [252]. Small hydrophobic molecules—including lipids, drugs, and fluorescent dyes—diffuse into the polymer matrix over time. This absorption is governed by classical diffusion physics expressed by Equation (29) [253]:

$$\frac{\partial C}{\partial t} = D_{PDMS}\nabla^2 C \tag{29}$$

where C is the analyte concentration and D_{PDMS} is the diffusion coefficient inside PDMS. Fluid-physics consequences include depletion of analytes from the flowing phase, distortion of concentration gradients, and loss of hydrophobic drugs. These effects interfere with drug-response studies and destabilize biochemical gradients [254]. The extent of absorption depends on molecular size, hydrophobicity, exposure duration, and local shear-enhanced transport. Plasma proteins like albumin and fibrinogen adsorb onto hydrophobic PDMS surfaces. The adsorption kinetics follow a Langmuir-type model given by Equation (30) [255]:

$$\frac{d\Gamma}{dt} = k_{on}C(\Gamma_{max} - \Gamma) - k_{off}\Gamma \tag{30}$$

where Γ is the surface-bound protein concentration. Adsorbed proteins form a conditioning layer that may alter platelet adhesion and endothelial behavior, trigger leukocyte activation, and initiate coagulation pathways. The simultaneous action of bulk absorption and surface adsorption creates a biochemical sink, removing molecules from the fluid and altering surface chemistry. The consequences include altered cell activation thresholds, inconsistent platelet activation, and perturbed coagulation modeling [256,257]. PDMS behaves as a compliant elastomer, meaning that its geometry, and therefore its hemodynamic environment, change under pressure, solvent exposure, and long-term operation. Table 10 shows the PDMS deformation modes in the blood-flow microfluidics.

Table 10. PDMS deformation modes in blood-flow microfluidics.

Deformation	Causes	Applications Affected	Solutions	References
Bulging	High inlet pressures Thin channel wall or roof	Alters shear stress profiles Distorts endothelial cell experiments	Increase PDMS curing ratio from 10:1 to 5:1 Bond PDMS to rigid substrates	[258]
Sagging	Large aspect ratio channels Vacuum degassing during priming	Channel occlusion Cell trapping or hypoxia in the collapsed regions	Reduce channel width/height ratio Stiffer PDMS	[259]
Absorption	Hydrophobic PDMS matrix absorbs hydrophobic drugs, dyes, lipids	Drug-response become inaccurate Altered platelet activation	Surface coatings Low absorption materials	[260]
Leaching	Incomplete curing Low-quality PDMS	Cytotoxicity to blood cells Platelet activation	Post-cure at high temperature Soxhlet extraction	[261]
Hydrophobic recovery	Reorientation of polymer chains Migration of oligomers to surface	Poor wetting during priming Bubble formation	Permanent coatings UV-ozone instead of plasma	[262]
Swelling	Exposure to organic solvents	Channel geometry distortion Membrane rupture in organ-on-chip devices	PDMS thermal aging Increase PDMS curing ratio from 10:1 to 5:1	[263]
Protein Fouling/Biofouling	PDMS hydrophobicity attracts proteins and cells	Non-specific adhesion of blood cells Altered platelet behavior	PEGylation Parylene-C caulking	[264]
Delamination	Poor plasma bonding Long-term perfusion	Leakage Flow interruption	Optimize plasma parameters Chemical bonding	[265]
Mechanical fatigue/creep	Long-term cycling loading Pulsatile pressure	Gradual channel deformation Inaccurate long-term blood perfusion	Stiffer PDMS Reinforce with glass polymer layers	[266]
Gas permeation and bubble formation	PDMS gas permeability	Bubble nucleation disrupts flow Endothelial detachment	High-pressure liquid phase PCR Bubble traps	[267]

PDMS has comparatively low Young's modulus, making it prone to deformation when exposed to elevated pressures or vacuum-driven flow [268]. The deformation can be approximated by Equation (31) [269]:

$$\delta = \frac{Pw^4}{Et^3} \tag{31}$$

where P is the applied pressure, w is the channel width, t is the PDMS roof thickness, and E is the PDMS Young's modulus. This deformation disrupts the flow profile, producing errors in shear-stress calculations, RBC, and platelet trajectories. This mechanical compliance limits PDMS under high pressure and motivates thicker channel roofs and hybrid PDMS–glass structures [270]. PDMS absorbs organic solvents, leading to swelling that distorts microchannel dimensions [271]. Swelling causes deformation, delamination, and changes in surface chemistry. Over time, PDMS undergoes mechanical aging due to migration of uncrosslinked oligomers and repeated mechanical stress [272,273]. In prolonged blood-flow experiments—such as endothelialized channels or chronic perfusion studies—aging may lead to gradual deformation, hydrophobic recovery, and increased protein adsorption [274]. The PDMS hydrophobic surface may lead to inconsistent cell adhesion, particularly for anchorage-dependent cells like endothelial cells [275]. Plasma oxidation increases hydrophilicity by generating silanol groups, reducing the contact angle from ~110° to ~20–30°. However, hydrophobic recovery occurs within hours due to migration of low-molecular-weight oligomers, being the time-dependent contact angle given by Equation (32) [276]:

$$\theta(t) = \theta_{hydrophilic} + \left(\theta_{native} - \theta_{hydrophilic}\right)e^{-kt} \tag{32}$$

where k is the hydrophobic-recovery rate constant. This recovery causes variability in endothelial adhesion and spreading, shear-stress distribution, and leukocyte and platelet interactions. Even with coatings (fibronectin, collagen, poly-L-lysine), adsorption variability and surface aging lead to heterogeneous cell behavior across experiments [277]. PDMS's high gas permeability promotes evaporation, altering medium osmolarity given by Equation (33) [278]:

$$\frac{dC_{solute}}{dt} = C_{solute}\left(\frac{1}{V}\frac{dV}{dt}\right) \tag{33}$$

where volume loss dV/dt increases solute concentration, affecting cell physiology. Hydrophobic molecules diffuse into PDMS according to Equation (34) [279]:

$$\frac{\partial C}{\partial t} = D_{PDMS}\nabla^2 C \tag{34}$$

reducing concentrations of lipids, hormones, drugs, and growth factors. This trend alters endothelial maturation, immune-cell activation, and vascular remodeling. PDMS releases uncrosslinked oligomers over time [280], which can reduce cell viability and interfere with biochemical assays. These issues limit PDMS suitability for long-term perfusion, organ-on-chip systems, and chronic endothelial studies. Oxygen flux through PDMS walls [281] can be approximated by Equation (35) [282]:

$$J_{O_2} = P_{O_2}\frac{\Delta p}{L} \tag{35}$$

where P_{O_2} is the oxygen permeability coefficient, Δp is the partial-pressure difference, and L is the wall thickness. Consequences include inability to maintain hypoxic conditions, and instability of controlled oxygen gradients [283].

7. Strategies to Overcome PDMS Limitations

7.1. Surface Modification

Several surface-modification strategies have been proposed to overcome the intrinsic hydrophobicity and biomolecule adsorption tendencies of PDMS. However, their applicability to blood-contacting microfluidic systems depends on factors such as coating stability, hemocompatibility, fabrication complexity, optical transparency, and long-term device performance. Oxygen plasma treatment is the simplest and most widely used approach.

It temporarily increases surface hydrophilicity [284] through the generation of silanol groups, facilitating channel filling and reducing initial protein adsorption. PEGylation provides enhanced resistance to protein adsorption and cellular adhesion by forming a hydrated steric barrier at the surface [285]. This strategy is attractive for blood-contacting applications because it can reduce nonspecific interactions between blood components and channel walls. However, grafting procedures can be complex, and long-term stability may be affected by PEG degradation or desorption. Polyvinyl alcohol forms hydrophilic films that improve wetting and reduce fouling [286]. Parylene coatings offer excellent chemical stability, reduced absorption of hydrophobic molecules, and long-term surface durability [287]. In addition, parylene acts as a barrier against gas and small-molecule transport through PDMS. These characteristics make parylene particularly suitable for prolonged blood perfusion studies. The main disadvantages are the requirement for specialized deposition equipment and the increased fabrication cost. Coatings can be applied via adsorption [288], covalent grafting [289], and chemical vapor deposition [290]. These methods are valuable for long-term perfusion and assays requiring precise biochemical control. Sol–gel-derived coatings can significantly improve chemical resistance and surface wettability while preserving optical transparency [291]. Their tunable composition enables adaptation to specific applications involving sensitive biomolecules [292]. However, coating uniformity inside complex microchannel networks can be challenging, and cracking or delamination may occur under mechanical deformation. From a blood-microfluidics perspective, no single modification strategy is universally optimal. Oxygen plasma treatment is generally sufficient for short-term experiments, whereas PEGylation is more appropriate when minimizing protein fouling and platelet adhesion is a primary objective. Parylene coatings are advantageous for long-duration studies requiring enhanced material stability, while sol–gel approaches may be preferred when tailored surface chemistry or barrier properties are desired. Patterned modification enables spatial control of wetting and biochemical interactions within microchannels. Techniques include plasma patterning [293], microcontact printing [294], and chemical grafting [295]. These methods create regions with distinct hydrophilicity/hydrophobicity, enabling controlled droplet formation and cell adhesion. In blood-flow studies, patterned surfaces mimic heterogeneous vascular environments, enabling control of cell–surface interactions [296]. Therefore, the selection of a surface-treatment strategy should be guided by the experimental duration, required hemocompatibility, fabrication constraints, and intended clinical or diagnostic application. Table 11 summarizes the benefits, limitations, and blood-contacting suitability for the main surface modification methods.

Table 11. Benefits, limitations, and blood-contacting suitability for surface modification methods.

Modification Technique	Benefits	Limitations	Blood-Contacting Suitability
Oxygen plasma	Simple and low-cost Improves wettability	Low-to-moderate (temporary) hydrophilicity stability Hydrophobic recovery	Not suitable for long-term experiments (unless combined with further surface modification)
PEGylation	Reduces protein adsorption and cell adhesion	Stability may decrease over time	Excellent
Parylene coating	Durable and chemically stable Reduces absorption	Costly Requires specialized equipment	Excellent for long-term experiments
Sol–Gel coating	Adjustable chemistry Improved barrier properties	Potential cracking and delamination	Generally good, but application-dependent

Figure 13 shows the relative efficiency of different PDMS surface modification techniques for blood-flow examination.

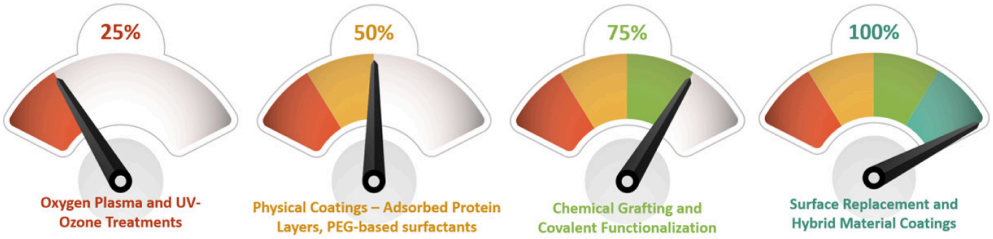

Figure 13. Relative efficiency of PDMS surface modification techniques for blood-flow studies.

7.2. Material Alternatives and Hybrids

Material alternatives and hybrid architectures have emerged as powerful strategies to overcome the intrinsic limitations of PDMS in blood-flow microfluidics. These approaches aim to preserve PDMS advantages while mitigating issues related to hydrophobicity, mechanical instability, and long-term biological compatibility. Figure 14 shows a pump-free paper/PDMS hybrid microfluidic chip for bacteria enrichment and fast detection.

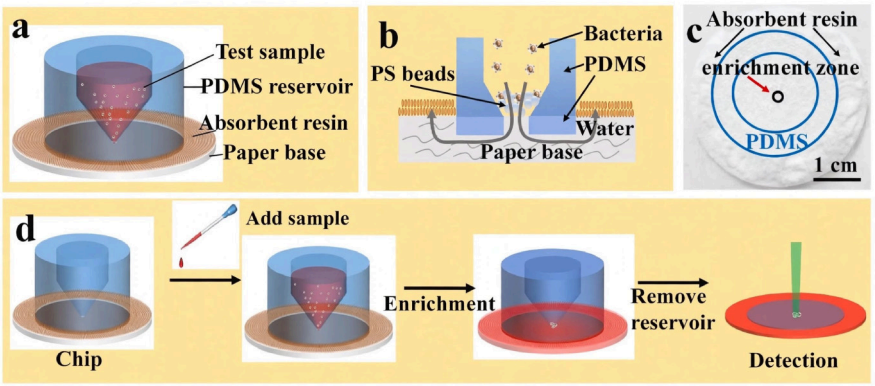

Figure 14. (**a**) Three-dimensional microfluidic chip, (**b**) chip cross-section, (**c**) optical image of the chip, and (**d**) detection procedure using the chip [297].

Table 12 presents the main PDMS hybrid formulations for blood-flow microfluidic devices.

Table 12. PDMS hybrid formulations employed in microfluidic devices for blood-flow analysis.

Composition	Device	Manufacturing Technique	Applications	References
PDMS and PC	Hybrid elastomer–plastic chip mimicking blood–brain barrier	Surface functionalization Bonding to PC	Blood–brain barrier permeability Blood–cell transport	[298]
Collagen/PET/PDMS	Device integrating nanofiber scaffolds	Collagen nanofiber deposition on PET PDMS microchannel integration	Cell–matrix interaction	[299]
PDMS with Surface Functionalization	PDMS microchannels with modified wettability	Plasma treatment Chemical surface modification	RBC deformation Platelet adhesion	[300]
PDMS/Glass	Hybrid PDMS–glass	Soft lithography Oxygen–plasma bonding	High-resolution imaging of RBCs Plasma separation	[301]

Table 12. *Cont.*

Composition	Device	Manufacturing Technique	Applications	References
PDMS/SU-8	Rigid–soft hybrid microchannels with SU-8 structural features	SU-8 photolithography PDMS casting and bonding	Micro-thrombosis Blood circulating tumor cells detection	[302]
PDMS/PMMA	Hybrid PDMS–PMMA microfluidic device	PDMS molding Thermal/adhesive bonding	Cancer cells adhesion to endothelial cells Point-of-care diagnostics	[303]
PDMS/PEG	Anti-fouling microfluidic channels	PEG-silane functionalization Soft lithography	Reduced protein adsorption Stable whole-blood flow	[304]
PDMS and Electrodes	Electrochemical or impedance-based microfluidic chip	PDMS casting over metal electrodes	Impedance cytometry Hematocrit and viscosity measurements	[305]
PDMS and Silicon	High-precision microchannels with silicon sensors	DRIE silicon etching PDMS bonding	Immunoassays RBC mechanics	[306]
PDMS and Hydrogel	Biohybrid vascular microfluidic models	Hydrogel photopolymerization PDMS microchannel integration	Endothelial barrier modeling Thrombosis and vessel-wall interaction	[307]
Nanoparticle-doped PDMS	Microchannels with enhanced mechanical strength	Nanoparticle dispersion in PDMS Soft lithography	High-shear blood flow Hemolysis and stenosis modeling	[308]

Material alternatives and hybrid architectures have emerged to overcome the limitations of PDMS in blood-flow microfluidics. These approaches preserve PDMS advantages—ease of fabrication, optical transparency, rapid prototyping—while mitigating issues related to hydrophobicity, mechanical instability, and long-term biological compatibility. By integrating PDMS with more rigid and chemically stable materials, more reproducible and physiologically relevant platforms can be built. Combining PDMS with glass is one of the strategies for improving device performance since glass provides improved chemical resistance and optical properties and minimal biomolecule absorption. Bonding PDMS to glass creates a stable structure that reduces channel deformation under pressure and improves long-term geometric fidelity [309]. These devices are valuable for applications requiring consistent shear stress including studies of platelet adhesion and endothelialized channels. Glass surfaces can be functionalized using silanes [310], enabling reproducible surface modification beyond what PDMS achieves. Thermoplastics like polymethyl methacrylate, Cyclic Olefin Copolymer (COC), and polycarbonate offer improved chemical resistance, lower biomolecule absorption, and greater mechanical rigidity. These materials can be micro-machined, hot-embossed, and injection-molded, enabling large-scale production. Composite devices that integrate PDMS layers with thermoplastic substrates provide a promising solution for blood-flow applications [311], enhancing mechanical robustness and long-term perfusion stability. Such hybrids are ideal for drug-screening assays, coagulation studies, and chronic endothelial perfusion. Another strategy involves applying thin barrier layers to PDMS surfaces to prevent absorption and improve chemical stability. Materials like parylene, silicon dioxide [312], and metal-oxide coatings can be deposited onto PDMS to create impermeable surfaces without compromising flexibility. Barrier layers reduce protein adsorption, prevent hydrophobic-molecule absorption, and stabilize biochemical gradients. Barrier-coated PDMS devices are useful for drug-response, coagulation, and long-term perfusion studies. Hybrid architectures allow PDMS to contribute flexibility, rapid prototyping, and optical access, while other materials provide rigidity (glass, PC), chemical inertness (COC, SiO_2), and barrier protection (parylene, metal oxides).

7.3. Device-Level Solutions

Device-level engineering strategies address PDMS limitations by redesigning microfluidic architecture, flow-control systems, and operational protocols. Microchannel geometry influences wetting behavior, shear stability, and deformability. They reduce corner-induced bubble trapping and promote uniform wetting, tapered inlets, and gradual expansions that minimize entrance effects, stabilize meniscus progression, and reduce flow separation, and increased channel height or reinforced ceilings. They reduce pressure-induced deformation, improving shear-stress accuracy in platelet adhesion, and leukocyte rolling assays. Channel deformation alters the velocity profile given by Equation (36) [313]:

$$u(y) = u_{max}\left(1 - \left(\frac{y}{R + \delta}\right)^2\right) \tag{36}$$

where δ is the deformation. Reinforced geometries minimize δ, preserving laminar flow even at varying hematocrit. Device-level flow-control solutions include pressure-driven flow systems, reduce pulsatility, and allow for rapid flow-rate adjustments [314,315]; flow-rate feedback loops maintain constant shear stress despite viscosity changes, on-chip resistors [316] that stabilize flow distribution in vascular networks, and flow-balancing networks [317] that ensure hemodynamic environments in bifurcations, stenoses, and microvascular mimics. Pressure-driven flow reduces oscillations compared to syringe pumps are expressed by Equation (37) [318]:

$$Q = \frac{\Delta P}{R_{hyd}} \tag{37}$$

where R_{hyd} is the hydraulic resistance. This ensures stable shear conditions for platelet and leukocyte assays. Mechanical compliance is a limitation of PDMS in high-pressure and long-duration experiments. Structural reinforcements include embedded supports and glass overlays [319]. These maintain dimensional stability, which is essential for stenosis models, microvascular networks, and endothelialized channels. Reinforced devices also improve compatibility with high-resolution imaging by reducing focal drift caused by PDMS flexing. Reinforcement reduces deformation. The bubble formation disrupts flow stability and activates blood cells. Device-level solutions include on-chip debubblers, gas-permeable side chambers, degassing membranes [320], hydrophilic priming channels, and bypass pathways. These features ensure wetting during startup and remove trapped air before it enters critical regions. Bubble nucleation probability decreases with reduced gas concentration $P_{bubble} \propto e^{-\frac{C_{gas}}{C_{sat}}}$ where degassing reduces C_{gas}, stabilizing flow. These solutions are especially important for whole-blood perfusion, where bubbles form spontaneously due to gas exchange.

8. Future Directions

8.1. Integration with Organ-on-Chip Systems

Organ-on-chip platforms increasingly incorporate microvascular networks to model tissue perfusion, immune interactions, and drug delivery. PDMS vascular-on-chip systems allow precise control of shear stress, endothelial function, and blood–tissue exchange, enabling more realistic models of human physiology [321]. These platforms support endothelial mechanobiology, immune-cell trafficking, platelet–vessel wall interactions, microvascular inflammation and thrombosis. Future directions are the multi-organ systems connected by microfluidic vasculature, enabling the study of responses like inflammation cascades, thrombotic propagation, multi-organ failure, and immune-system coordination [322].

8.2. Advanced Materials and Fabrication

New hybrid materials emerge as alternatives to PDMS, offering enhanced chemical stability and biocompatibility and reduced biomolecule absorption. These include Cyclic Olefin Copolymer (COC), Polystyrene (PS), Polycarbonate (PC), glass–polymer composites, and elastomer–thermoplastic hybrids. Additive manufacturing enables rapid fabrication of complex 3D vascular geometries previously impossible with soft lithography [323]. Multi-material bioprinting allows for the integration of rigid supports, flexible membranes, biomimetic extracellular matrices, and perfusable vascular networks [324]. These advances expand the design for microvascular models and support more physiologically accurate blood-flow studies. Recent trends involve hybrid manufacturing strategies where PDMS is used only for active components, such as elastomeric valves, deformable membranes, and pneumatic actuation layers, while thermoplastics like COC and polystyrene form structural microchannels. This mitigates uncontrolled absorption of hydrophobic drugs and biomolecules. COC has emerged as an alternative to PDMS due to lower sorption of hydrophobic molecules, excellent optical clarity, and compatibility with surface passivation strategies [325]. COC and PS are increasingly used in organ-on-chip platforms and immune-cell perfusion models. Table 13 shows a comparative analysis of PDMS, thermoplastics (COC/COP/PMMA), and 3D printing resins (SLA/DLP).

Table 13. Comparative analysis of PDMS, thermoplastics, and 3D printing resins for blood-flow microfluidics.

Property	PDMS	Thermoplastics	3D Printing Resins
Optical Transparency	Excellent (>90%) [3,12,13]	Excellent-to-Good [3,269]	Variable [50] (clear resins improving > 80–95%)
Drug/Analyte Absorption	High [3,13]	Low [3,269]	Low-to-Moderate [50,51]
Fabrication Speed	Fast [3,13]	Slow [3]	Very Fast [50]
Ease of Fabrication	High [3,12,13]	Low [3]	High [50]
Scalability	Low [3,12,13]	Very High [3]	Moderate [50,51]
Cost	Low [3,12,13]	High [3]	Low [50,51]
Surface Modification	Unstable [3,12,13]	Stable [3]	Material dependent [50,51]

8.3. Sensing and Integrated Analytics

Modern systems integrate optical, electrochemical, and mechanical sensors into PDMS or hybrid substrates. These sensors quantify oxygen tension, shear stress, coagulation factor levels, and endothelial barrier integrity. Shear stress can be measured using deformable micro-pillars or piezoresistive films where embedded sensors provide real-time estimates of $\frac{du}{dy}$ across the channel. Electrochemical sensors detect thrombin, fibrinogen, and platelet-derived factors via Equation (38) [326]:

$$I = kC \tag{38}$$

where I is the current and C is the analyte concentration. Machine-learning-based image analysis is revolutionizing microfluidic blood-flow quantification [327]. AI extracts leukocyte rolling velocity, platelet aggregation kinetics, thrombus growth rate, and flow-field reconstruction. These tools provide high-throughput, unbiased quantification with precision far exceeding manual analysis. The convergence of embedded sensors and AI transforms the microfluidic systems into diagnostic tools with autonomous data interpretation.

8.4. Patient-Specific Microfluidics

Microfluidic platforms increasingly support patient-specific blood analysis, enabling personalized assessment of coagulation disorders, platelet function, RBC mechanical abnormalities, and inflammatory responses [328]. Rapid prototyping and modular device design allow researchers to tailor microchannel geometry, biochemical gradients, shear-stress profiles, and endothelial phenotypes to individual patient needs. Future microfluidic assays may support point-of-care diagnostics for sickle-cell disease, thrombophilia, diabetes-related hemorheology, and inflammatory disorders [329,330]. These systems promise rapid, minimally invasive insights into patient physiology, enabling personalized treatment strategies. Microfluidics allow for the reconstruction of patient-specific vascular conditions using individualized hematocrit, platelet reactivity, and plasma composition. This enables precision hemodynamics, where device geometry and flow conditions are tuned to match patient physiology.

8.5. Active Hydraulic Regulation

Future microfluidic blood-flow platforms will likely benefit from active hydraulic regulation technologies capable of dynamically adjusting the flow resistance. Inspired by biological valves, magnetic microfluidic rheostats have been proposed as a means of achieving continuous and precise hydraulic-resistance tuning via geometry-controlled flow restriction, opening new possibilities for adaptive blood-flow control in biomimetic microvascular networks [331].

8.6. Convergence of Computational and Experimental Hemodynamics

Computational Fluid Dynamics (CFD) and Dynamic Numerical Simulation (DNS) are increasingly integrated with microfluidic experiments to provide deeper insight into hemodynamic behavior [332]. PDMS and hybrid platforms offer controlled environments for validating CFD models of shear-stress distribution, RBC and platelet trajectories, leukocyte rolling, thrombus formation [333]. Future systems may include real-time feedback loops between simulations and experiments CFD predicts flow behavior, sensors measure actual flow, and algorithms adjust pressure/flow rate. This enables adaptive control of microfluidic conditions and automated optimization of device design. The convergence of CFD, DNS, embedded sensors, and AI will produce digital-twin microfluidic systems, where each experiment has a computational replica.

9. Conclusions

PDMS microfluidics have transformed blood-flow research by bridging the gap between conventional in vitro assays and the physiological complexity of the microcirculation. Their optical transparency, biocompatibility, gas permeability, and compatibility with soft lithography have enabled the development of microvascular-scale platforms for studying RBC deformability, platelet adhesion, leukocyte dynamics, thrombosis, and other key hemodynamic processes. These systems provide controlled flow environments and high-resolution visualization capabilities that have significantly advanced the understanding of blood rheology and cellular transport phenomena.

Despite these advantages, important challenges remain. Intrinsic PDMS properties, including hydrophobic recovery, absorption of biomolecules, gas permeation, and mechanical compliance, can influence flow behavior and compromise experimental reproducibility. In blood-flow studies, these effects may alter wall shear stress, hydraulic resistance, cell–surface interactions, and biochemical conditions, thereby affecting the quantitative interpretation of experimental results.

To address these limitations, recent efforts have focused on surface engineering, improved fabrication strategies, and hybrid material platforms. The integration of PDMS with thermoplastics, glass, barrier coatings, and advanced manufacturing approaches combines the prototyping flexibility of PDMS with improved chemical stability, mechanical robustness, and long-term reliability. These developments are contributing to more standardized and physiologically relevant microfluidic systems suitable for translational research and large-scale implementation.

Looking ahead, the field is moving toward intelligent and multifunctional microfluidic platforms that integrate embedded sensors, automated data acquisition, computational modeling, and artificial intelligence. Coupling microfluidic experiments with real-time monitoring and predictive simulations may enable more accurate characterization of blood-flow behavior and support personalized diagnostic approaches. As these technologies mature, blood-flow microfluidics are expected to evolve from laboratory research tools into robust platforms for disease modeling, therapeutic screening, and clinically relevant precision-medicine applications.

Author Contributions: Conceptualization: J.P.; methodology: J.P., R.S. and A.M.; software, A.M.; validation, A.M.; formal analysis, J.P. and A.M.; investigation: J.P. and R.S.; resources: A.M.; data curation: J.P. and R.S.; original draft: J.P. and R.S.; Final revision and edition: J.P. and R.S.; project administration: A.M. All authors have read and agreed to the published version of the manuscript.

Funding: This work was supported by the Fundação para a Ciência e a Tecnologia (FCT), Avenida D. Carlos I, 126, 1249-074 Lisboa, Portugal, through multiple grants and projects. Additional funding was provided by FCT through LA/P/0083/2020 IN +-IST-ID and for financing Dr. Reinaldo Rodrigues de Souza through FCT-Tenure. Ana Moita acknowledges support from CEECINST/00043/2021/CP2797/CT0005 (https://doi.org/10.54499/CEECINST/00043/2021/CP2797/CT0005, accessed on 15 October 2026).

Institutional Review Board Statement: Not applicable.

Informed Consent Statement: Not applicable.

Data Availability Statement: No new data were created or analyzed in this study. Data sharing is not applicable to this article.

Conflicts of Interest: The authors declare no conflicts of interest.

Abbreviations

The following abbreviations are used in this manuscript:

CFD	Computational Fluid Dynamics
CFL	Cell Free Layer
COC	Cyclic Olefin Copolymer
COP	Cyclic Olefin Polymer
CTC	Circulating Tumor Cell
DLD	Deterministic Lateral Displacement
DLP	Digital Light Processing
DNS	Dynamic Numerical Simulation
ECM	Extracellular Matrix
FDM	Fused Deposition Modeling
MEMS	Microelectromechanical Systems
PDMS	Polydimethylsiloxane
PC	Polycarbonate
PCR	Polymerase Chain Reaction
PEG	Polyethylene Glycol
PET	Polyethylene Terephthalate
PIV	Particle Image Velocimetry
PMMA	Polymethylmethacrylate

PS	Polystyrene
PTV	Particle Tracking Velocimetry
RBC	Red Blood Cell
SLA	Stereolithography
vWF	von Willebrand factor
WSS	Wall Shear Stress
WBC	White Blood Cell

References

1. Wajihah, S.A.; Sankar, D.S. A review on non-Newtonian fluid models for multi-layered blood rheology in constricted arteries. *Arch. Appl. Mech.* **2023**, *93*, 1771–1796. [CrossRef] [PubMed]
2. Feuer, D.S.; Handberg, E.M.; Mehrad, B.; Wei, J.; Merz, C.N.B.; Pepine, C.J.; Keeley, E.C. Microvascular Dysfunction as a Systemic Disease: A Review of the Evidence. *Am. J. Med.* **2022**, *135*, 1059–1068. [CrossRef] [PubMed]
3. Ren, K.; Zhou, J.; Wu, H. Materials for Microfluidic Chip Fabrication. *Acc. Chem. Res.* **2013**, *46*, 2396–2406. [CrossRef] [PubMed]
4. Shakeri, A.; Khan, S.; Didar, T.F. Conventional and emerging strategies for the fabrication and functionalization of PDMS-based microfluidic devices. *Lab Chip* **2021**, *21*, 3053–3075. [CrossRef] [PubMed]
5. Xu, T.; Lim, Y.J.; Zheng, Y.; Jung, M.S.; Gaus, K.; Gardiner, E.E.; Lee, W.M. Modified inverted selective plane illumination microscopy for sub-micrometer imaging resolution in polydimethylsiloxane soft lithography devices. *Lab Chip* **2020**, *20*, 3960–3969. [CrossRef] [PubMed]
6. Khaustov, I.A.; Safronova, Y.A.; Chebotareva, O.E.; Brianton, J.A.; Knyazev, E.N. Optimization of Gas Permeability in PDMS Microfluidic Chips for Organ-on-Chip Modeling. *Appl. Biochem. Microbiol.* **2025**, *61*, 1753–1759. [CrossRef]
7. Vo, T.; Tran, A.S.; Tran, T.N. A Simple and Low-Cost Method for Fabrication of Non-Planar PDMS Microfluidic Channel. *Int. J. Autom. Smart Technol.* **2025**, *15*. [CrossRef]
8. Newman, G.; Leclerc, A.; Arditi, W.; Calzuola, S.T.; Feaugas, T.; Roy, E.; Perrault, C.M.; Porrini, C.; Bechelany, M. Challenge of material haemocompatibility for microfluidic blood-contacting applications. *Front. Bioeng. Biotechnol.* **2023**, *11*, 1249753. [CrossRef] [PubMed]
9. Venzac, B. Light-based 3D printing and post-treatments of molds for PDMS soft lithography. *Lab Chip* **2025**, *25*, 2129–2147. [CrossRef] [PubMed]
10. Raj, A.; Suthanthiraraj, P.P.A.; Sen, A.K. Pressure-driven flow through PDMS-based flexible microchannels and their applications in microfluidics. *Microfluid. Nanofluid* **2018**, *22*, 128. [CrossRef]
11. Sebastian, B.; Dittrich, P.S. Microfluidics to Mimic Blood Flow in Health and Disease. *Annu. Rev. Fluid Mech.* **2018**, *50*, 483–504. [CrossRef]
12. Cai, D.; Heise, H.M. Spectroscopic Aspects of Polydimethylsiloxane (PDMS) Used for Optical Waveguides. In *Molecular Spectroscopy—Experiment and Theory, Challenges and Advances in Computational Chemistry and Physics*; Koleżyński, A., Król, M., Eds.; Springer: Cham, Switzerland, 2019; Volume 26. [CrossRef]
13. Lima, R.A. The Impact of Polydimethylsiloxane (PDMS) in Engineering: Recent Advances and Applications. *Fluids* **2025**, *10*, 41. [CrossRef]
14. Merkel, T.C.; Bondar, V.I.; Nagai, K.; Freeman, B.D.; Pinnau, I. Gas sorption, diffusion, and permeation in poly(dimethylsiloxane). *J. Polym. Sci. Part B Polym. Phys.* **2000**, *38*, 415–434. [CrossRef]
15. Mark James, E. (Ed.) *Polymer Data Handbook*, 2nd ed.; Oxford Academic: New York, NY, USA, 2009. [CrossRef]
16. Regehr, K.J.; Domenech, M.; Koepsel, J.T.; Carver, K.C.; Ellison-Zelski, S.J.; Murphy, W.L.; Schuler, L.A.; Alarid, E.T.; Beebe, D.J. Biological implications of polydimethylsiloxane-based microfluidic cell culture. *Lab Chip* **2009**, *9*, 2132–2139. [CrossRef] [PubMed]
17. Seo, S.; Kim, T. Gas transport mechanisms through gas-permeable membranes in microfluidics: A perspective. *Biomicrofluidics* **2023**, *17*, 061301. [CrossRef] [PubMed]
18. Varner, H.; Cohen, T. Explaining the spread in measurement of PDMS elastic properties: Influence of test method and curing protocol. *Soft Matter* **2024**, *20*, 9174–9183. [CrossRef] [PubMed]
19. Teixeira, I.; Castro, I.; Carvalho, V.; Rodrigues, C.; Souza, A.; Lima, R.; Teixeira, S.; Ribeiro, J. Polydimethylsiloxane mechanical properties: A systematic review. *AIMS Mater. Sci.* **2021**, *8*, 952–973. [CrossRef]
20. White, F.M. *Fluid Mechanics*, 9th ed.; McGraw-Hill Education: New York, NY, USA, 2021; ISBN 978-1260575762.
21. Gervais, T.; El-Ali, J.; Günther, A.; Jensen, K.F. Flow-induced deformation of shallow microfluidic channels. *Lab Chip* **2006**, *6*, 500–507. [CrossRef] [PubMed]
22. Tupin, S.; Saqr, K.M.; Ohta, M. Effects of wall compliance on multiharmonic pulsatile flow in idealized cerebral aneurysm models: Comparative PIV experiments. *Exp. Fluids* **2020**, *61*, 164. [CrossRef]

23. Raj, A.; Sen, A.K. Flow-induced deformation of compliant microchannels and its effect on pressure–flow characteristics. *Microfluid. Nanofluid* **2016**, *20*, 31. [CrossRef]
24. Christov, I.C.; Cognet, V.; Shidhore, T.C.; Stone, H.A. Flow rate–pressure drop relation for deformable shallow microfluidic channels. *J. Fluid Mech.* **2018**, *841*, 267–286. [CrossRef]
25. Lavanchy, F.; Sasaki, Y.; Minami, T.; Chevalier, S. Operando Measurements of Pressure-Based PDMS Deformations in Electrochemical Microfluidic Devices. *J. Electrochem. Soc.* **2026**, *173*, 5. [CrossRef]
26. Berthier, E.; Young, E.W.K.; Beebe, D. Engineers are from PDMS-land, Biologists are from Polystyrenia. *Lab Chip* **2012**, *12*, 1224–1237. [CrossRef] [PubMed]
27. Sreekantan, S.; Hassan, M.; Sundera Murthe, S.; Seeni, A. Biocompatibility and Cytotoxicity Study of Polydimethylsiloxane (PDMS) and Palm Oil Fuel Ash (POFA) Sustainable Super-Hydrophobic Coating for Biomedical Applications. *Polymers* **2020**, *12*, 3034. [CrossRef] [PubMed]
28. Sackmann, E.; Fulton, A.; Beebe, D. The present and future role of microfluidics in biomedical research. *Nature* **2014**, *507*, 181–189. [CrossRef] [PubMed]
29. Clarson, S.J.; Semlyen, J.A. (Eds.) *Siloxane Polymers*; Prentice Hall: Englewood Cliffs, NJ, USA, 1993.
30. Torres-Alvarez, D.; Aguirre-Soto, A. Polydimethylsiloxane chemistry for the fabrication of microfluidics—Perspective on its uniqueness, limitations and alternatives. *Mater. Today Proc.* **2022**, *48*, 88–95. [CrossRef]
31. Wong, I.; Ho, C.M. Surface molecular property modifications for poly(dimethylsiloxane) (PDMS) based microfluidic devices. *Microfluid. Nanofluid* **2009**, *7*, 291–306. [CrossRef] [PubMed]
32. Bhattacharya, S.; Datta, A.; Berg, J.; Gangopadhyay, S. Studies on surface wettability of poly(dimethyl) siloxane (PDMS) and glass under oxygen-plasma treatment and correlation with bond strength. *J. Microelectromechanical Syst.* **2005**, *14*, 590–597. [CrossRef]
33. Liu, X.; Zhou, J.; Yan, R.; Tang, T.; Wei, S.; Li, R.; Hou, D.; Weng, Y.; Wang, D.; Shen, H.; et al. An optimized PDMS microfluidic device for ultra-fast and high-throughput imaging flow cytometry. *Lab Chip* **2023**, *23*, 3571–3580. [CrossRef] [PubMed]
34. Brown, X.Q.; Ookawa, K.; Wong, J.Y. Evaluation of polydimethylsiloxane scaffolds with physiologically-relevant elastic moduli: Interplay of substrate mechanics and surface chemistry effects on vascular smooth muscle cell response. *Biomaterials* **2005**, *26*, 3123–3129. [CrossRef] [PubMed]
35. Gonçalves, M.; Gonçalves, I.M.; Borges, J.; Faustino, V.; Soares, D.; Vaz, F.; Minas, G.; Lima, R.; Pinho, D. Polydimethylsiloxane Surface Modification of Microfluidic Devices for Blood Plasma Separation. *Polymers* **2024**, *16*, 1416. [CrossRef] [PubMed]
36. Gökaltun, A.; Abraham Kang, Y.B.; Yarmush, M.L.; Usta, O.B.; Asatekin, A. Simple Surface Modification of Poly(dimethylsiloxane) via Surface Segregating Smart Polymers for Biomicrofluidics. *Sci. Rep.* **2019**, *9*, 7377. [CrossRef] [PubMed]
37. Gómez-Varela, A.I.; Viña, A.; Bao-Varela, C.; Flores-Arias, M.T.; Carnero, B.; González-Peteiro, M.; González-Juanatey, J.R.; Álvarez, E. Biocompatibility Testing of UV-Curable Polydimethylsiloxane for Human Umbilical Vein Endothelial Cell Culture on-a-Chip. *ACS Omega* **2024**, *9*, 30281–30293. [CrossRef] [PubMed]
38. Gomez-Sjoberg, R.; Leyrat, A.A.; Houseman, B.T.; Shokat, K.; Quake, S.R. Biocompatibility and Reduced Drug Absorption of Sol−Gel-Treated Poly (dimethyl siloxane) for Microfluidic Cell Culture Applications. *Anal. Chem.* **2010**, *82*, 8954–8960. [CrossRef] [PubMed]
39. Xia, Y.; Chu, X.; Zhao, C.; Wang, N.; Yu, J.; Jin, Y.; Sun, L.; Ma, S. A Glass-Ultra-Thin PDMS Film-Glass Microfluidic Device for Digital PCR Application Based on Flexible Mold Peel-Off Process. *Micromachines* **2022**, *13*, 1667. [CrossRef] [PubMed]
40. Yao, K.; Kelly, S. Replicable 2.5D PDMS microfluidics with precision nanoscale features expand the dimensions of pore-scale flow studies. *Soft Matter* **2026**, *22*, 2466–2473. [CrossRef] [PubMed]
41. Bento, D.; Lopes, S.; Maia, I.; Lima, R.; Miranda, J.M. Bubbles Moving in Blood Flow in a Microchannel Network: The Effect on the Local Hematocrit. *Micromachines* **2020**, *11*, 344. [CrossRef] [PubMed]
42. Menon, N.V.; Su, C.; Pang, K.T.; Phua, Z.J.; Tay, H.M.; Dalan, R.; Wang, X.; Li, K.H.H.; Hou, H.W. Recapitulating atherogenic flow disturbances and vascular inflammation in a perfusable 3D stenosis model. *Biofabrication* **2020**, *12*, 4. [CrossRef] [PubMed]
43. Peng, R.; Li, D. Fabrication of polydimethylsiloxane (PDMS) nanofluidic chips with controllable channel size and spacing. *Lab Chip* **2016**, *16*, 3767–3776. [CrossRef] [PubMed]
44. Carugo, D.; Lee, J.Y.; Pora, A.; Browning, R.J.; Capretto, L.; Nastruzzi, C.; Stride, E. Facile and cost-effective production of microscale PDMS architectures using a combined micromilling-replica molding (μMi-REM) technique. *Biomed. Microdevices* **2016**, *18*, 4. [CrossRef] [PubMed]
45. Folch, A.; Ayon, A.; Hurtado, O.; Schmidt, M.A.; Toner, M. Molding of Deep Polydimethylsiloxane Microstructures for Microfluidics and Biological Applications. *ASME J. Biomech. Eng.* **1999**, *121*, 28–34. [CrossRef] [PubMed]
46. Chen, C.-f.; Wharton, K. Characterization and failure mode analyses of air plasma oxidized PDMS–PDMS bonding by peel testing. *RSC Adv.* **2017**, *7*, 1286–1289. [CrossRef]
47. Chai, H.; Chen, F.; Song, Z.; Xiong, L.; Xiao, G.; Lu, Z.; Yu, L. A versatile wax assisted double replica molding and its application in flexible electronic skin. *Sens. Actuators B Chem.* **2021**, *343*, 130132. [CrossRef]

48. Unger, M.A.; Chou, H.-P.; Thorsen, T.; Scherer, A.; Quake, S.R. Monolithic Microfabricated Valves and Pumps by Multilayer Soft Lithography. *Science* **2000**, *288*, 113–116. [CrossRef] [PubMed]
49. Zhou, L.; Zhuang, G.; Li, G. A facile method for the fabrication of glass-PDMS-glass sandwich microfluidic devices by sacrificial molding. *Sens. Actuators B Chem.* **2018**, *261*, 364–371. [CrossRef]
50. Guler, M.T. Fabricating plasma bonded microfluidic chips by CO_2 laser machining of PDMS by the application of viscoelastic particle focusing and droplet generation. *J. Manuf. Process.* **2022**, *73*, 260–268. [CrossRef]
51. Su, W.; Li, Y.; Zhang, L.; Sun, J.; Liu, S.; Ding, X. Typography-Like 3D-Printed Templates for the Lithography-Free Fabrication of Microfluidic Chips. *SLAS Technol.* **2020**, *25*, 82–87. [CrossRef] [PubMed]
52. Hoang, T.; Truong, H.; Han, J.; Lee, S.; Lee, J.; Parajuli, S.; Lee, J.; Cho, G. Room temperature roll-to-roll additive manufacturing of polydimethylsiloxane-based centrifugal microfluidic device for on-site isolation of ribonucleic acid from whole blood. *Mater. Today Bio* **2023**, *23*, 100838. [CrossRef] [PubMed]
53. Díaz Lantada, A.; Resnick, J.; Mousa, J.; de Alba, M.Á.; Hengsbach, S.; Ramos Gómez, M. Rapid Prototyping of Biomedical Microsystems for Interacting at a Cellular Level. In *Microsystems for Enhanced Control of Cell Behavior. Studies in Mechanobiology. Tissue Engineering and Biomaterials*; Díaz Lantada, A., Ed.; Springer: Cham, Switzerland, 2016; Volume 18. [CrossRef]
54. Nguyen, T.; Sarkar, T.; Tran, T.; Moinuddin, S.M.; Saha, D.; Ahsan, F. Multilayer Soft Photolithography Fabrication of Microfluidic Devices Using a Custom-Built Wafer-Scale PDMS Slab Aligner and Cost-Efficient Equipment. *Micromachines* **2022**, *13*, 1357. [CrossRef] [PubMed]
55. Okuno, T.; Ito, K.; Funamoto, K.; Yoshino, D. Cell-cultured PDMS vascular model to allow placement of implant devices. *BMC Methods* **2026**, *3*, 16. [CrossRef]
56. Tůma, P. Casting of PDMS microfluidics into 3D printed moulds and their application in capillary electrophoresis. *Talanta* **2026**, *298*, 129037. [CrossRef] [PubMed]
57. Gonzalez, G.; Chiappone, A.; Dietliker, K.; Pirri, C.F.; Roppolo, I. Fabrication and Functionalization of 3D Printed Polydimethylsiloxane-Based Microfluidic Devices Obtained through Digital Light Processing. *Adv. Mater. Technol.* **2020**, *5*, 2000374. [CrossRef]
58. Dzikonski, D.; Bekker, E.; Zamboni, R.; Ciechanska, D.; Schwab, A.; Denz, C.; Imbrock, J. Hybrid Microfluidic Chip Design with Two-Photon Polymerized Protein-Based Hydrogel Microstructures for Single Cell Experiments. *Adv. Mater. Technol.* **2025**, *10*, 2401571. [CrossRef]
59. Kim, S.-Y.; Son, H.-B.; Lim, H.-R. One-Step Fabrication of Microfluidic Channels in Polydimethylsiloxane: Influence of Laser Power on Channel Formation. *Micromachines* **2025**, *16*, 282. [CrossRef] [PubMed]
60. Filion, R.; St-Georges-Robillard, A.; Chaudoir, H.; Ritch, S.; Ndongo, M.; Chua, X.Y.; Laurent, E.; Mes-Masson, A.-M.; Ajji, A.; Gervais, T. Mass fabrication of PDMS microfluidic devices by injection molding and applications in sensitive 3D spheroid and explant culture. *Sci. Rep.* **2025**, *15*, 33218. [CrossRef] [PubMed]
61. Jang, M.; Kwon, Y.J.; Lee, N.Y. Non-photolithographic plastic-mold-based fabrication of cylindrical and multi-tiered poly(dimethylsiloxane) microchannels for biomimetic lab-on-a-chip applications. *RSC Adv.* **2015**, *5*, 100905–100911. [CrossRef]
62. Chen, P.-C.; Zhang, R.-H.; Chen, L.-T. Using Micromachined Molds, Partial-curing PDMS Bonding Technique, and Multiple Casting to Create Hybrid Microfluidic Chip for Microlens Array. *Micromachines* **2019**, *10*, 572. [CrossRef] [PubMed]
63. Testa, G.; Persichetti, G.; Sarro, P.M.; Bernini, R. A hybrid silicon-PDMS optofluidic platform for sensing applications. *Biomed. Opt. Express* **2014**, *5*, 417–426. [CrossRef] [PubMed]
64. Stoecklein, D.; Di Carlo, D. Nonlinear Microfluidics. *Anal. Chem.* **2019**, *91*, 296–314. [CrossRef] [PubMed]
65. Bruus, H. *Theoretical Microfluidics*; Oxford Academic: Oxford, UK, 1997. [CrossRef]
66. Jo, B.-H.; Van Lerberghe, L.M.; Motsegood, K.M.; Beebe, D.J. Three-dimensional micro-channel fabrication in polydimethylsiloxane (PDMS) elastomer. *J. Microelectromechanical Syst.* **2000**, *9*, 76–81. [CrossRef]
67. Tovar-Lopez, F.; Thurgood, P.; Gilliam, C.; Nguyen, N.; Pirogova, E.; Khoshmanesh, K.; Baratchi, S. A Microfluidic System for Studying the Effects of Disturbed Flow on Endothelial Cells. *Front. Bioeng. Biotechnol.* **2019**, *7*, 81. [CrossRef] [PubMed]
68. Antonova, N.; Khristov, K. Microrheological and Microfluidic Approaches for Evaluation of the Mechanical Properties of Blood Cells. *Appl. Sci.* **2025**, *15*, 8291. [CrossRef]
69. Chien, S. Red Cell Deformability and its Relevance to Blood Flow. *Annu. Rev. Physiol.* **1987**, *49*, 177–192. [CrossRef] [PubMed]
70. Chien, S.; Sung, L. Molecular basis of red cell membrane rheology. Part 1. *Biorheology* **1990**, *27*, 327–344. [CrossRef] [PubMed]
71. Viallat, A.; Abkarian, M. Red blood cell: From its mechanics to its motion in shear flow. *Int. Jnl. Lab. Hem.* **2014**, *36*, 237–243. [CrossRef] [PubMed]
72. Chien, S. Chapter 26—Biophysical Behavior of Red Cells in Suspensions. In *The Red Blood Cell*, 2nd ed.; Surgenor, D.M., Ed.; Academic Press: Cambridge, MA, USA, 1975; pp. 1031–1133. [CrossRef]
73. Chien, S. Shear Dependence of Effective Cell Volume as a Determinant of Blood Viscosity. *Science* **1970**, *168*, 977–979. [CrossRef] [PubMed]

74. Chien, S.; Usami, S.; Skalak, R. Blood Flow in Small Tubes. In *American Physiological Society Handbook of Physiology, Section 2, The Cardiovascular System, 4*; Renkins, E.M., Michel, C.C., Eds.; American Physiological Society: Bethesda MD, USA, 1984; pp. 217–249.
75. Connes, P.; Nader, E. Blood Rheology: Key Parameters and Impact on Blood Flow. In *Handbook of Red Blood Cells*; Kaestner, L., Bogdanova, A., Eds.; Springer: Cham, Switzerland, 2025. [CrossRef]
76. Kim, S.; Ong, P.K.; Yalcin, O.; Intaglietta, M.; Johson, P.C. The cell-free layer in microvascular blood flow. *Biorheology* **2009**, *46*, 181–189. [CrossRef] [PubMed]
77. Fedosov, D.A.; Caswell, B.; Karniadakis, G.E. A multiscale red blood cell model with accurate mechanics, rheology, and dynamics. *Biophys. J.* **2010**, *98*, 2215–2225. [CrossRef] [PubMed]
78. Merrill, E.W.; Benis, A.M.; Gilliland, E.R.; Sherwood, T.K.; Salzman, E.W. Pressure-flow relations of human blood in hollow fibers at low flow rates. *J. Appl. Physiol.* **1965**, *20*, 954–967. [CrossRef] [PubMed]
79. Yasuda, K.; Armstrong, R.C.; Cohen, R.E. Shear flow properties of concentrated solutions of linear and star branched polystyrenes. *Rheol. Acta* **1981**, *20*, 163–178. [CrossRef]
80. Quemada, D. Rheology of concentrated disperse systems and minimum energy dissipation principle. I. Viscosity–concentration relationship. *Rheol. Acta* **1977**, *16*, 82–94. [CrossRef]
81. Johnston, B.M.; Johnston, P.R.; Corney, S.; Kilpatrick, D. Non-Newtonian blood flow in human right coronary arteries: Steady state simulations. *J. Biomech.* **2004**, *37*, 709–720. [CrossRef] [PubMed]
82. Nouaman, M.; Darras, A.; Wagner, C.; Recktenwald, S.M. Confinement effect on the microcapillary flow and shape of red blood cells. *Biomicrofluidics* **2024**, *18*, 024104. [CrossRef] [PubMed]
83. Jain, A.; Munn, L.L. Determinants of Leukocyte Margination in Rectangular Microchannels. *PLoS ONE* **2009**, *4*, e7104. [CrossRef] [PubMed]
84. Souza, A.; Nobrega, G.; Neves, L.B.; Barbosa, F.; Ribeiro, J.; Ferrera, C.; Lima, R.A. Recent Advances of PDMS In Vitro Biomodels for Flow Visualizations and Measurements: From Macro to Nanoscale Applications. *Micromachines* **2024**, *15*, 1317. [CrossRef] [PubMed]
85. Rashidi, Y.; Wagner, C.; Recktenwald, S.M. Impact of sequential bifurcations on the cell-free layer of healthy and rigid red blood cells. *Lab Chip* **2025**, *25*, 5055–5064. [CrossRef] [PubMed]
86. Taylor, D.J.; Feher, J.; Halliday, I.; Hose, D.R.; Gosling, R.; Aubiniere-Robb, L.; Veer, M.v.; Keulards, D.; Tonino, P.A.L.; Rochette, M.; et al. Refining Our Understanding of the Flow Through Coronary Artery Branches; Revisiting Murray's Law in Human Epicardial Coronary Arteries. *Front. Physiol.* **2022**, *13*, 871912. [CrossRef] [PubMed]
87. Davidovits, P. Chapter 8—The Motion of Fluids. In *Physics in Biology and Medicine*, 5th ed.; Davidovits, P., Ed.; Academic Press: Cambridge, MA, USA, 2019; pp. 103–117. [CrossRef]
88. Xu, T.; Lizarralde-Iragorri, M.A.; Roman, J.; Ghasemi, R.; Lefèvre, J.-P.; Martincic, E.; Brousse, V.; Français, O.; El Nemer, W.; Le Pioufle, B. Characterization of red blood cell microcirculatory parameters using a bioimpedance microfluidic device. *Sci. Rep.* **2020**, *10*, 9869. [CrossRef] [PubMed]
89. Reinhart, W.H.; Piety, N.Z.; Shevkoplyas, S.S. Influence of feeding hematocrit and perfusion pressure on hematocrit reduction (Fåhræus effect) in an artificial microvascular network. *Microcirculation* **2017**, *24*, e12396. [CrossRef] [PubMed]
90. Fenech, M.; Girod, V.; Claveria, V.; Meance, S.; Abkarian, M.; Charlot, B. Microfluidic blood vasculature replicas using backside lithography. *Lab Chip* **2019**, *19*, 2096–2106. [CrossRef] [PubMed]
91. Pries, A.R.; Secomb, T.W. Microvascular blood viscosity in vivo and the endothelial surface layer. *Am. J. Physiol. Heart Circ. Physiol.* **2005**, *289*, H2657–H2664. [CrossRef] [PubMed]
92. Popel, A.S.; Johnson, P.C. Microcirculation and Hemorheology. *Annu. Rev. Fluid. Mech.* **2005**, *37*, 43–69. [CrossRef] [PubMed]
93. Shen, F.; Li, Z.; Ai, M.; Gao, H.; Liu, Z. Round cavity-based vortex sorting of particles with enhanced holding capacity. *Phys. Fluids* **2021**, *33*, 082002. [CrossRef]
94. Shayor, A.A.; Kabir, M.E.; Rifath, M.S.A.; Rashid, A.B.; Oh, K.W. A Synergistic Overview between Microfluidics and Numerical Research for Vascular Flow and Pathological Investigations. *Sensors* **2024**, *24*, 5872. [CrossRef] [PubMed]
95. Tomaiuolo, G. Biomechanical properties of red blood cells in health and disease towards microfluidics. *Biomicrofluidics* **2014**, *8*, 051501. [CrossRef] [PubMed]
96. Sosa, J.M.; Nielsen, N.D.; Vignes, S.M.; Chen, T.G.; Shevkoplyas, S.S. The relationship between red blood cell deformability metrics and perfusion of an artificial microvascular network. *Clin. Hemorheol. Microcirc.* **2014**, *57*, 275–289. [CrossRef] [PubMed]
97. Hou, H.W.; Bhagat, A.A.; Chong, A.G.; Mao, P.; Tan, K.S.; Han, J.; Lim, C.T. Deformability based cell margination–a simple microfluidic design for malaria-infected erythrocyte separation. *Lab Chip* **2010**, *10*, 2605–2613. [CrossRef] [PubMed]
98. Lee, T.R.; Yoo, S.S.; Yang, J. Generalized plasma skimming model for cells and drug carriers in the microvasculature. *Biomech. Model. Mechanobiol.* **2017**, *16*, 497–507. [CrossRef] [PubMed]
99. Tripathi, S.; Kumar, Y.V.B.V.; Prabakhar, A.; Joshi, S.S.; Agrawal, A. Passive blood plasma separation at the microscale: A review of design principles and microdevices. *J. Micromech. Microeng.* **2015**, *25*, 083001. [CrossRef]

100. Yang, S.; Undar, A.; Zahn, J.D. A microfluidic device for continuous, real time blood plasma separation. *Lab Chip* **2006**, *6*, 871–880. [CrossRef] [PubMed]
101. Bakhtiaridoost, S.; Habibiyan, H.; Ghafoorifard, H. A microfluidic device to separate high-quality plasma from undiluted whole blood sample using an enhanced gravitational sedimentation mechanism. *Anal. Chim. Acta* **2023**, *1239*, 340641. [CrossRef] [PubMed]
102. Liu, S.C.; Yoo, P.B.; Garg, N.; Lee, A.P.; Rasheed, S. A microfluidic device for blood plasma separation and fluorescence detection of biomarkers using acoustic microstreaming. *Sens. Actuators A Phys.* **2021**, *317*, 112482. [CrossRef]
103. Chen, Y.; Li, D.; Li, Y.; Wan, J.; Li, J.; Chen, H. Margination of Stiffened Red Blood Cells Regulated by Vessel Geometry. *Sci. Rep.* **2017**, *7*, 15253. [CrossRef] [PubMed]
104. Akther, F.; Yakob, S.B.; Nguyen, N.-T.; Ta, H.T. Surface Modification Techniques for Endothelial Cell Seeding in PDMS Microfluidic Devices. *Biosensors* **2020**, *10*, 182. [CrossRef] [PubMed]
105. Bischel, L.L.; Sung, K.E.; Jiménez-Torres, J.A.; Mader, B.; Keely, P.J.; Beebe, D.J. The importance of being a lumen. *FASEB J.* **2014**, *28*, 4583–4590. [CrossRef] [PubMed]
106. Lima, R.; Wada, S.; Tanaka, S.; Takeda, M.; Ishikawa, T.; Tsubota, K.-I.; Imai, Y.; Yamaguchi, T. In vitro blood flow in a rectangular PDMS microchannel: Experimental observations using a confocal micro-PIV system. *Biomed. Microdevices* **2008**, *10*, 153–167. [CrossRef] [PubMed]
107. Wang, C.K.; Liao, W.H.; Wu, H.M.; Tung, Y.C. One-Step Approach to Fabricating Polydimethylsiloxane Microfluidic Channels of Different Geometric Sections by Sequential Wet Etching Processes. *J. Vis. Exp.* **2018**, *139*, 57868. [CrossRef] [PubMed]
108. Mane, S.; Hemadri, V.; Tripathi, S. Margination of white blood cells within straight and curved microchannels. *AIP Conf. Proc.* **2023**, *2584*, 060006. [CrossRef]
109. Zhang, Z.; Hou, T.; Ren, Y.; Wang, C.; Wang, Z.; Pan, H.; Li, P.; Smith, R.; Wang, J. Real-time embedded pressure and flow rate sensor in polydimethylsiloxane-based microchannel using fiber Bragg grating technique. *Flow Meas. Instrum.* **2024**, *96*, 102551. [CrossRef]
110. Dupuy, A.; Ju, L.A.; Passam, F.H. Straight Channel Microfluidic Chips for the Study of Platelet Adhesion under Flow. *Bio Protoc.* **2019**, *9*, e3195. [CrossRef] [PubMed]
111. Chu, P.-Y.; Hsieh, H.-Y.; Chung, P.-S.; Wang, P.-W.; Wu, M.-C.; Chen, Y.-Q.; Kuo, J.-C.; Fan, Y.-J. Development of vessel mimicking microfluidic device for studying mechano-response of endothelial cells. *iScience* **2023**, *26*, 106927. [CrossRef] [PubMed]
112. Zervantonakis, I.K.; Hughes-Alford, S.K.; Charest, J.L.; Condeelis, J.S.; Gertler, F.B.; Kamm, R.D. Three-dimensional microfluidic model for tumor cell intravasation and endothelial barrier function. *Proc. Natl. Acad. Sci. USA* **2012**, *109*, 13515–13520. [CrossRef] [PubMed]
113. Nagashima, S.; Hasebe, T.; Hotta, A.; Suzuki, T. Endothelial cell adhesion and proliferation on wrinkled diamond-like carbon films on grooved PDMS substrates. *RSC Appl. Interfaces* **2026**, *3*, 1409–1414. [CrossRef]
114. Yadhuraj, S.R.; Gandla, S.B.; Omprakash, S.S.; Sudarshan, B.G.; Kumar, S.C.P. Design and Development of Micro-channel using PDMS for Biomedical Applications. *Mater. Today Proc.* **2018**, *5*, 21392–21397. [CrossRef]
115. Hsu, C.-H.; Chen, T.-W.; Soong, W.-J.; Chen, C. Independent parallel production of tunable blood clot analogues in hourglass-profiled circular PDMS fluidic channels. *Lab Chip* **2026**, *26*, 3425–3434. [CrossRef] [PubMed]
116. Elham, K.; Andrea, F.; Antoni, L.M.J.; Simin, N.; Jasmina, C.T.; Luigi, M.S.; Behrouz, A. Capillary microfluidics for diagnostic applications: Fundamentals, mechanisms, and capillarics. *Front. Lab A Chip Technol.* **2025**, *4*, 1502127. [CrossRef]
117. Richmond, T.; Tompkins, N. 3D microfluidics in PDMS: Manufacturing with 3D molding. *Microfluid. Nanofluid* **2021**, *25*, 76. [CrossRef]
118. Higgins, J.M.; Eddington, D.T.; Bhatia, S.N.; Mahadevan, L. Sickle cell vasoocclusion and rescue in a microfluidic device. *Proc. Natl. Acad. Sci. USA* **2007**, *104*, 20496–20500. [CrossRef] [PubMed]
119. Kim, Y.C.; Kim, S.-H.; Kim, D.; Park, S.-J.; Park, J.-K. Plasma extraction in a capillary-driven microfluidic device using surfactant-added poly(dimethylsiloxane). *Sens. Actuators B Chem.* **2010**, *145*, 861–868. [CrossRef]
120. Souza, A.; Souza, M.S.; Ferrera, C.; Puga, H.; Lima, R.; Ribeiro, J. Flow Visualizations in a PDMS Cerebral Aneurysm Biomodel. In *Innovations in Mechanical Engineering II. Icieng 2022*; Machado, J., Soares, F., Trojanowska, J., Ottaviano, E., Valášek, P., Reddy D., M., Perondi, E.A., Basova, Y., Eds.; Lecture Notes in Mechanical Engineering; Springer: Cham, Switzerland, 2023. [CrossRef]
121. Stathoulopoulos, A.; Passos, A.; Kaliviotis, E.; Balabani, S. Partitioning of dense RBC suspensions in single microfluidic bifurcations: Role of cell deformability and bifurcation angle. *Sci. Rep.* **2024**, *14*, 535. [CrossRef] [PubMed]
122. Aye, S.S.S.; Fang, Z.; Wu, M.C.L.; Lim, K.S.; Ju, L.A. Integrating microfluidics, hydrogels, and 3D bioprinting for personalized vessel-on-a-chip platforms. *Biomater. Sci.* **2025**, *13*, 1131–1160. [CrossRef] [PubMed]
123. Tataranu, L.G.; Munteanu, O.; Kamel, A.; Gheorghita, K.L.; Rizea, R.E. Advancements in Brain Aneurysm Management: Integrating Neuroanatomy, Physiopathology, and Neurosurgical Techniques. *Medicina* **2024**, *60*, 1820. [CrossRef] [PubMed]
124. Shen, F.; Lu, X.; Pang, Y.; Liu, Z. Experimental study on transient flow patterns in simplified saccular intracranial aneurysm models using particle image velocimetry. *Acta Mech. Sin.* **2022**, *38*, 322162. [CrossRef]

125. Cernik, M.; Poláková, K.; Kubala, L.; Wunschová, A.V.; Danylevska, A.M.G.; Peskova, M.; Vitecek, J. Luminal Surface Plasma Treatment of Closed Cylindrical Microchannels: A Tool toward the Creation of On-Chip Vascular Endothelium. *ACS Biomater. Sci. Eng.* **2023**, *9*, 2755–2763. [CrossRef] [PubMed]
126. Duchamp, M.; Bakht, S.M.; Ju, J.; Yazdi, I.K.; Zhang, W.; Zhang, Y.S. Perforated and Endothelialized Elastomeric Tubes for Vascular Modeling. *Adv. Mater. Technol.* **2019**, *4*, 1800741. [CrossRef] [PubMed]
127. Teh, Y.; Lin, R.; Hung, L.-H.; Lee, A.P. Droplet microfluidics. *Lab Chip* **2008**, *8*, 198–220. [CrossRef] [PubMed]
128. Choi, W.; Park, J.H.; Byeon, H.; Lee, S.J. Flow characteristics around a deformable stenosis under pulsatile flow condition. *Phys. Fluids* **2018**, *30*, 011902. [CrossRef]
129. Tomaiuolo, G.; Simeone, M.; Martinelli, V.; Rotoli, B.; Guido, S. Red blood cell deformation in microconfined flow. *Soft Matter* **2009**, *5*, 3736–3740. [CrossRef]
130. Zhou, Q.; Fidalgo, J.; Bernabeu, M.O.; Oliveira, M.S.N.; Krüger, T. Emergent cell-free layer asymmetry and biased haematocrit partition in a biomimetic vascular network of successive bifurcations. *Soft Matter* **2021**, *17*, 3619–3633. [CrossRef] [PubMed]
131. Xu, X.; Qiu, Y.; Chen, C.-Y.; Carton, M.; Campbell, P.M.R.; Chowdhury, A.M.; Bandyopadhyay, B.C.; Bentley, W.E.; Smith, B.R.; Sochol, R.D. 3D nanoprinting of PDMS microvessels with tailored tortuosity and microporosity via direct laser writing. *Lab Chip* **2025**, *25*, 1947–1958. [CrossRef] [PubMed]
132. Yue, T.; Zhao, D.; Phan, D.T.T.; Wang, X.; Park, J.J.; Biviji, Z.; Hughes, C.C.W.; Lee, A.P. A modular microfluidic system based on a multilayered configuration to generate large-scale perfusable microvascular networks. *Microsyst. Nanoeng.* **2021**, *7*, 4. [CrossRef] [PubMed]
133. Shin, M.; Matsuda, K.; Ishii, O.; Terai, H.; Kaazempur-Mofrad, M.; Borenstein, J.; Detmar, M.; Vacanti, J.P. Endothelialized Networks with a Vascular Geometry in Microfabricated Poly (dimethyl siloxane). *Biomed. Microdevices* **2004**, *6*, 269–278. [CrossRef] [PubMed]
134. Zheng, Y.; Chen, J.; Craven, M.; Choi, N.W.; Totorica, S.; Diaz-Santana, A.; Kermani, P.; Hempstead, B.; Fischbach-Teschl, C.; López, J.A.; et al. In vitro microvessels for the study of angiogenesis and thrombosis. *Proc. Natl. Acad. Sci. USA* **2012**, *109*, 9342–9347. [CrossRef] [PubMed]
135. Pham Do, T.; Nguyen, T.; Huynh, K.; Nguyen, T. Fabrication of Circular Cross-section Microchannels with Stenosis via DLP 3D Printing and PDMS Membrane Inflation for Microfluidic Vascular Models. *J. Vis. Exp.* **2026**, *229*, e69706. [CrossRef] [PubMed]
136. Souza, A.; Lopes, D.; Souza, S.; Ribeiro, J.; Lima, R.; Ferrera, C. Experimental and numerical analyses of the hemodynamics impact on real intracranial aneurysms: A particle tracking approach. *Results Eng.* **2024**, *24*, 103566. [CrossRef]
137. Dibble, M.; Di Cio', S.; Luo, P.; Balkwill, F.; Gautrot, J.E. The impact of pericytes on the stability of microvascular networks in response to nanoparticles. *Sci. Rep.* **2023**, *13*, 5729. [CrossRef] [PubMed]
138. Shin, S.; Choi, Y.; Jang, W.; Ulziituya, B.; Ha, G.; Kang, R.; Park, S.; Kim, M.; Zhang, Y.S.; Kim, H.-J.; et al. A vascularized tumors-on-a-chip model for studying tumor-angiogenesis interplay, heterogeneity and drug responses. *Mater. Today Bio* **2025**, *32*, 101741. [CrossRef] [PubMed]
139. Nguyen, T.Q.; Park, W.-T. Fabrication method of multi-depth circular microchannels for investigating arterial thrombosis-on-a-chip. *Sens. Actuators B Chem.* **2020**, *321*, 128590. [CrossRef]
140. Liu, D.; Sun, M.; Zhang, J.; Hu, R.; Fu, W.; Xuanyuan, T.; Liu, W. Single-cell droplet microfluidics for biomedical applications. *Analyst* **2022**, *147*, 2294–2316. [CrossRef] [PubMed]
141. Jin, G.J.; Rahman, M.M.; Yoo, M.; Uddin, M.J.; Sarkar, B.; Shim, J.S. Wrist-wearable blood flow meter by biomimetically structured conductive PDMS composite. *Sens. Actuators A Phys.* **2025**, *393*, 116813. [CrossRef]
142. Siddique, A.; Pause, I.; Narayan, S.; Kruse, L.; Stark, R.W. Endothelialization of PDMS-based microfluidic devices under high shear stress conditions. *Colloids Surf. B Biointerfaces* **2021**, *197*, 111394. [CrossRef] [PubMed]
143. Cameron, T.C.; Randhawa, A.; Grist, S.M.; Bennet, T.; Hua, J.; Alde, L.G.; Caffrey, T.M.; Wellington, C.L.; Cheung, K.C. PDMS Organ-On-Chip Design and Fabrication: Strategies for Improving Fluidic Integration and Chip Robustness of Rapidly Prototyped Microfluidic In Vitro Models. *Micromachines* **2022**, *13*, 1573. [CrossRef] [PubMed]
144. Maia, R.; Sousa, P.; Pinto, V.; Soares, D.; Lima, R.; Minas, G.; Rodrigues, R.O. PDMS porous microneedles used as engineered tool in advanced microfluidic devices and their proof-of-concept for biomarker detection. *Chem. Eng. J.* **2024**, *485*, 149725. [CrossRef]
145. Song, S.; Lu, J.; Jiang, X.; Zhao, J.; Xiang, X.; Shang, Y. Droplet microfluidics for single-cell analysis: From improved cell encapsulation and sorting technologies to innovative applications. *Biotechnol. Adv.* **2026**, *87*, 108777. [CrossRef] [PubMed]
146. Bounab, Y.; Eyer, K.; Dixneuf, S.; Rybczynska, M.; Chauvel, C.; Mistretta, M.; Tran, T.; Aymerich, N.; Chenon, G.; Llitjos, J.-F.; et al. Dynamic single-cell phenotyping of immune cells using the microfluidic platform DropMap. *Nat. Protoc.* **2020**, *15*, 2920–2955. [CrossRef] [PubMed]
147. Ma, T.; Wang, Y.; Sun, S.; Pan, T.; Li, B.; Chu, J. Size-tunable droplet microfluidic system using an on-chip microfluidic peristaltic pump. *Sens. Actuators A Phys.* **2022**, *334*, 113332. [CrossRef]
148. Hintermüller, A.; Offenzeller, C.; Jakoby, B. A Microfluidic Viscometer with Capacitive Readout Using Screen-Printed Electrodes. *IEEE Sens. J.* **2021**, *21*, 2565–2572. [CrossRef]

149. Sun, J.; Han, K.; Xu, M.; Li, L.; Qian, J.; Li, L.; Li, X. Blood Viscosity in Subjects with Type 2 Diabetes Mellitus: Roles of Hyperglycemia and Elevated Plasma Fibrinogen. *Front. Physiol.* **2022**, *13*, 827428. [CrossRef] [PubMed]
150. Fan, D.; Liu, Y.; Liu, Y. The Latest Advances in Microfluidic DLD Cell Sorting Technology: The Optimization of Channel Design. *Biosensors* **2025**, *15*, 126. [CrossRef] [PubMed]
151. Zhang, J.; Tang, H.; Zhang, J.; Zhang, Z. Mesoscopic simulation of multi-scheme particle separation in deterministic lateral displacement devices using two-piece hybrid pillars. *J. Chromatogr. A* **2023**, *1711*, 464434. [CrossRef] [PubMed]
152. Wu, J.; Yan, Z.; He, Y.; Liu, J.; Lv, Y. Two-Dimensional Simulation on the Critical Diameter of Particles in Asymmetric I-Shaped DLD Arrays. *Micromachines* **2025**, *16*, 270. [CrossRef] [PubMed]
153. Zeming, K.K.; Vernekar, R.; Chua, M.T.; Quek, K.Y.; Sutton, G.; Krüger, T.; Kuan, W.S.; Han, J. Label-Free Biophysical Markers from Whole Blood Microfluidic Immune Profiling Reveal Severe Immune Response Signatures. *Small* **2021**, *17*, 2006123. [CrossRef] [PubMed]
154. Pandit, P.; Kong, L.; Samuel, G.L. Design and fabrication of a polydimethylsiloxane device for evaluating the effect of pillar geometry and configuration in the flow separation using deterministic lateral displacement. *RSC Adv.* **2024**, *14*, 1563–1575. [CrossRef] [PubMed]
155. Al-Fandi, M.; Al-Rousan, M.; Jaradat, M.A.; Al-Ebbini, L. New design for the separation of microorganisms using microfluidic deterministic lateral displacement. *Robot. Comput.-Integr. Manuf.* **2011**, *27*, 237–244. [CrossRef]
156. Chen, J.; Huang, X.; Xuan, W.; Sun, L. A 3D modeling framework for accurate trajectory-based prediction of critical diameter in deterministic lateral displacement microfluidics. *Microsyst. Nanoeng.* **2026**, *12*, 78. [CrossRef] [PubMed]
157. Qian, G.; Wang, L.; Wu, Z.; Wang, T.; Wan, S.; Zeng, J.; Sun, H.; Yan, H.; Shi, L.; Zhou, T. Coupling inertial effects and deterministic lateral displacement for high-purity microalgae separation in a microfluidic platform. *Chem. Eng. J.* **2025**, *526*, 170904. [CrossRef]
158. Dong, H.; Huang, L.; Zhao, L. Influence of the internal structure of straight microchannels on inertial transport behavior of particles. *Heliyon* **2024**, *10*, e29577. [CrossRef] [PubMed]
159. Tanriverdi, S.; Cruz, J.; Habibi, S.; Amini, K.; Costa, M.; Lundell, F.; Mårtensson, G.; Brandt, L.; Tammisola, O.; Russom, A. Elasto-inertial focusing and particle migration in high aspect ratio microchannels for high-throughput separation. *Microsyst. Nanoeng.* **2024**, *10*, 87. [CrossRef] [PubMed]
160. Bhagat, A.A.S.; Kuntaegowdanahalli, S.S.; Papautsky, I. Continuous particle separation in spiral microchannels using dean flows and differential migration. *Lab Chip* **2008**, *8*, 1906–1914. [CrossRef] [PubMed]
161. Yuan, D.; Sluyter, R.; Zhao, Q.; Tang, S.; Yan, S.; Yun, G.; Li, M.; Zhang, J.; Li, W. Dean-flow-coupled elasto-inertial particle and cell focusing in symmetric serpentine microchannels. *Microfluid. Nanofluid* **2019**, *23*, 41. [CrossRef]
162. Ozyilmaz, E.; Gediz Ilis, G. Design and Performance Analysis of Spiral Microchannels for Efficient Particle Separation Using Inertial Microfluidics. *Micromachines* **2025**, *16*, 349. [CrossRef] [PubMed]
163. Kuntaegowdanahalli, S.S.; Bhagat, A.A.S.; Kumar, G.; Papautsky, I. Inertial microfluidics for continuous particle separation in spiral microchannels. *Lab Chip* **2009**, *9*, 2973–2980. [CrossRef] [PubMed]
164. Nivedita, N.; Papautsky, I. Continuous separation of blood cells in spiral microfluidic devices. *Biomicrofluidics* **2013**, *7*, 54101. [CrossRef] [PubMed]
165. Kim, B.; Lee, S.; Kim, J.I.; Lee, D.H.; Koo, B.; Kim, S.; Ryu, S.; Kim, B.; Seo, M.; Jeong, J. Liquid Metal-Based Multimodal Wearable Sensor Platform Enabled by Highly Accessible Microfabrication of PDMS with Tuned Mechanical Properties. *Adv. Mater. Technol.* **2025**, *10*, 2400859. [CrossRef]
166. Sourani, S.; Bayareh, M. Manipulation of microparticles using acoustic actuators: A review. *Microfluid. Nanofluid* **2026**, *30*, 11. [CrossRef]
167. Li, P.; Mao, Z.; Peng, Z.; Zhou, L.; Chen, Y.; Huang, P.-H.; Truica, C.I.; Drabick, J.J.; El-Deiry, W.S.; Dao, M.; et al. Acoustic separation of circulating tumor cells. *Proc. Natl. Acad. Sci. USA* **2015**, *112*, 4970–4975. [CrossRef] [PubMed]
168. Song, H.; Rosano, J.M.; Wang, Y.; Garson, C.J.; Prabhakarpandian, B.; Pant, K.; Klarmann, G.J.; Perantoni, A.; Alvarez, L.M.; Lai, E. Continuous-flow sorting of stem cells and differentiation products based on dielectrophoresis. *Lab Chip* **2015**, *15*, 1320–1328. [CrossRef] [PubMed]
169. Noosawat, P.; Srituravanich, W.; Damrongplasit, N.; Suzuki, Y.; Kaewthamasorn, M.; Pimpin, A. A microfluidic device for capturing malaria-infected red blood cells by magnetophoretic force using an array of V- and W-shaped nickel microstructures. *Microfluid. Nanofluid* **2022**, *26*, 78. [CrossRef]
170. Khashan, S.; Odhah, A.A.; Taha, M.; Alazzam, A.; Al-Fandi, M. Enhanced microfluidic multi-target separation by positive and negative magnetophoresis. *Sci. Rep.* **2024**, *14*, 13293. [CrossRef] [PubMed]
171. Xie, P.; Yao, X.; Chu, Z.; Yang, Y.; Li, H.; Tan, S.; Tang, H.; Zhou, J.; Jin, W. Homoporous polydimethylsiloxane membrane microfilter for ultrafast label-free isolation and recognition of circulating tumor cells in peripheral blood. *iScience* **2023**, *26*, 108246. [CrossRef] [PubMed]
172. Ebrahimi, S.; Bagchi, P. A computational study of red blood cell deformability effect on hemodynamic alteration in capillary vessel networks. *Sci. Rep.* **2022**, *12*, 4304. [CrossRef] [PubMed]

173. Dixit, D.D.; Graf, T.P.; McHugh, K.J.; Lillehoj, P.B. Artificial intelligence-enabled microfluidic cytometer using gravity-driven slug flow for rapid CD4$^+$ T cell quantification in whole blood. *Microsyst. Nanoeng.* **2025**, *11*, 36. [CrossRef]
174. Hosokawa, K.; Ohmori, H. Digital PCR using a simple PDMS microfluidic chip and standard laboratory equipment. *Anal. Sci.* **2023**, *39*, 2067–2074. [CrossRef] [PubMed]
175. Chang, Y.-N.; Yao, D.-J. Development of a Microfluidic Viscometer for Non-Newtonian Blood Analog Fluid Analysis. *Bioengineering* **2024**, *11*, 1298. [CrossRef]
176. Kurkuri, M.D.; Al-Ejeh, F.; Shi, J.Y.; Palms, D.; Prestidge, C.; Griesser, H.J.; Brown, M.P.; Thierry, B. Plasma functionalized PDMS microfluidic chips: Towards point-of-care capture of circulating tumor cells. *J. Mater. Chem.* **2011**, *21*, 8841–8848. [CrossRef]
177. Yan, R.; Wei, S.; Weng, Y.; Li, R.; Jin, Y.; Liu, X.; Hou, J.; Xu, Y.; Li, S.; Wang, D.; et al. Rapid-manufacturing and cost-effective single-layer microfluidic device for high-throughput three-dimensional hydrodynamic focusing. *Microsyst. Nanoeng.* **2026**, *12*, 87. [CrossRef] [PubMed]
178. Darboui, M.; Fatehi, M.; Zareifar, R.; Tolgari, H.R.T.; Khoshmardan, H.E. Multi-level DLD microfluidic chip for plasma separation: A novel approach using Cu-ACE. *Results Phys.* **2025**, *71*, 108209. [CrossRef]
179. Rossi, J.M.; Diamond, S.L. Scalable manufacture of a disposable, storage-stable eight-channel microfluidic device for rapid testing of platelet, coagulation, and drug function under whole blood flow. *Biomicrofluidics* **2020**, *14*, 054103. [CrossRef] [PubMed]
180. Neeves, K.B.; Illing, D.A.R.; Diamond, S.L. Thrombin Flux and Wall Shear Rate Regulate Fibrin Fiber Deposition State during Polymerization under Flow. *Biophys. J.* **2010**, *98*, 1344–1352. [CrossRef]
181. Boas, L.V.; Faustino, V.; Lima, R.; Miranda, J.M.; Minas, G.; Fernandes, C.S.V.; Catarino, S.O. Assessment of the Deformability and Velocity of Healthy and Artificially Impaired Red Blood Cells in Narrow Polydimethylsiloxane (PDMS) Microchannels. *Micromachines* **2018**, *9*, 384. [CrossRef] [PubMed]
182. Condelipes, P.G.M.; Petrou, I.; Iria, I.; Gonçalves, J.; Santos, R.; Chu, V.; Conde, J.P. Microfluidic capillary platform with hydrophilic PDMS for point-of-care immunoassays. *Sens. Actuators B Chem.* **2025**, *423*, 136831. [CrossRef]
183. Açıkgöz, H.N.; Karaman, A.; Şahin, M.A.; Çaylan, Ö.R.; Büke, G.C.; Yıldırım, E.; Eroğlu, İ.C.; Erson-Bensan, A.E.; Çetin, B.; Özer, M.B. Assessment of silicon, glass, FR4, PDMS and PMMA as a chip material for acoustic particle/cell manipulation in microfluidics. *Ultrasonics* **2023**, *129*, 106911. [CrossRef] [PubMed]
184. Lin, B.-S.; Yang, Y.-C.; Ho, C.-Y.; Yang, H.-Y.; Wang, H.-Y. A PDMS-Based Cylindrical Hybrid Lens for Enhanced Fluorescence Detection in Microfluidic Systems. *Sensors* **2014**, *14*, 2967–2980. [CrossRef]
185. Shrirao, A.B.; Fritz, Z.; Novik, E.M.; Yarmush, G.M.; Schloss, R.S.; Zahn, J.D.; Yarmush, M.L. Microfluid flow cytometry: The role of microfabrication methodologies, performance and functional specification. *Technology* **2018**, *6*, 1–23. [CrossRef] [PubMed]
186. Zeng, N.F.; Mancuso, J.E.; Zivkovic, A.M.; Smilowitz, J.T.; Ristenpart, W.D. Red Blood Cells from Individuals with Abdominal Obesity or Metabolic Abnormalities Exhibit Less Deformability upon Entering a Constriction. *PLoS ONE* **2016**, *11*, e0156070. [CrossRef] [PubMed]
187. Pinho, D.; Muñoz-Sánchez, B.N.; Anes, C.F.; Vega, E.J.; Lima, R. Flexible PDMS microparticles to mimic RBCs in blood particulate analogue fluids. *Mech. Res. Commun.* **2019**, *100*, 103399. [CrossRef]
188. Wagner, C.; Steffen, P.; Svetina, S. Aggregation of red blood cells: From rouleaux to clot formation. *Comptes Rendus Phys.* **2013**, *14*, 459–469. [CrossRef]
189. Baskurt, O.K.; Meiselman, H.J. Blood Rheology and Hemodynamics. *Semin. Thromb. Hemost.* **2003**, *29*, 435–450. [CrossRef] [PubMed]
190. Kang, Y.J. Periodic and simultaneous quantification of blood viscosity and red blood cell aggregation using a microfluidic platform under in-vitro closed-loop circulation. *Biomicrofluidics* **2018**, *12*, 024116. [CrossRef] [PubMed]
191. Merrill, E.W. Rheology of blood. *Physiol. Rev.* **1969**, *49*, 863–888. [CrossRef] [PubMed]
192. Kang, Y.J. Microfluidic-based measurement of RBC aggregation and the ESR using a driving syringe system. *Anal. Methods* **2018**, *10*, 1805–1816. [CrossRef]
193. Mehri, R.; Mavriplis, C.; Fenech, M. Red blood cell aggregates and their effect on non-Newtonian blood viscosity at low hematocrit in a two-fluid low shear rate microfluidic system. *PLoS ONE* **2018**, *13*, e0199911. [CrossRef] [PubMed]
194. Carneiro, J.; Doutel, E.; Campos, J.B.L.M.; Miranda, J.M. PDMS droplet formation and characterization by hydrodynamic flow focusing technique in a PDMS square microchannel. *J. Micromech. Microeng.* **2016**, *26*, 105013. [CrossRef]
195. Chen, Q.; Singh, N.; Schirrmann, K.; Zhou, Q.; Chernysvky, I.L.; Juel, A. Robust fabrication of ultra-soft tunable PDMS microcapsules as a biomimetic model for red blood cells. *Soft Matter* **2023**, *19*, 5249–5261. [CrossRef] [PubMed]
196. Skalak, R.; Chien, S. *Handbook of Bioengineering*; McGraw-Hill: Columbus, OH, USA, 1987.
197. Jang, T.; Poplawska, M.; Cimpeanu, E.; Mo, G.; Dutta, D.; Lim, S.H. Vaso-occlusive crisis in sickle cell disease: A vicious cycle of secondary events. *J. Transl. Med.* **2021**, *19*, 397. [CrossRef]
198. Pozrikidis, C. *Modeling and Simulation of Capsules and Biological Cells*; Chapman & Hall/CRC: Boca Raton, FL, USA, 2003.
199. Belyaev, A.V.; Panteleev, M.A.; Ataullakhanov, F.I. Threshold of Microvascular Occlusion: Injury Size Defines the Thrombosis Scenario. *Biophys. J.* **2015**, *109*, 450–456. [CrossRef] [PubMed]

200. Man, Y.; Kucukal, E.; An, R.; Watson, Q.D.; Bosch, J.; Zimmerman, P.A.; Little, J.A.; Gurkan, U.A. Microfluidic assessment of red blood cell mediated microvascular occlusion. *Lab Chip* **2020**, *20*, 2086–2099. [CrossRef]
201. Albers, H.J.; Passier, R.; van den Berg, A.; van der Meer, A.D. Automated Analysis of Platelet Aggregation on Cultured Endothelium in a Microfluidic Chip Perfused with Human Whole Blood. *Micromachines* **2019**, *10*, 781. [CrossRef]
202. Ye, T.; Shi, H.; Phan-Thien, N.; Lim, C.T. The key events of thrombus formation: Platelet adhesion and aggregation. *Biomech. Model. Mechanobiol.* **2020**, *19*, 943–955. [CrossRef] [PubMed]
203. Lin, J.; Chen, S.; Zhang, C.; Liao, J.; Chen, Y.; Deng, S.; Mao, Z.; Zhang, T.; Tian, N.; Song, Y.; et al. Recent advances in microfluidic technology of arterial thrombosis investigations. *Platelets* **2024**, *35*, 2316743. [CrossRef]
204. Springer, T.A. Biology and physics of von Willebrand factor concatamers. *J. Thromb. Haemost.* **2011**, *9*, 130–143. [CrossRef]
205. Zhang, Y.; Ramasundara, S.Z.; Preketes-Tardiani, R.E.; Cheng, V.; Lu, H.; Ju, L.A. Emerging Microfluidic Approaches for Platelet Mechanobiology and Interplay with Circulatory Systems. *Front. Cardiovasc. Med.* **2021**, *8*, 766513. [CrossRef] [PubMed]
206. Ansarizadeh, M.; Nguyen, H.-T.; Lazovic, B.; Kettunen, J.; De Silva, L.; Sivakumar, R.; Junttila, P.; Rissanen, S.-L.; Hicks, R.; Singh, P.; et al. Microfluidic vessel-on-chip platform for investigation of cellular defects in venous malformations and responses to various shear stress and flow conditions. *Lab Chip* **2025**, *25*, 613–630. [CrossRef] [PubMed]
207. Zilberman-Rudenko, J.; McCarty, O.J.T. Utility and development of microfluidic platforms for platelet research. *Platelets* **2017**, *28*, 425–426. [CrossRef] [PubMed]
208. Ethier, A.; Simmons, C.A. *Introductory Biomechanics: From Cells to Organisms*; Cambridge Texts in Biomedical Engineering; Cambridge University Press: Cambridge, UK, 2007.
209. Fischer, R.A. The Wave of Advance of Advantageous Genes. *Ann. Eugen.* **1937**, *7*, 355–369. [CrossRef]
210. Rahman, S.M.; Hlady, V. Microfluidic assay of antiplatelet agents for inhibition of shear-induced platelet adhesion and activation. *Lab Chip* **2021**, *21*, 174–183. [CrossRef]
211. Starikova, E.A.; Mammedova, J.T.; Rubinstein, A.A.; Sokolov, A.V.; Kudryavtsev, I.V. Activation of the Coagulation Cascade as a Universal Danger Sign. *Curr. Issues Mol. Biol.* **2025**, *47*, 108. [CrossRef]
212. Colace, T.V.; Tormoen, G.W.; McCarty, O.J.; Diamond, S.L. Microfluidics and coagulation biology. *Annu. Rev. Biomed. Eng.* **2013**, *15*, 283–303. [CrossRef] [PubMed]
213. Mussbacher, M.; Kral-Pointner, J.B.; Salzmann, M.; Schrottmaier, W.C.; Assinger, A. Mechanisms of Hemostasis: Contributions of Platelets, Coagulation Factors, and the Vessel Wall. In *Fundamentals of Vascular Biology. Learning Materials in Biosciences*; Geiger, M., Ed.; Springer: Cham, Switzerland, 2024. [CrossRef]
214. Guan, W.; Ma, F.; Luo, Y.; Han, C.; Su, F.; Xing, X. Deformable U-shaped microelectrodes made of carbon-PDMS for blood coagulation test. *Sens. Actuators B Chem.* **2025**, *443*, 138236. [CrossRef]
215. Fogelson, A.L.; Neeves, K.B. Fluid Mechanics of Blood Clot Formation. *Annu. Rev. Fluid Mech.* **2015**, *47*, 377–403. [CrossRef] [PubMed]
216. Neeves, K.B.; Diamond, S.L. A membrane-based microfluidic device for controlling the flux of platelet agonists into flowing blood. *Lab Chip* **2008**, *8*, 701–709. [CrossRef] [PubMed]
217. Westein, E.; Van der Meer, A.D.; Kuijpers, J.E.; Frimat, J.-P.; Van der Berg, A.; Heemskerk, J.W.M. Atherosclerotic Geometries Exacerbate Pathological Thrombus Formation Poststenosis in a von Willebrand Factor-Dependent Manner. *Proc. Natl. Acad. Sci. USA* **2013**, *110*, 1357–1362. [CrossRef] [PubMed]
218. Stalker, T.J.; Traxler, E.A.; Wu, J.; Wannemacher, K.M.; Cermignano, S.L.; Voronov, R.; Diamond, S.L.; Brass, L.F. Hierarchical organization in the hemostatic response and its relationship to the platelet-signaling network. *Blood* **2013**, *121*, 1875–1885. [CrossRef] [PubMed]
219. Nourshargh, S.; Alon, R. Leukocyte migration into inflamed tissues. *Immunity* **2014**, *41*, 694–707. [CrossRef] [PubMed]
220. Lai, A.; Zhou, Y.; Chheang, C.; Mirabedini, A.; Mirzaalikhan, Y.; Noonan, J.; Watson, A.; Dayawansa, N.H.; Huang, W.; Khanmohammadi, M.; et al. Decoding vascular aging: Substrate stiffness and shear stress orchestrate endothelial inflammation and remodelling via mechanosensitive pathways. *Biomaterials* **2026**, *329*, 123932. [CrossRef] [PubMed]
221. Hammer, D.A.; Apte, S.M. Simulation of cell rolling and adhesion on surfaces in shear flow: General results and analysis of selectin-mediated neutrophil adhesion. *Biophys. J.* **1992**, *63*, 35–57. [CrossRef] [PubMed]
222. Kourtzelis, I.; Mitroulis, I. Leukocyte Recruitment. In *Compendium of Inflammatory Diseases*; Parnham, M.J., Ed.; Springer: Basel, Switzerland, 2016. [CrossRef]
223. Hernández Vera, R.; O'Callaghan, P.; Fatsis-Kavalopoulos, N.; Kreuger, J. Modular microfluidic systems cast from 3D-printed molds for imaging leukocyte adherence to differentially treated endothelial cultures. *Sci. Rep.* **2019**, *9*, 11321. [CrossRef] [PubMed]
224. Sundd, P.; Gutierrez, E.; Koltsova, E.K.; Kuwano, Y.; Fukuda, S.; Pospieszalska, M.K.; Groisman, A.; Ley, K. 'Slings' enable neutrophil rolling at high shear. *Nature* **2012**, *488*, 399–403. [CrossRef] [PubMed]
225. Lämmermann, T.; Germain, R.N. The multiple faces of leukocyte interstitial migration. *Semin. Immunopathol.* **2014**, *36*, 227–251. [CrossRef] [PubMed]

226. Boneschansker, L.; Yan, J.; Wong, E.; Briscoe, D.M.; Irimia, D. Microfluidic platform for the quantitative analysis of leukocyte migration signatures. *Nat. Commun.* **2014**, *5*, 4787. [CrossRef] [PubMed]
227. Keller, E.F.; Segel, L.A. Initiation of slime mold aggregation viewed as an instability. *J. Theor. Biol.* **1970**, *26*, 399–415. [CrossRef] [PubMed]
228. Batchelor, G.K. *An Introduction to Fluid Dynamics*; Cambridge University Press: Cambridge, UK, 2000.
229. Irimia, D. Chapter 10—Cell Migration in Confined Environments. In *Methods in Cell Biology*; Piel, M., Théry, M., Eds.; Academic Press: Cambridge, MA, USA, 2014; Volume 121, pp. 141–153. [CrossRef] [PubMed]
230. Chung, S.; Sudo, R.; Mack, P.J.; Wan, C.R.; Vickerman, V.; Kamm, R.D. Cell migration into scaffolds under co-culture conditions in a microfluidic platform. *Lab Chip* **2009**, *9*, 269–275. [CrossRef] [PubMed]
231. Reátegui, E.; Jalali, F.; Khankhel, A.H.; Wong, E.; Cho, H.; Lee, J.; Serhan, C.N.; Dalli, J.; Elliott, H.; Irimia, D. Microscale arrays for the profiling of start and stop signals coordinating human-neutrophil swarming. *Nat. Biomed. Eng.* **2017**, *1*, 0094. [CrossRef] [PubMed]
232. Wu, X.; Xu, Y.; Zhao, X.; Mi, X. A Four-Channel Microfluidic Vascular-Wall Chip for Modeling Early Atherosclerosis-Related Endothelial Dysfunction and Evaluating Combined Anti-Inflammatory Treatment. *Micromachines* **2026**, *17*, 734. [CrossRef] [PubMed]
233. Bogseth, A.; Ramirez, A.; Vaughan, E.; Maisel, K. In Vitro Models of Blood and Lymphatic Vessels-Connecting Tissues and Immunity. *Adv. Biol.* **2023**, *7*, e2200041. [CrossRef] [PubMed]
234. Griep, L.M.; Wolbers, F.; de Wagenaar, B.; ter Braak, P.M.; Weksler, B.B.; Romero, I.A.; Couraud, P.O.; Vermes, I.; van der Meer, A.D.; van den Berg, A. BBB on chip: Microfluidic platform to mechanically and biochemically modulate blood-brain barrier function. *Biomed. Microdevices* **2013**, *15*, 145–150. [CrossRef] [PubMed]
235. Aoun, L.; Nègre, P.; Gonsales, C.; de Noray, V.S.; Brustlein, S.; Biarnes-Pelicot, M.; Valignat, M.-P.; Theodoly, O. Leukocyte transmigration and longitudinal forward-thrusting force in a microfluidic Transwell device. *Biophys. J.* **2021**, *120*, 2205–2221. [CrossRef] [PubMed]
236. Jalili-Firoozinezhad, S.; Gazzaniga, F.S.; Calamari, E.L.; Camacho, D.M.; Fadel, C.W.; Bein, A.; Swenor, B.; Nestor, B.; Cronce, M.J.; Tovaglieri, A.; et al. A complex human gut microbiome cultured in an anaerobic intestine-on-a-chip. *Nat. Biomed. Eng.* **2019**, *3*, 520–531. [CrossRef] [PubMed]
237. Bevilacqua, M.P. Endothelial-Leukocyte Adhesion Molecules. *Annu. Rev. Immunol.* **1993**, *11*, 767–804. [CrossRef] [PubMed]
238. Keller, E.F.; Segel, L.A. Model for chemotaxis. *J. Theor. Biol.* **1971**, *30*, 225–234. [CrossRef] [PubMed]
239. Lawrence, M.B.; Springer, T.A. Leukocytes roll on a selectin at physiologic flow rates: Distinction from and prerequisite for adhesion through integrins. *Cell* **1991**, *65*, 859–873. [CrossRef] [PubMed]
240. Lauffenburger, D.; Horwitz, A. Cell Migration: A Physically Integrated Molecular Process. *Cell* **1996**, *84*, 359–369. [CrossRef] [PubMed]
241. Jain, R.K. Transport of molecules across tumor vasculature. *Cancer Metast Rev.* **1987**, *6*, 559–593. [CrossRef] [PubMed]
242. Chumbimuni-Torres, K.Y.; Coronado, R.E.; Mfuh, A.M.; Castro-Guerrero, C.; Silva, M.F.; Negrete, G.R.; Bizios, R.; Garcia, C.D. Adsorption of proteins to thin-films of PDMS and its effect on the adhesion of human endothelial cells. *RSC Adv.* **2011**, *1*, 706–714. [CrossRef] [PubMed]
243. Kizhakkedathu, J.N.; Conway, E.M. Biomaterial and cellular implants: Foreign surfaces where immunity and coagulation meet. *Blood* **2022**, *139*, 1987–1998. [CrossRef] [PubMed]
244. Gennes, P.G.; Brochard-Wyart, F.; Quéré, D. *Capillarity and Wetting Phenomena: Drops, Bubbles, Pearls, Waves*; Springer: Berlin/Heidelberg, Germany, 2004.
245. Jahangiri, F.; Hakala, T.; Jokinen, V. Long-term hydrophilization of polydimethylsiloxane (PDMS) for capillary filling microfluidic chips. *Microfluid. Nanofluid* **2020**, *24*, 2. [CrossRef]
246. Ruben, B.; Elisa, M.; Leandro, L.; Victor, M.; Gloria, G.; Marina, S.; Mian, K.S.; Pandiyan, R.; Nadhira, L. Oxygen plasma treatments of polydimethylsiloxane surfaces: Effect of the atomic oxygen on capillary flow in the microchannels. *Micro Nano Lett.* **2017**, *12*, 754–757. [CrossRef]
247. Neves, L.B.; Afonso, I.S.; Nobrega, G.; Barbosa, L.G.; Lima, R.A.; Ribeiro, J.E. A Review of Methods to Modify the PDMS Surface Wettability and Their Applications. *Micromachines* **2024**, *15*, 670. [CrossRef] [PubMed]
248. Bento, D.; Sousa, L.; Yaginuma, T.; Garcia, V.; Lima, R.; Miranda, J.M. Microbubble moving in blood flow in microchannels: Effect on the cell-free layer and cell local concentration. *Biomed. Microdevices* **2017**, *19*, 6. [CrossRef] [PubMed]
249. Moramarco, T.; Dingman, S.L. On the theoretical velocity distribution and flow resistance in natural channels. *J. Hydrol.* **2017**, *555*, 777–785. [CrossRef]
250. Keiser, L.; Stamoulis, L.; Georjon, L.; Marmottant, P.; Dollet, B. Bubble removal in microfluidic channels surrounded by gas-permeable media: Experiments and a predictive model. *Lab Chip* **2025**, *25*, 5030–5042. [CrossRef] [PubMed]
251. Walker, G.M.; Beebe, D.J. A passive pumping method for microfluidic devices. *Lab Chip* **2002**, *2*, 131–134. [CrossRef] [PubMed]

252. Nesbitt, W.S.; Westein, E.; Tovar-Lopez, F.J.; Tolouei, E.; Mitchell, A.; Fu, J.; Carberry, J.; Fouras, A.; Jackson, S.P. A shear gradient-dependent platelet aggregation mechanism drives thrombus formation. *Nat. Med.* **2009**, *15*, 665–673. [CrossRef] [PubMed]
253. Crank, J. *The Mathematics of Diffusion*, 2nd ed.; Oxford University Press: Oxford, UK, 1979.
254. Finger, E.B.; Puri, K.D.; Alon, R.; Lawrence, M.B.; von Andrian, U.H.; Springer, T.A. Adhesion through L-selectin requires a threshold hydrodynamic shear. *Nature* **1996**, *379*, 266–269. [CrossRef] [PubMed]
255. Roach, L.S.; Song, H.; Ismagilov, R.F. Controlling Nonspecific Protein Adsorption in a Plug-Based Microfluidic System by Controlling Interfacial Chemistry Using Fluorous-Phase Surfactants. *Anal. Chem.* **2005**, *77*, 785–796. [CrossRef] [PubMed]
256. Liu, J.; Yao, Y.; Li, X.; Zhang, Z. Fabrication of advanced polydimethylsiloxane-based functional materials: Bulk modifications and surface functionalization. *Chem. Eng. J.* **2021**, *408*, 127262. [CrossRef]
257. Crago, M.; Lee, A.; Hoang, T.P.; Talebian, S.; Naficy, S. Protein adsorption on blood-contacting surfaces: A thermodynamic perspective to guide the design of antithrombogenic polymer coatings. *Acta Biomater.* **2024**, *180*, 46–60. [CrossRef] [PubMed]
258. Roh, C.; Lee, J.; Kang, C. The Deformation of Polydimethylsiloxane (PDMS) Microfluidic Channels Filled with Embedded Circular Obstacles under Certain Circumstances. *Molecules* **2016**, *21*, 798. [CrossRef] [PubMed]
259. Lee, J.-Y.; Yun, Y.-K.; Kim, Y.-R.; Jo, K.-B. PDMS Nanoslits without Roof Collapse. *Bull. Korean Chem. Soc.* **2009**, *30*, 1793–1797. [CrossRef]
260. Yao, J.; Guan, Y.; Park, Y.; Choi, Y.E.; Kim, H.S.; Park, J. Optimization of PTFE Coating on PDMS Surfaces for Inhibition of Hydrophobic Molecule Absorption for Increased Optical Detection Sensitivity. *Sensors* **2021**, *21*, 1754. [CrossRef] [PubMed]
261. Carter, S.-S.D.; Atif, A.-R.; Kadekar, S.; Lanekoff, I.; Engqvist, H.; Varghese, O.P.; Tenje, M.; Mestres, G. PDMS leaching and its implications for on-chip studies focusing on bone regeneration applications. *Organs-On-A-Chip* **2020**, *2*, 100004. [CrossRef]
262. Tsuzuki, T.; Baassiri, K.; Mahmoudi, Z.; Perumal, A.S.; Rajendran, K.; Rubies, G.M.; Nicolau, D.V. Hydrophobic Recovery of PDMS Surfaces in Contact with Hydrophilic Entities: Relevance to Biomedical Devices. *Materials* **2022**, *15*, 2313. [CrossRef] [PubMed]
263. "Mike Kim", M.; Huang, Y.; Choi, K.; Hidrovo, C.H. The improved resistance of PDMS to pressure-induced deformation and chemical solvent swelling for microfluidic devices. *Microelectron. Eng.* **2014**, *124*, 66–75. [CrossRef]
264. Liu, Y.; Zhang, L.; Wu, W.; Zhao, M.; Wang, W. Restraining non-specific adsorption of protein using Parylene C-caulked polydimethylsiloxane. *Biomicrofluidics* **2016**, *10*, 024126. [CrossRef] [PubMed]
265. Jiang, B.; Guo, H.; Chen, D.; Zhou, M. Microscale investigation on the wettability and bonding mechanism of oxygen plasma-treated PDMS microfluidic chip. *Appl. Surf. Sci.* **2022**, *574*, 151704. [CrossRef]
266. Johnston, I.D.; McCluskey, D.K.; Tan, C.K.L.; Tracey, M.C. Mechanical characterization of bulk Sylgard 184 for microfluidics and microengineering. *Micromech. Microeng.* **2014**, *24*, 035017. [CrossRef]
267. Gao, S.; Xu, T.; Wu, L.; Zhu, X.; Wang, X.; Jian, X.; Li, X. Overcoming bubble formation in polydimethylsiloxane-made PCR chips: Mechanism and elimination with a high-pressure liquid seal. *Microsyst. Nanoeng.* **2024**, *10*, 136. [CrossRef] [PubMed]
268. Grindulis, K.; Matusevica, N.G.; Kozlova, V.; Rimsa, R.; Klavins, K.; Mozolevskis, G. Sorption and release of small molecules in PDMS and COC for Organs on chip. *Sci. Rep.* **2025**, *15*, 14012. [CrossRef] [PubMed]
269. Shidhore, T.C.; Christov, I.C. Static response of deformable microchannels: A comparative modelling study. *J. Phys. Condens. Matter* **2018**, *30*, 5. [CrossRef] [PubMed]
270. Zhou, J.; Ellis, A.V.; Voelcker, N.H. Recent developments in PDMS surface modification for microfluidic devices. *Electrophoresis* **2010**, *31*, 2–16. [CrossRef] [PubMed]
271. Inglis, D.W. A method for reducing pressure-induced deformation in silicone microfluidics. *Biomicrofluidics* **2010**, *4*, 026504. [CrossRef] [PubMed]
272. Xia, Y.; Whitesides, G.M. Soft Lithography. *Angew. Chem. Int. Ed.* **1998**, *37*, 550–575. [CrossRef]
273. Zhang, S.; Staples, A.E. Effects of natural aging on hydrophilicity and mechanical properties of PDMS in various storage environments. *npj Mater. Degrad.* **2025**, *9*, 109. [CrossRef] [PubMed]
274. Morawska-Chochół, A.; Szumera, M.; Młyniec, A.; Pielichowska, K. The Effect of Aging Process Conditions on the Thermal Properties of Poly (Dimethylsiloxane)-Based Silicone Rubber. *Materials* **2024**, *17*, 5608. [CrossRef] [PubMed]
275. Mata, A.; Fleischman, A.J.; Roy, S. Characterization of polydimethylsiloxane (PDMS) properties for biomedical micro/Nanosystems. *Biomed. Microdevices* **2005**, *7*, 281–293. [CrossRef] [PubMed]
276. Kim, J.; Chaudhury, M.K.; Owen, M.J. Hydrophobic Recovery of Polydimethylsiloxane Elastomer Exposed to Partial Electrical Discharge. *J. Colloid Interface Sci.* **2000**, *226*, 231–236. [CrossRef]
277. Makamba, H.; Kim, J.H.; Lim, K.; Park, N.; Hahn, J.H. Surface modification of poly(dimethylsiloxane) microchannels. *Electrophoresis* **2003**, *24*, 3607–3619. [CrossRef] [PubMed]
278. Heo, Y.S.; Cabrera, L.M.; Song, J.W.; Futai, N.; Tung, Y.-C.; Smith, G.D.; Takayama, S. Characterization and Resolution of Evaporation-Mediated Osmolality Shifts That Constrain Microfluidic Cell Culture in Poly(dimethylsiloxane) Devices. *Anal. Chem.* **2007**, *79*, 1126–1134. [CrossRef] [PubMed]

279. Rodrigues, P.M.; Xavier, M.; Calero, V.; Pastrana, L.; Gonçalves, C. Partitioning of Small Hydrophobic Molecules into Polydimethylsiloxane in Microfluidic Analytical Devices. *Micromachines* **2022**, *13*, 713. [CrossRef] [PubMed]
280. van der Valk, J.; Brunner, D.; De Smet, K.; Svenningsen, Å.F.; Honegger, P.; Knudsen, L.E.; Lindl, T.; Noraberg, J.; Price, A.; Scarino, M.L.; et al. Optimization of chemically defined cell culture media–replacing fetal bovine serum in mammalian in vitro methods. *Toxicol. Vitr.* **2010**, *24*, 1053–1063. [CrossRef] [PubMed]
281. Wang, J.D.; Douville, N.J.; Takayama, S.; ElSayed, M. Quantitative Analysis of Molecular Absorption into PDMS Microfluidic Channels. *Ann. Biomed. Eng.* **2012**, *40*, 1862–1873. [CrossRef] [PubMed]
282. Firpo, G.; Angeli, E.; Repetto, L.; Valbusa, U. Permeability thickness dependence of polydimethylsiloxane (PDMS) membranes. *J. Membr. Sci.* **2015**, *481*, 1–8. [CrossRef]
283. Shiku, H.; Saito, T.; Wu, C.-C.; Yasukawa, T.; Yokoo, M.; Abe, H.; Matsue, T.; Yamada, H. Oxygen Permeability of Surface-modified Poly(dimethylsiloxane) Characterized by Scanning Electrochemical Microscopy. *Chem. Lett.* **2006**, *35*, 234–235. [CrossRef]
284. Bodas, D.; Khan-Malek, C. Hydrophilization and hydrophobic recovery of PDMS by oxygen plasma and chemical treatment—An SEM investigation. *Sens. Actuators B Chem.* **2007**, *123*, 368–373. [CrossRef]
285. Zhang, Z.; Wang, J.; Tu, Q.; Nie, N.; Sha, J.; Liu, W.; Liu, R.; Zhang, Y.; Wang, J. Surface modification of PDMS by surface-initiated atom transfer radical polymerization of water-soluble dendronized PEG methacrylate. *Colloids Surf. B Biointerfaces* **2011**, *88*, 85–92. [CrossRef] [PubMed]
286. Yu, L.; Li, C.M.; Zhou, Q.; Luong, J.H.T. Poly(vinyl alcohol) Functionalized Poly(dimethylsiloxane) Solid Surface for Immunoassay. *Bioconjugate Chem.* **2007**, *18*, 281–284. [CrossRef] [PubMed]
287. Sasaki, H.; Onoe, H.; Osaki, T.; Kawano, R.; Takeuchi, S. Parylene-coating in PDMS microfluidic channels prevents the absorption of fluorescent dyes. *Sens. Actuators B Chem.* **2010**, *150*, 478–482. [CrossRef]
288. Hill-West, J.L.; Chowdhury, S.M.; Slepian, M.J.; Hubbell, J.A. Inhibition of thrombosis and intimal thickening by in situ photopolymerization of thin hydrogel barriers. *Proc. Natl. Acad. Sci. USA* **1994**, *91*, 5967–5971. [CrossRef] [PubMed]
289. Wang, Y.; Chen, B.; Luo, X.; Feng, W.; Guo, T.; Gao, Y.; Bai, S.; Gao, P.; Xu, J.; Gao, Y.; et al. Covalently grafted PDMS chains enable UV-curable hyperbranched PUA coatings with synergistic omniphobicity and optical transparency. *Prog. Org. Coat.* **2026**, *211*, 109766. [CrossRef]
290. Silverio, V.; Canane, P.A.G.; Cardoso, S. Surface wettability and stability of chemically modified silicon, glass and polymeric surfaces via room temperature chemical vapor deposition. *Colloids Surf. A Physicochem. Eng. Asp.* **2019**, *570*, 210–217. [CrossRef]
291. Zhang, X.; Ye, H.; Xiao, B.; Yan, L.; Lv, H.; Jiang, B. Sol−Gel Preparation of PDMS/Silica Hybrid Antireflective Coatings with Controlled Thickness and Durable Antireflective Performance. *J. Phys. Chem. C* **2010**, *114*, 19979–19983. [CrossRef]
292. Aymerich, M.; Gómez-Varela, A.I.; Álvarez, E.; Flores-Arias, M.T. Study of Different Sol-Gel Coatings to Enhance the Lifetime of PDMS Devices: Evaluation of Their Biocompatibility. *Materials* **2016**, *9*, 728. [CrossRef] [PubMed]
293. Kim, S.-H.; Lee, S.; Ahn, D.; Park, J.Y. PDMS double casting method enabled by plasma treatment and alcohol passivation. *Sens. Actuators B Chem.* **2019**, *293*, 115–121. [CrossRef]
294. Gimenez, R.; Pérez-Sosa, C.; Bourguignon, N.; Miriuka, S.; Bhansali, S.; Arroyo, C.R.; Debut, A.; Lerner, B.; Pérez, M.S. Simple Microcontact Printing Technique to Obtain Cell Patterns by Lithography Using Grayscale, Photopolymer Flexographic Mold, and PDMS. *Biomimetics* **2022**, *7*, 155. [CrossRef] [PubMed]
295. Sheng, S.; Wang, M.; Mu, L. An innovative and rapid method for permanent hydrophilic modification of polydimethylsiloxane (PDMS) chip surfaces. *J. Appl. Phys.* **2025**, *137*, 015301. [CrossRef]
296. Gleghorn, J.P.; Nelson, C.M. Nanopatterned Surfaces for Exploring and Regulating Cell Behavior. In *Encyclopedia of Nanotechnology*; Bhushan, B., Ed.; Springer: Dordrecht, The Netherlands, 2016. [CrossRef]
297. Zhu, Z.; Lv, Z.; Wang, L.; Tan, H.; Xu, Y.; Li, S.; Chen, L. A pump-free paper/PDMS hybrid microfluidic chip for bacteria enrichment and fast detection. *Talanta* **2024**, *275*, 126155. [CrossRef] [PubMed]
298. Nguyen, P.Q.H.; Duong, D.D.; Kwun, J.D.; Lee, N.Y. Hybrid elastomer-plastic microfluidic device as a convenient model for mimicking the blood-brain barrier in vitro. *Biomed. Microdevices* **2019**, *21*, 90. [CrossRef] [PubMed]
299. Eslam, H.M.; Hataminia, F.; Asadi-Saghandi, H.; Fayazbakhsh, F.; Tabatabaei, N.; Ghanbari, H. Characterization and numerical simulation of a new microfluidic device for studying cells-nanofibers interactions based on collagen/PET/PDMS composite. *Front. Lab. Chip. Technol.* **2024**, *3*, 1411171. [CrossRef]
300. Xue, P.; Li, Q.; Li, Y.; Sun, L.; Zhang, L.; Xu, Z.; Kang, Y. Surface Modification of Poly(dimethylsiloxane) with Polydopamine and Hyaluronic Acid to Enhance Hemocompatibility for Potential Applications in Medical Implants or Devices. *ACS Appl. Mater. Interfaces* **2017**, *9*, 33632–33644. [CrossRef] [PubMed]
301. Amini, H.; Sokhansanj, A.; Akrami, M.; Haririan, I. Design and Fabrication of a High-Performance Microfluidic Chip for Blood Plasma Separation: Modelling and Prediction of System Behavior via CFD Method. *Int. J. Anal. Chem.* **2023**, 3648247. [CrossRef] [PubMed]
302. Qin, T.; Yang, X.; Zhang, J.; Cao, X. Developing a non-fouling hybrid microfluidic device for applications in circulating tumor cell detections. *Colloids Surf. B Biointerfaces* **2017**, *151*, 39–46. [CrossRef] [PubMed]

303. Tsai, H.-F.; Toda-Peters, K.; Shen, A.Q. Glioblastoma adhesion in a quick-fit hybrid microdevice. *Biomed. Microdevices* **2019**, *21*, 30. [CrossRef] [PubMed]
304. DeMeulemeester, J.A.; Thompson, A.J.; Potkay, J.A. Surface Modification of Poly(dimethylsiloxane) Blood Flow Chambers with a Poly (ethylene glycol) Conjugate and Factor XII Inhibitor. *Langmuir* **2025**, *41*, 5048–5059. [CrossRef] [PubMed]
305. Ren, C.; Zhang, S.; Song, D.; Guo, J. Lab on dielectric film deposited PCB device for characterization of electrical property of biological cells. *IEEE Trans. Dielectr. Electr. Insul.* **2016**, *23*, 1895–1897. [CrossRef]
306. Pereira, A.T.; Novo, P.; Prazeres, D.M.F.; Chu, V.; Conde, J.P. Heterogeneous immunoassays in microfluidic format using fluorescence detection with integrated amorphous silicon photodiodes. *Biomicrofluidics* **2011**, *5*, 014102. [CrossRef] [PubMed]
307. Fukushi, M.; Kinoshita, K.; Yamada, M.; Yajima, Y.; Utoh, R.; Seki, M. Formation of pressurizable hydrogel-based vascular tissue models by selective gelation in composite PDMS channels. *RSC Adv.* **2019**, *9*, 9136–9144. [CrossRef] [PubMed]
308. Li, C.-X.; Liu, Y.; Li, Y.; Li, J.-J.; Qu, S.-L. Micro-velocity fiber probe based on Fe3O4-PDMS filled microcavity for on-chip microfluidic. *Measurement* **2024**, *224*, 113924. [CrossRef]
309. Casanova-Moreno, J.; To, J.; Yang, C.W.T.; Turner, R.F.B.; Bizzotto, D.; Cheung, K.C. Fabricating devices with improved adhesion between PDMS and gold-patterned glass. *Sens. Actuators B Chem.* **2017**, *246*, 904–909. [CrossRef]
310. Das, A.; Santhosh, S.; Giridhar, M.; Behr, J.; Michel, T.; Schaudy, E.; Ibáñez-Redín, G.; Lietard, J.; Somoza, M.M. Dipodal Silanes Greatly Stabilize Glass Surface Functionalization for DNA Microarray Synthesis and High-Throughput Biological Assays. *Anal. Chem.* **2023**, *95*, 15384–15393. [CrossRef] [PubMed]
311. Miranda, I.; Souza, A.; Sousa, P.; Ribeiro, J.; Castanheira, E.M.S.; Lima, R.; Minas, G. Properties and Applications of PDMS for Biomedical Engineering: A Review. *J. Funct. Biomater.* **2022**, *13*, 2. [CrossRef] [PubMed]
312. Cunha, F.M.; Freitas, J.R.; Pimenta, S.; Silva, M.F.; Correia, J.H. Silicon dioxide atomic layer deposition at low temperature for PDMS microlenses coating. *Opt. Mater.* **2024**, *157*, 116167. [CrossRef]
313. Hardy, B.S.; Uechi, K.; Zhen, J.; Kavehpour, H.P. The deformation of flexible PDMS microchannels under a pressure driven flow. *Lab Chip* **2009**, *9*, 935–938. [CrossRef] [PubMed]
314. Zhang, L.; Liu, Z.; Pang, Y.; Wang, X.; Li, M.; Ren, Y. Trapping a moving droplet train by bubble guidance in microfluidic networks. *RSC Adv.* **2018**, *8*, 8787–8794. [CrossRef] [PubMed]
315. De Graaf, M.N.S.; Vivas, A.; van der Meer, A.D.; Mummery, C.L.; Orlova, V.V. Pressure-Driven Perfusion System to Control, Multiplex and Recirculate Cell Culture Medium for Organs-on-Chips. *Micromachines* **2022**, *13*, 1359. [CrossRef] [PubMed]
316. Lee, J.D.; Kumar, A.; Mathur, T.; Jain, A. Vascular architecture-on-chip: Engineering complex blood vessels for reproducing physiological and heterogeneous hemodynamics and endothelial function. *Lab Chip* **2025**, *25*, 2620–2631. [CrossRef] [PubMed]
317. Kim, S.; Lai, D.; Park, J.Y.; Yokokawa, R.; Takayama, S. Microfluidic automation using elastomeric valves and droplets: Reducing reliance on external controllers. *Small* **2012**, *8*, 2925–2934. [CrossRef] [PubMed]
318. Zeng, W.; Li, S.; Wang, Z. Characterization of syringe-pump-driven versus pressure-driven microfluidic flows. In Proceedings of the 2015 International Conference on Fluid Power and Mechatronics (FPM), Harbin, China, 5–7 August 2015; pp. 711–715. [CrossRef]
319. Ariati, R.; Sales, F.; Souza, A.; Lima, R.A.; Ribeiro, J. Polydimethylsiloxane Composites Characterization and Its Applications: A Review. *Polymers* **2021**, *13*, 4258. [CrossRef] [PubMed]
320. Xu, J.; Vaillant, R.; Attinger, D. Use of a porous membrane for gas bubble removal in microfluidic channels: Physical mechanisms and design criteria. *Microfluid. Nanofluid* **2010**, *9*, 765–772. [CrossRef]
321. Becher, C.; Frauenlob, M.; Selinger, F.; Ertl, P.; Goumans, M.-J.; Sanchez-Duffhues, G. A cost-effective vessel-on-a-chip for high shear stress applications in vascular biology. *Microvasc. Res.* **2025**, *160*, 104814. [CrossRef] [PubMed]
322. Qiao, L.; Chang, S.; Zou, L.; Zhang, F.; Cui, C.; Huang, N. Multiorgan-on-a-chip: An advanced platform for disease modeling, drug toxicity assessment, and therapeutic screening. *Bio-des. Manuf.* **2025**, *8*, 1035–1062. [CrossRef]
323. Grigoryan, B.; Paulsen, S.J.; Corbett, D.C.; Sazer, D.W.; Fortin, C.L.; Zaita, A.J.; Greenfield, P.T.; Calafat, N.J.; Gounley, J.P.; Ta, A.H.; et al. Multivascular networks and functional intravascular topologies within biocompatible hydrogels. *Science* **2019**, *364*, 458–464. [CrossRef] [PubMed]
324. Nazir, A.; Gokcekaya, O.; Billah, K.M.M.; Ertugrul, O.; Jiang, J.; Sun, J.; Hussain, S. Multi-material additive manufacturing: A systematic review of design, properties, applications, challenges, and 3D printing of materials and cellular metamaterials. *Mater. Des.* **2023**, *226*, 111661. [CrossRef]
325. Shakeri, A.; Jarad, N.A.; Khan, S.; Didar, T.F. Bio-functionalization of microfluidic platforms made of thermoplastic materials: A review. *Anal. Chim. Acta* **2022**, *1209*, 339283. [CrossRef] [PubMed]
326. Gong, H.; Bao, C.; Li, J.; Yu, Y.; Yang, W. Label-free and high-sensitivity electrochemical sensor for thrombin detection based on target-induced hybridization chain reaction and host-guest interaction. *Electrochim. Acta* **2026**, *548*, 147913. [CrossRef]
327. Foy, B.H.; Stefely, J.A.; Bendapudi, P.K.; Hasserjian, R.P.; Al-Samkari, H.; Louissaint, A.; Fitzpatrick, M.J.; Hutchison, B.; Mow, C.; Collins, J.; et al. Computer vision quantitation of erythrocyte shape abnormalities provides diagnostic, prognostic, and mechanistic insight. *Blood Adv.* **2023**, *7*, 4621–4630. [CrossRef] [PubMed]

328. Zilberman-Rudenko, J.; Sylman, J.L.; Lakshmanan, H.H.S.; McCarty, O.J.T.; Maddala, J. Dynamics of Blood Flow and Thrombus Formation in a Multi-Bypass Microfluidic Ladder Network. *Cel. Mol. Bioeng.* **2017**, *10*, 16–29. [CrossRef] [PubMed]
329. Du, E.; Diez-Silva, M.; Kato, G.J.; Dao, M.; Suresh, S. Kinetics of sickle cell biorheology and implications for painful vasoocclusive crisis. *Proc. Natl. Acad. Sci. USA* **2015**, *112*, 1422–1427. [CrossRef] [PubMed]
330. Zhang, B.; Radisic, M. Organ-on-a-chip devices advance to market. *Lab Chip* **2017**, *17*, 2395–2420. [CrossRef] [PubMed]
331. Miao, J.; Jiang, C.; Li, J.; Tsang, A.C.H. Biologically motivated magnetic microfluidic rheostats for precise and scalable flow control. *Microsyst. Nanoeng.* **2026**, *12*, 314. [CrossRef] [PubMed]
332. Balogh, P.; Bagchi, P. Analysis of red blood cell partitioning at bifurcations in simulated microvascular networks. *Phys. Fluids* **2018**, *30*, 051902. [CrossRef]
333. Muthard, R.W.; Diamond, S.L. Side view thrombosis microfluidic device with controllable wall shear rate and transthrombus pressure gradient. *Lab Chip* **2013**, *13*, 1883–1891. [CrossRef] [PubMed]

Disclaimer/Publisher's Note: The statements, opinions and data contained in all publications are solely those of the individual author(s) and contributor(s) and not of MDPI and/or the editor(s). MDPI and/or the editor(s) disclaim responsibility for any injury to people or property resulting from any ideas, methods, instructions or products referred to in the content.